



<https://theses.gla.ac.uk/>

Theses Digitisation:

<https://www.gla.ac.uk/myglasgow/research/enlighten/theses/digitisation/>

This is a digitised version of the original print thesis.

Copyright and moral rights for this work are retained by the author

A copy can be downloaded for personal non-commercial research or study,
without prior permission or charge

This work cannot be reproduced or quoted extensively from without first
obtaining permission in writing from the author

The content must not be changed in any way or sold commercially in any
format or medium without the formal permission of the author

When referring to this work, full bibliographic details including the author,
title, awarding institution and date of the thesis must be given

Enlighten: Theses

<https://theses.gla.ac.uk/>
research-enlighten@glasgow.ac.uk

OPTICAL FIBRE COUPLING DEVICES

A thesis

submitted to the Faculty of Engineering
of the University of GLASGOW

for the degree of

Master of Science

by

Yann H.B. Kerr

March, 1981

ProQuest Number: 10647719

All rights reserved

INFORMATION TO ALL USERS

The quality of this reproduction is dependent upon the quality of the copy submitted.

In the unlikely event that the author did not send a complete manuscript and there are missing pages, these will be noted. Also, if material had to be removed, a note will indicate the deletion.



ProQuest 10647719

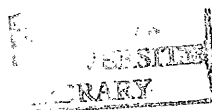
Published by ProQuest LLC (2017). Copyright of the Dissertation is held by the Author.

All rights reserved.

This work is protected against unauthorized copying under Title 17, United States Code
Microform Edition © ProQuest LLC.

ProQuest LLC.
789 East Eisenhower Parkway
P.O. Box 1346
Ann Arbor, MI 48106 – 1346

Thesis
6373
Copy 2



This work is dedicated to my parents and my wife

ACKNOWLEDGEMENTS

I wish to express my sincere gratitude to Professor J. Lamb for his help, interest and encouragements during the course of this work as well as for providing the research facilities in the Department of Electronics and Electrical Engineering.

I would also like to thank Dr. P.J.R. Laybourn for the supervision of this work and his help in the preparation of this thesis.

Mention must also be made of Dr. R. Dunsmuir for many helpful discussions.

I would also like to address my special thanks to Dr. A. Yi Yan for his constant help and advice during the study concerned with the second part of this thesis.

I am also greatly indebted to Mr. R.H. Hutchins for his help and for looking after my personal well-being.

The technical assistance of Mrs. L. Hobbs, Mr. G. Boyle, Mr. J. Clark, Mr. K. Piechowiak, Mr. B. Miller, Mr. D. Thompson and Mr. H. Anderson is greatly acknowledged.

Grateful acknowledgement is made to the Stevenson Scholarship Committee, the Royal Society, the Centre National de la Recherche Scientifique and the Science Research Council for financial support of this work.

Finally I am greatly indebted to my wife for her constant support and encouragement as well as for her help in the preparation of this thesis.

SUMMARY

This thesis deals with optical coupling systems and is divided in two parts.

The first one is concerned with directional coupling between two graded index fibres made by a diffusion process. The theory and physics of ion exchange is studied, providing a theoretical description of the refractive index change. A mathematical method of solving the concentration dependent diffusion equation is given. Theoretical index distributions are thus obtained for circular waveguides. To compare theory with experiment, a device directly measuring the index profile of a circular fibre is described.

The theory of propagation in round graded index fibres is reviewed and a simplified coupling coefficient derived in order to determine the coupling efficiency. The coupling arrangement is described and the results discussed. It is shown that efficient tapping of power can be done with the high order modes, and eventually, at a much lower efficiency with the low order ones.

The second part describes a theoretical study of optical contra-directional coupling between a single mode sandwich ribbon fibre and a thin film planar waveguide, longitudinal phase matching being achieved by means of a periodic corrugation, which is typically a grating etched into the film.

Film-fibre couplers were tested and achieved an estimated efficiency of only 20% due to the poor quality of the gratings. With several improvements in the set-up and specimens, an efficiency of over 60% is quite feasible. The application of the method for linking integrated optical devices is considered as well as a possible demultiplexer.

The study presented provides the ground work for future development of integrated optical devices links and an active device.

II-2.3.	The multimode fibre coupler	30
II-2.3.1.	The coupling coefficient	31
II-2.3.2.	Simplified coupling coefficient	33
II-2.3.3.	Coupling efficiency	34
II-2.4.	Conclusion	36
<u>CHAPTER III FABRICATION AND MEASUREMENTS OF GRADED INDEX FIBRES</u>		39
II-3.1.	Fabrication process of the fibres	39
II-3.1.1.	Production of the raw fibre	39
	a) The preform	39
	b) Fibre pulling	40
	c) Checking the fibres	40
II-3.1.2.	Production of graded index fibres by the	
	two melt method	44
	a) The furnace design	44
	b) The melts	46
	c) Results	46
	d) Conclusion	47
II-3.1.3.	The repulling method	47
II-3.1.4.	Selfoc fibres	49
	a) Fabrication process	49
	b) Properties of the fibres	49
II-3.2.	Study of the index profile	52
II-3.2.1.	Indirect methods of measurements	52
	a) "Potting" fibres	52
	b) End fire launching	52
	c) Prism launching	62
	d) Conclusion	62
II-3.2.2.	Direct methods of profile measurements	64
	II-3.2.2.1. Interferometric measurements	64

a) The Michelson interferometer	64
b) The Mach-Zehnder interferometer	64
c) Conclusion	67
II-3.2.2.2. Index profile from refracted light	
from fibre	67
a) Introduction	67
b) Principle and description of the method	69
c) Theory of the refracted light method	72
d) Experimental results and conclusion	75
<u>CHAPTER IV INDEX MODIFICATION AND COUPLING</u>	79
II-4.1. Introduction	79
II-4.2. Principle of index modification	79
II-4.3. Index modification apparatus	79
II-4.3.1. Silver diffused fibres	79
II-4.3.2. Selfoc fibres	82
II-4.4. Coupling devices	90
II-4.4.1. Short coupling method	90
II-4.4.2. Coupling block method	90
II-4.5. Results and conclusion	93
<u>PART III GRATING COUPLERS</u>	96
<u>CHAPTER I INTRODUCTION</u>	97
<u>CHAPTER II PROPAGATION IN A SLAB AND IN A RECTANGULAR WAVEGUIDE</u>	99
III-2.1. Introduction	99
III-2.2. Slab waveguide	99
III-2.3. Stripe waveguide	101
<u>CHAPTER III COUPLING COEFFICIENT</u>	108
III-3.1. Coupled mode theory	108
III-3.2. Coupling by means of a grating (TE modes)	109
III-3.3. Numerical results	114
III-3.3.1. Description of the model	114

a) Fibre	116
b) Film	116
c) Grating	116
d) Coupler	117
II-3.3.2. Computed results and conclusion	117
<u>CHAPTER IV EXPERIMENTAL RESULTS AND CONCLUSION</u>	128
III-4.1. Experimental apparatus	128
III-4.2. The fibres	128
III-4.3. Slab waveguides and gratings	135
III-4.4. Results	137
III-5 Conclusion	143
<u>PART IV CONCLUSION</u>	144
IV-1 First part	145
IV-2 Second part	147
IV-3 Suggestions for future work	148
References	152

PART 1

INTRODUCTION

I-1 General

Optical fibres have been used for many years to relay images over short distances. In 1966 Kao [1] suggested their use over long distances and led the way to many successful attempts to reduce their optical losses [2].

Now several types of fibres are industrially produced. The Japanese Selfoc fibres have, for example, losses of less than 8dB/km [3]. Beales et al have reported losses of 5.7dB/km at 840nm [4] while Payne and Gambling achieved even better results by manufacturing their fibres with a Chemical Vapour Deposition (C.V.D.) process [5] - [9]. Now, with this method, very low-loss fibres are produced (0.25dB/km) [10]. Because of the very low losses achieved and because of important reductions of the pulse broadening obtained by profiling the index profile, optical fibres are now able to compete with more conventional techniques for carrying information. When compared with coaxial cables, for instance, they present several advantages [11]: low size and weight, they are not subject to electromagnetic interference and hold out the promise of low manufacturing costs. Several complete optical fibre systems have already been installed and put into operational use by the British Post Office [12].

However, the realisation of practical fibre systems, especially the data bus, has been hampered by the inefficiency of light coupling into and out of fibres and thin film waveguides. Research on different coupling schemes of fibres to thin film waveguides, fibres to fibres, thin film waveguides to thin film waveguides and sources to fibres is currently being conducted in several laboratories [13] - [19]. All the coupling methods investigated can be divided in two categories: direct excitation and evanescent field coupling. The first requires the field patterns of input and output to match closely. It demands extreme accuracy in both alignment and preparation of the waveguides.

For the second method, coupling takes place in the overlapping region of the evanescent tail and requires the latter to be strong and the coupled guides to have matched phase velocities.

I-2 Motivation and aim of the work

At the beginning of this research, in October 1978, Stewart [20] had stated the possibility of using the ion exchange process in the modification of optical fibres for coupling purposes, but little had been done in actually looking at the feasibility of the process. On the other hand it seemed that Selfoc fibres would be readily available in the near future and could be suitably modified.

Coupling between a fibre and an integrated circuit being a very important problem to be solved, the investigation of means to overcome the difficulties encountered when the fibre and circuit have refractive indices which are very different were also carried out.

Bearing this in mind, the aims of this work were:

- a)
 - i) To manufacture graded index fibres using an ion exchange process similar to the one used to produce Selfoc fibres, using, as a starting point, the work done by Stewart et al. [21],[22].
 - ii) To modify locally the index profiles of these fibres so that they could be coupled together and could be then used as "bus-bars" around, for example, a system of limited extent (ship, aircraft) directional couplers being formed at intermediate points along the fibre.
 - iii) To apply these results to Selfoc fibres as soon as they were available.
- b) To investigate a way of coupling a fibre of relatively low effective index (typically round 1.5) to a waveguide of higher effective index (Lithium Niobate or Arsenic Trisulphide) with good efficiency.

I-3 Review of the Thesis

Considering the rather different aspects of the two main parts of this study, the thesis is divided in two.

I-3.1 First part

The first chapter deals with the theory of ion exchange in glass by studying the different factors affecting the process. The theory leads to a diffusion equation which is then solved analytically for round fibres.

The following chapter is devoted to the propagation of light in a fibre with particular attention to one having a graded index profile. A simplified theory of the multimode fibre coupling is then developed.

The third chapter is concerned with the experimental manufacturing and testing of graded index ion-exchanged round fibres.

In chapter four the transverse coupling of two fibres is considered, with particular application to Selfoc fibres. The chapter ends with the results of the foregoing work which are summarised and discussed.

I-3.2 Second part

This part deals with the contradirectional coupling between a sandwich ribbon (S.R.) fibre and a thin film waveguide by means of a grating.

The second chapter is devoted to the propagation of light in a slab and a rectangular waveguide while the following one deals with the coupled mode theory necessary to be able to evaluate the coupling coefficient of the device. Some numerical results are given in chapter three. In chapter four the experimental apparatus is described with the results gained. Finally in chapter five the results are discussed. There is ample scope for applications and suggestions for the continuation of the work are given in the general conclusion.

PART II

DIRECTIONAL COUPLING TO
MULTIMODE GLASS FIBRES

CHAPTER I

The Ion Exchange Process

II-1.1 Theory of ion-exchange

As it is necessary to be able to predict the shape of the refractive index profile of a graded index fibre produced by ion-exchange, the theory of diffusion and the mathematical techniques for solving the concentration-dependent diffusion equation have to be studied. The bulk of this chapter is thus devoted to diffusion theory in cylindrical dielectric rods. However the first thing will be to decide what raw materials are most suitable for the diffusion process when the physics of ion-exchange are known.

II-1.1 The physics of ion exchange: Theory

Not all the glasses have properties that are suitable for allowing the ion-exchange process to take place. Generally speaking, glass is made up from different inorganic oxides fused together in given proportions [23]. A given type can be considered more or less pure (elements such as Fe_2O_3 , MgO can be considered as impurities) and cause the glass to have very different properties.

Glasses do not have a long range structure so it is possible for some of the ionic constituents to diffuse. Some of them are too tightly bound to the network (Si, O), but others can be quite mobile. They obey a law which can be characterised by a diffusion constant of the type:

$$D = D_0 \exp\left(-\frac{\Delta H}{RT}\right) \quad (1-1)$$

where: D is the self-diffusion constant

ΔH is the energy of activation

R is the gas constant

T is the temperature (absolute)

The mobility of the cations is variable but, in general, the monovalent ones are more mobile and thus more interesting for this study. In the inter-diffusion process, the monovalent cations in the glass can diffuse through the relatively immobile structure of the substrate to be exchanged at the surface with ions in the melt which, in turn, migrate through the silicate structure.

We shall consider a piece of glass containing a cation A and a melt, containing a cation B, of sufficient volume so that the depletion of the ions will not be a sufficient factor and can be ignored. The inter-diffusion and exchange of the two ions only will be considered. Generally speaking, in the glass A and B do not have the same mobility, inducing an electrical field which will damp the movement of the faster and speed up the slower species. As electrical neutrality must be preserved, the fluxes of the two ions must remain identical.

Using these two conditions, it is possible to derive an equation for monovalent ions [20].

$$D_{AB} = \frac{D_B}{1 - \alpha \frac{C_B}{C_{AO}}} \quad (1-2)$$

where:

- D_{AB} is the inter-diffusion coefficient
- D_A is the self-diffusion coefficient for A,
- D_B is the self-diffusion coefficient for B,
- C_A is the concentration of A in the glass,
- C_B is the concentration of B in the glass,
- C_{AO} is the original concentration of A in the glass,

and

$$C_{AO} = C_A + C_B$$

$$\alpha = 1 - \frac{D_B}{D_A}$$

The flux for A and B might be written according to Stewart [20]:

$$J_A = -D_{AB} \frac{\partial C_A}{\partial x} \quad (1-3)$$

$$J_B = -D_{AB} \frac{\partial C_B}{\partial x} \quad (1-4)$$

leading to:

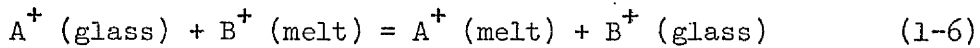
$$\frac{\partial}{\partial x} \left(D_{AB} \frac{\partial C_B}{\partial x} \right) = \frac{\partial C_B}{\partial t} \quad (1-5)$$

which can determine the concentration profile of B.

To solve equations (1-2) and (1-3), knowledge of the degree of exchange must be known. This is given by the expression C_{BS}/C_{AO} where C_{BS} is the surface concentration of B. The exchange can be complete for some melts containing only the cation B but, for dilute melts, it is necessary to evaluate it.

II-1.1.2 Surface concentration for dilute melts.

It is assumed that the glass has remained in the melt long enough for equilibrium to be reached. Consider the glass/melt interface. The exchange process verifies the equation:



which leads to the equilibrium constant

$$K_{AB} = \frac{a_{GSB} a_{MA}}{a_{GSA} a_{MB}} \quad (1-7)$$

where a is the thermodynamic activity of A^+ and B^+ (subscripts A, B) at the glass surface (subscript GS) or in the melt (subscript M).

It is found [22] that the ratio C_{BS}/C_{AO} can be computed from the equation:

$$\ln \left[\frac{M_B}{M_A} \right] - \frac{E_M}{RT} (1 - 2M_A) = \gamma \ln \frac{C_{BS}}{C_{AO} - C_{BS}} - \ln(K_{AB}) \quad (1-8)$$

where M_A and M_B are the mole fractions of A and B, E_M is the net interaction energy of the ions, γ is a constant ($\gamma \geq 1$) [24].

Thus it appears that the surface concentration is only dependent on the melt dilution.

The diffusion theory as expressed here is greatly simplified as many other factors may influence it. The main ones are the following:

i) The diffusional motion of the cations is assumed to be random.

In some glasses they move in a direction related to their previous motion [25], and to take this into account, the self-diffusion constants must be multiplied by a factor F [26].

However it will be assumed here that for the two ions the factors F_A and F_B are equivalent (since they are moving in the same medium) [27], leaving the inter-diffusion coefficient roughly unaffected.

ii) Film diffusion can also occur, especially with dilute melts where the amount of B available at the time can be insufficient to satisfy the demand of the glass [28], [29].

II-1.1.3 Relationship between concentration and index change.

For a glass the refractive index is modified when ions of different polarisability are exchanged, and for many substrates it can be computed from the Gladstone-Dale equation [30],[31]:

$$n = 1 + \rho \sum_{i=1}^n r_i w_i \quad (1-9)$$

where ρ , the density [32], is given by

$$\rho = \frac{1}{\sum_{i=1}^n v_i w_i} \quad (1-10)$$

and where

w_i is the weight fraction of the i^{th} component oxide,

v_i is the specific volume of the i^{th} component oxide,

r_i is the specific reflectivity of the i^{th} component oxide.

Assuming that (1-9) is valid for ion diffused glass and that only minor constituents are exchanged, ρ is almost constant giving:

$$\Delta n = \rho \sum_{i=1}^n r_i \Delta w_i \quad (1-11)$$

For the case of the exchange of two ions only:

$$\Delta W_B = -\frac{W_B}{W_A} \Delta W_A \quad (1-12)$$

where W_i is the molecular weight of the oxide i . Thus

$$\Delta n = \rho \left(r_B - r_A \frac{W_A}{W_B} \right) \Delta W_B \quad (1-13)$$

Consequently there is a linear relation between the concentration of the ion of the melt in the glass and the change of refractive index.

For example (1-8) can be written for a dilute melt:

$$\ell_n \left(\frac{M_B}{M_A} \right) - \frac{EM}{RT} (1 - 2M_A) = \gamma \ln \left(\frac{\Delta n_s}{\Delta n_{sp} - \Delta n_s} \right) - \ell_n K_{AB} \quad (1-14)$$

where: Δn_{sp} is the surface index change with a pure melt,

Δn_s is the surface index change with a dilute melt.

It is thus possible to predict quite easily what the index change will be for a given dilute melt. In Fig. 1-1 the ratio $\Delta n_s/\Delta n_{sp}$ is plotted against M_B/M_A . It shows that to achieve a significant index change only small quantities of the ion B are required ($M_B/M_A \leq 5 \cdot 10^{-2}$). In Fig. 1-2 the experimental results are plotted according to equation (1-14). It gives $K_{AB} = 131$ and $\gamma = 1.32$.

II-1.1.4 Glass composition

In glasses the oxides are not organised as in a crystalline solid (as the x-ray diffraction pictures show), but more as a rather viscous liquid. The molecular aspect of glass is a random arrangement, as in liquids, with molecules which are not very mobile [33]. W.H. Zachariasen [34] considered the structure of glass as a random network of SiO_2 altered by the addition of oxides such as Na_2O , K_2O , Li_2O , CaO , MgO , ZnO which modify the network by breaking its continuity. Other oxides such as Al_2O_3 , BeO , TiO_2 , called intermediates, can either disrupt or join the network. In this work, it will be assumed that Zachariasen's theory concerning the structure of glass is valid, for although it proves to have some imperfections, the main features of the theory are

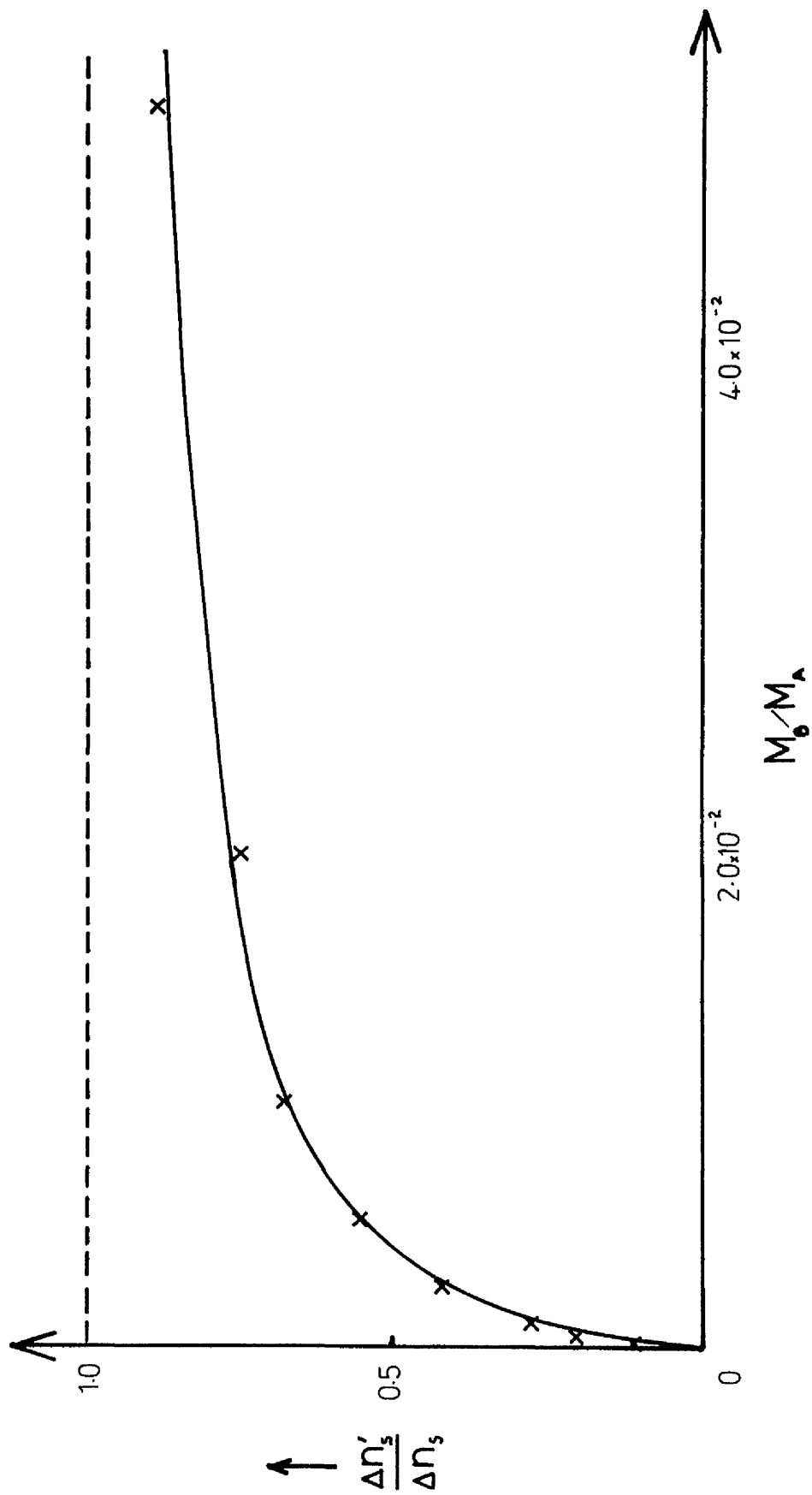


Figure 1.1: EXPERIMENTAL RELATIONSHIP BETWEEN SURFACE REFRACTIVE INDEX AND MELT COMPOSITION. (Reference 20)

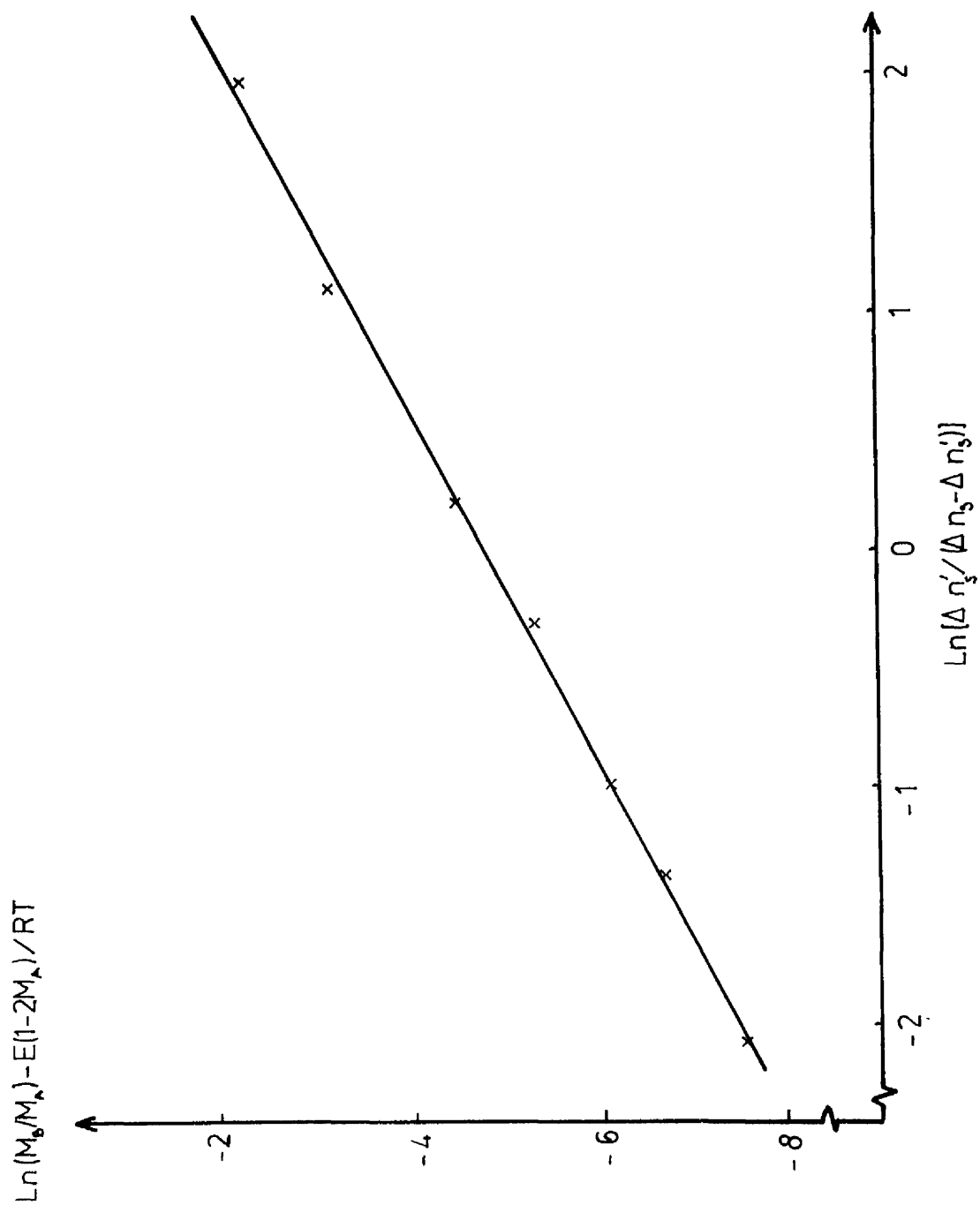


Figure 1.2: EXPERIMENTAL RESULTS ON THE RELATIONSHIP BETWEEN MELT DILUTION AND THE SURFACE INDEX. (eq.1.14) (Reference 20)

sufficient to understand the diffusion process.

II-1.1.5 Conclusion. Choice of materials

The glass chosen should possess cations as mobile as possible and it has been shown that this condition was fulfilled with monovalent modifying cations [20]. Thus the glass should have either Na_2O or K_2O or Li_2O , the possible exchangeable ions being then Li^+ , Ag^+ , K^+ , Tl^+ , Na^+ . It is also better to have a high value for K_{AB} so that the glass is "fond" of the ion in the melt.

It has also been shown experimentally [35] that the mobility of sodium ions in many silica glasses decreases when the concentration of CaO is increased, as though the oxide was inhibating the diffusion. Consequently the best choice seems to be an alumino-silicate glass (Al_2O_3 concentration has a direct effect on K_{AB}) with exchange between the ions:

K^+ , Na^+ or

Ag^+ , Na^+ or

Tl^+ , Na^+

Since the sodium ions are to be exchanged, the proportion of NaO in the glass is related to the maximum index change possible.

The work in this study was done with soda lime glass because of its availability and the ease in which it can be pulled into fibres.

The ideal glass composition would be [20]:

Silica	75%
Sodium oxide	14%
Aluminium oxide	11%
Calcium oxide	0%

But the one used had the following composition [36]

Silica	71%
Sodium oxide	15%

Aluminium oxide 2.2%

Calcium oxide 5.7%

The Silver ions of a very dilute melt (0.3%) containing Ag NO_3 were chosen for the exchange.

For these, the constants in equations (1-2) - (1-8), (1-14) are the following [22], [25].

$$E_M = 3.5 \times 10^3 \text{ J mole}^{-1}$$

$$K_{AB} = 120$$

$$\gamma = 1.08$$

$$D_{Na} = 5.75 \times 10^{-7} \exp - \frac{8.5 \times 10^4}{RT} \text{ m}^2 \text{ s}^{-1}$$

$$D_{Ag} = 1.59 \times 10^{-7} \exp - \frac{9.1 \times 10^4}{RT} \text{ m}^2 \text{ s}^{-1}$$

The melting point of NaNO_3 is 310°C .

II-1.2 Solution of the diffusion equation

The bulk of this part is devoted to the solution of the diffusion equation for the concentration profile which, as has been shown, is directly related to the refractive index profile.

Cylindrical geometry only is considered.

II-1.2.1. The equations

The exchange of monovalent ions can be described by the equations (1-2) - (1-5). Considering the new parameter C:

$$C = \frac{C_B}{C_{A_0}} \quad (1-15)$$

we have $C = 1$ at the surface and D_{AB} can be written:

$$D_{AB} = \frac{D_B}{1 - \alpha C} \quad (1-16)$$

For dilute melts, at the surface, $C_{BS} < C_{AO}$ but the condition $C = 1$ may still be used if α is replaced by α^I given by:

$$\alpha^I = \alpha \frac{C_{BS}}{C_{AO}} \quad (1-17)$$

which yields for dilute melts:

$$D_{AB} = \frac{D_B}{1 - \alpha^1 C} \quad (1-18)$$

The general form for (1-3) and (1-4) may be written:

$$J_A = -D_{AB} \vec{\text{grad}} C_A \quad (1-19)$$

$$J_B = -D_{AB} \vec{\text{grad}} C_B \quad (1-20)$$

Combining equation (1-19)(1-20) with the continuity equation yields the diffusion equation in vector notation:

$$\text{div} \left(D_{AB} \vec{\text{grad}} C \right) = \frac{\partial C}{\partial t} \quad (1-21)$$

which can be written in cylindrical coordinates (fig. 1-3a):

$$\frac{1}{r} \frac{\partial}{\partial r} \left(r D_{AB} \frac{\partial C}{\partial r} \right) + \frac{1}{r^2} \frac{\partial}{\partial \phi} \left(D_{AB} \frac{\partial C}{\partial \phi} \right) + \frac{\partial}{\partial z} \left(D_{AB} \frac{\partial C}{\partial z} \right) = \frac{\partial C}{\partial t} \quad (1-22)$$

In the case considered we have:

$$\frac{\partial C}{\partial \phi} = \frac{\partial C}{\partial z} = 0 \quad (1-23)$$

Hence, the diffusion equation can be written:

$$\frac{1}{r} \frac{\partial}{\partial r} \left(r D_{AB} \frac{\partial C}{\partial r} \right) = \frac{\partial C}{\partial t} \quad (1-24)$$

II-1.2.2. Solution using the finite difference method

The finite difference method is the most suitable for cylindrical geometry as it is described on Fig. (1-3). In order to have a general solution, the non-dimensional variables:

$$T = \frac{D_B t}{b^2} \quad (1-25)$$

$$R = \frac{r}{b} \quad (1-26)$$

$$s = \frac{\ln(1 - \alpha C)}{\ln(1 - \alpha)} \quad (1-27)$$

are used, t being the time of diffusion and b the outside diameter of the fibre. In terms of these new variables, the diffusion equation (1-24) can be written:

$$\frac{\partial s}{\partial T} - e^{\beta s} \left(\frac{1}{R} \frac{\partial}{\partial R} \left[R \frac{\partial s}{\partial R} \right] \right) = 0 \quad (1-28)$$

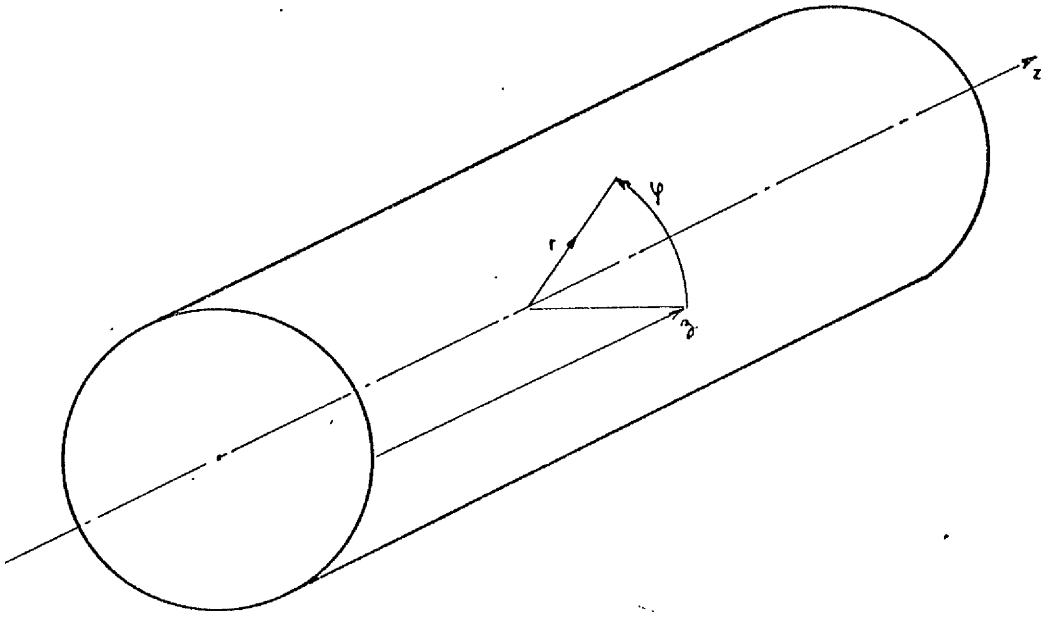


FIG:1-3a The Cylindrical Coordinate System

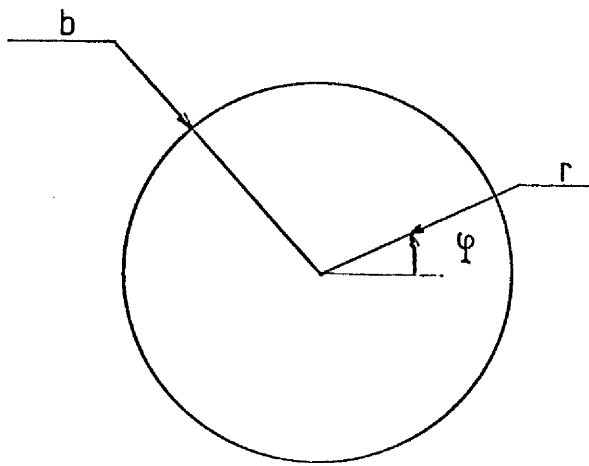
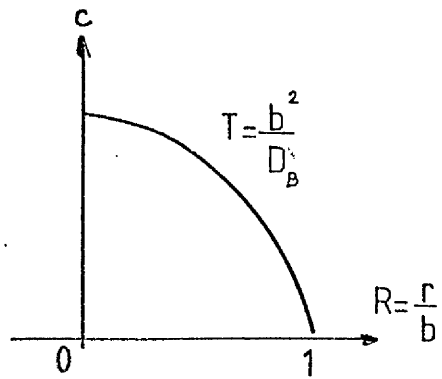


FIG:1-3b Coordinate System For The Fibre.



with $\beta = -\ln(1 - \alpha)$

In order to solve this equation, it is possible to approximate the partial derivatives by the corresponding Taylor series. Hence,

$$\frac{\partial s}{\partial T} = \frac{s(R, T + \delta T) - s(R, T)}{\delta T} + \epsilon_1(R, T) \quad (1-29)$$

$$\frac{\partial s}{\partial R} = \frac{s(R + \delta R, T) - s(R - \delta R, T)}{2\delta R} + \epsilon_2(R, T) \quad (1-30)$$

$$\frac{\partial^2 s}{\partial R^2} = \frac{s(R + \delta R, T) - 2s(R, T) + s(R - \delta R, T)}{(\delta R)^2} + \epsilon_3(R, T) \quad (1-31)$$

Since:

$$\frac{1}{R} \frac{\partial}{\partial R} \left(R \frac{\partial s}{\partial R} \right) = \frac{\partial^2 s}{\partial R^2} + \frac{1}{R} \frac{\partial s}{\partial R} \quad (1-32)$$

then:

$$\begin{aligned} \frac{1}{R} \frac{\partial}{\partial R} \left[R \frac{\partial s}{\partial R} \right] &= \frac{s(R + \delta R, T) - 2s(R, T) + s(R - \delta R, T)}{(\delta R)^2} + \\ &\frac{1}{R} \frac{s(R + \delta R, T) - s(R - \delta R, T)}{2\delta R} + \epsilon_4(R, T) \end{aligned} \quad (1-33)$$

which can be written:

$$\frac{1}{R} \frac{\partial}{\partial R} \left[R \frac{\partial s}{\partial R} \right] = \sum_{i=1}^2 \left(\frac{2R + (-1)^i \delta R}{2R} \right) \left(\frac{s(R + (-1)^i \delta R, T) - s(R, T)}{(\delta R)^2} \right) + \epsilon_4(R, T) \quad (1-34)$$

Substituting (1-34) and (1-29) in (1-28) leads to the finite difference formula (if we neglect $\epsilon_1(R, T)$), valid as long as $R \neq 0$:

$$\begin{aligned} s(R, T + \delta T) = s(R, T) + e^{\beta s(R, T) \frac{\delta T}{(\delta R)^2}} \sum_{i=1}^2 \left(1 + (-1)^i \frac{\delta R}{2R} \right) &\left(s(R + (-1)^i \delta R, T) \right. \\ &\left. - s(R, T) \right) \end{aligned} \quad (1-35)$$

This equation is always true for a hollow cylinder as R is never zero. However, in the case of a solid one another equation must be found for the case $R = 0$ in order to be able to solve the diffusion equation.

Consider the case

$$R \ll \delta R$$

$$\delta R \ll 1$$

It is possible to consider $\frac{\partial s}{\partial R} = 0$ for $R = 0$ (If it were not, the circular

symmetry would imply a gradient discontinuity which is not physically possible). Thus s can be approximated by:

$$s(R,T) = s(0,T) + \left[s(\delta R,T) - s(0,T) \right] \left(\frac{R}{\delta R} \right)^2 + \epsilon_5(R,T) \quad (1-36)$$

which yields:

$$\frac{\partial^2 s}{\partial R^2} + \frac{1}{R} \frac{\partial s}{\partial R} = \frac{4}{(\delta R)^2} \left(s(\delta R,T) - s(0,T) \right) + \epsilon_6(R,T) \quad (1-37)$$

and for $R = 0$

$$s(0,T + \delta T) \approx s(0,T) + \frac{4\delta T}{(\delta R)^2} e^{\beta s(0,T)} \left(s(\delta R,T) - s(0,T) \right) \quad (1-38)$$

For the boundary conditions it is possible to specify:

$$s(1,T) = \frac{\ln(1 - \alpha C_s(T))}{\ln(1 - \alpha)} \quad (1-39)$$

$$s\left(\frac{a}{b}, T\right) = s\left(\frac{a}{b} + \delta R, T\right) \quad (1-40)$$

for a hollow cylinder:

$$s(R,0) = \frac{\ln(1 - \alpha C_i(R))}{\ln(1 - \alpha)} \quad (1-41)$$

A Fortran IV programme, developed by Stewart, was used to carry out the computations. Fig. 1-4 shows the result for a plain fibre and for two values of α . It shows also the parabolic shape compared with each concentration profile. It is clearly visible that in some cases ($\alpha = 0.92$, $T = 0.12$ for example) the two profiles are quite similar, and so a parabolic shape may be obtained by suitable choice of the diffusion time.

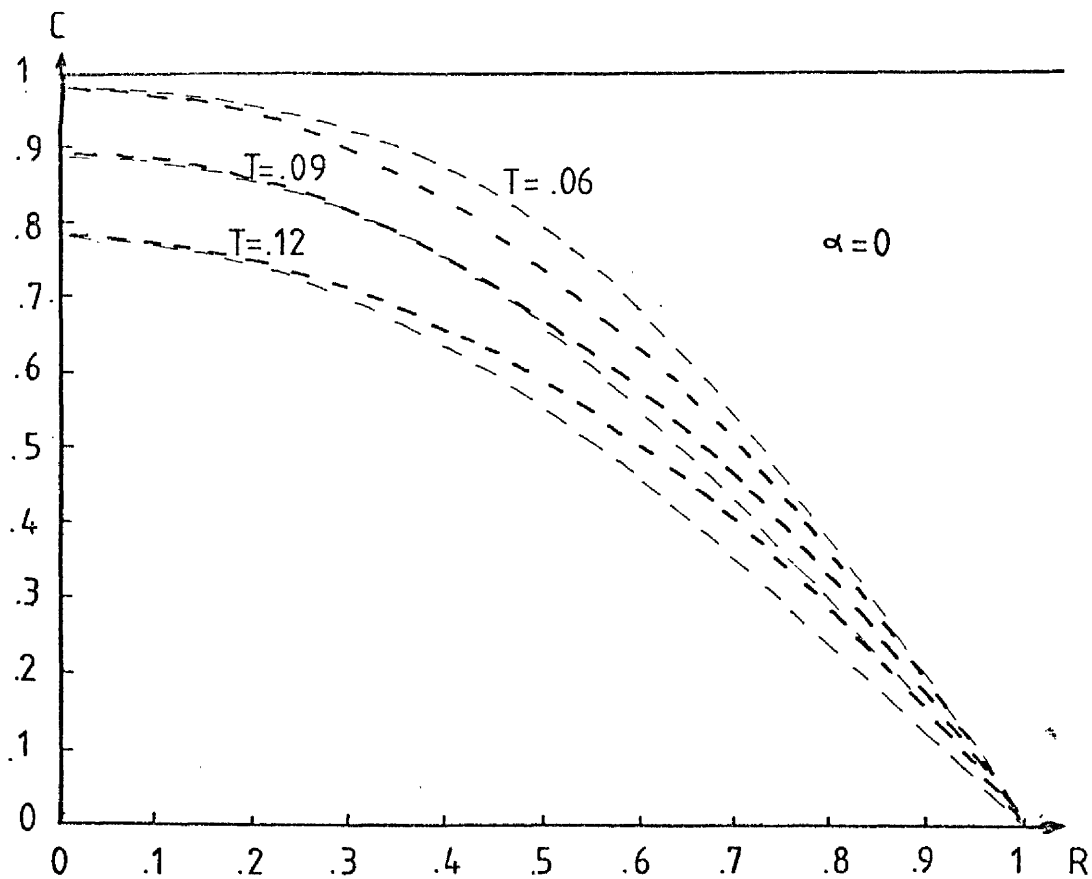
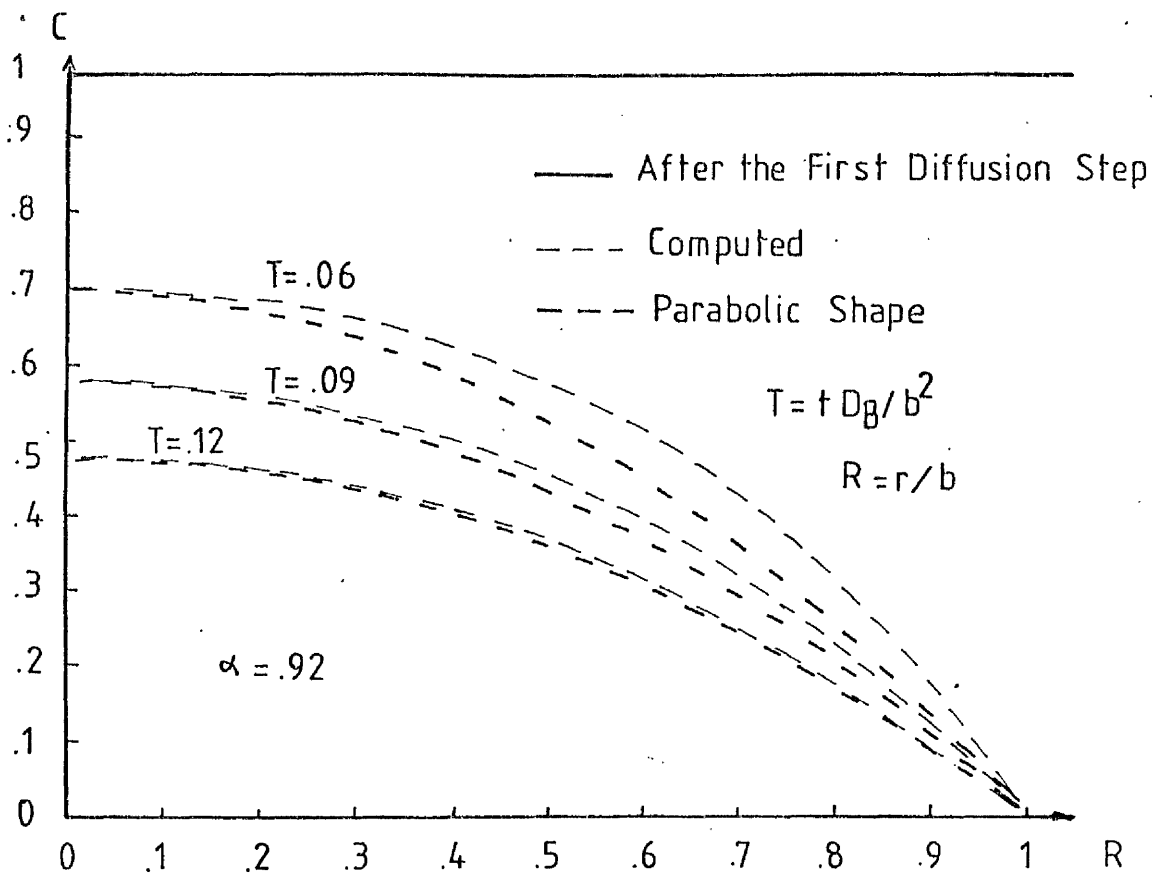


Fig.1.4 Computed Concentration Profiles.

CHAPTER II

Theory of Propagation in a Circular

Dielectric Waveguide and Simplified

Theory of the Multimode Coupler.

II-2.1 Introduction

Glass optical fibres are probably the simplest form of optical waveguides and the circular type is certainly the most common [39] among a large variety. Various types are depicted on fig. 2.1.

Generally speaking a fibre consists of two main parts (fig. 2.2):

- a) The core whose refractive index n , is slightly higher than that of the surrounding medium.
- b) The cladding of index n_0 which surrounds the core.

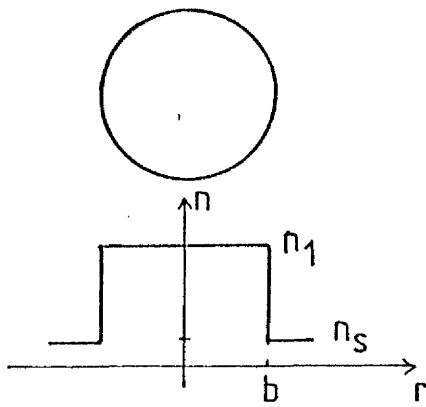
In optical communications single-mode fibres are the best with regard to transmission bandwidth, but the small dimensions of the core make the handling of such fibres (when splicing for example) quite delicate. Moreover, input coupling efficiency is poor when a multimode source is being used. Hence multimode fibres are of greater interest.

For the step-index fibre, the mode delay difference can considerably reduce the bandwidth. The possible solution lies in graded index fibres, as the mode delay differences can be minimised by shaping the profile. For example a nearly parabolic refractive index profile gives very satisfactory results [38].

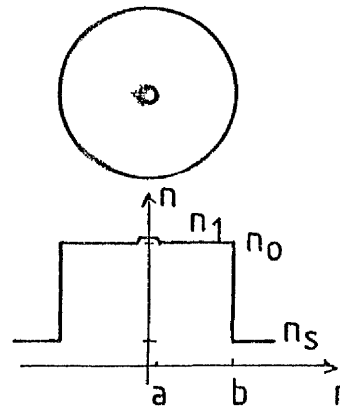
For these reasons it was decided to produce and work with multimode graded index fibres. The aim of this chapter is to provide the basic theory of propagation in circular graded index fibres in order to be able to evaluate their coupling efficiency.

II-22 Theory of propagation.

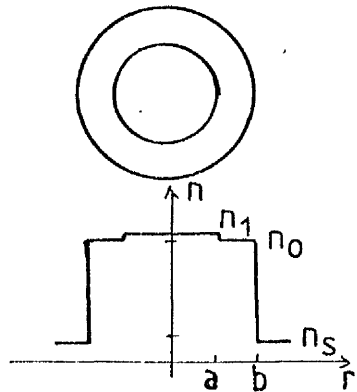
Maxwell's equations have a solution for propagation in circular fibres with infinite cladding whether they are of the step-index or



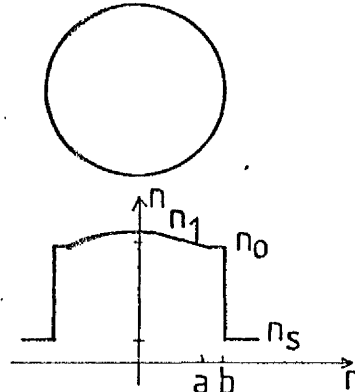
a) Unclad Fibre



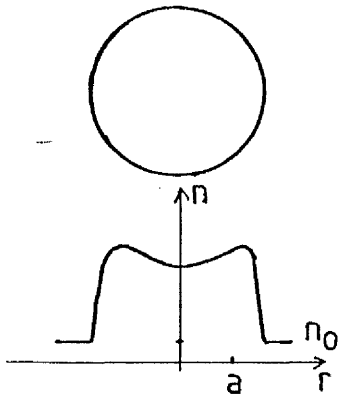
b) Single Mode Clad Fibre



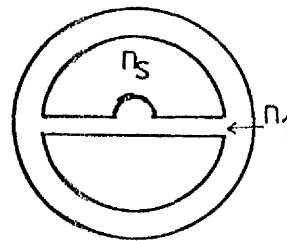
c) Multimode Clad Fibre



d) Parabolic Index Fibre



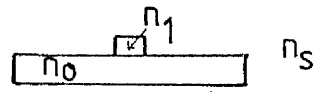
e) Graded Index Fibre



f) Single Material Fibre

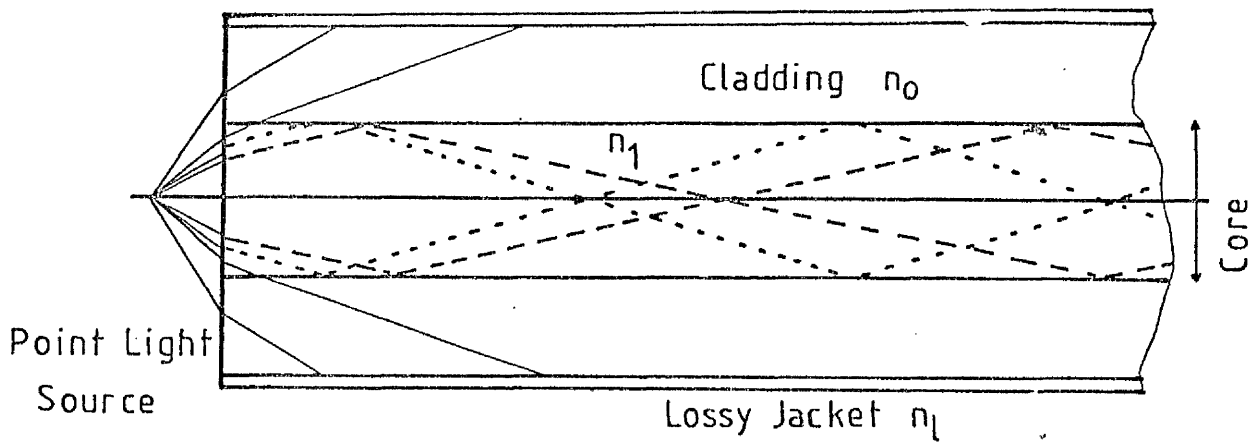


g) Thin Ribbon Fibre



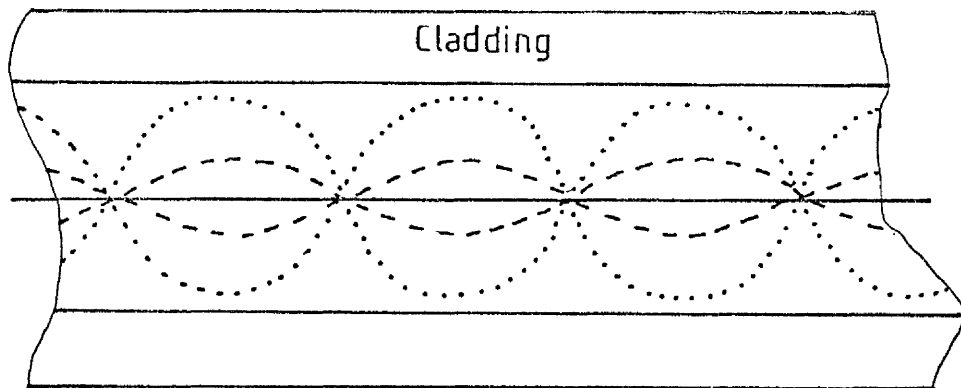
h) Sandwich Ribbon Fibre

Fig.2.1. Various Types of Optical Fibres



(a)

— Fundamental - - - Medium Order ····· High Order
Ray Paths



(b)

Fig.2.2 Collection And Guidance of Light

From a Point Source By a:

a) Clad Glass Fibre.

b) Graded Index Fibre.

graded-index type [40]. However the solutions are rather cumbersome and it is very often necessary to use one of the various approximate techniques developed. The basic ideas and results of some of them are briefly reviewed in the following sections.

II-22] Weakly guiding fibres.

A technique developed by Gloge [41] gives the approximate solution for all the modes of a weakly guiding fibre, that is, a fibre where the index difference Δ between the core and the cladding is small

$$\Delta = \frac{n_1 - n_0}{n_1} \quad (2-1)$$

$$\Delta \ll 1 \quad (2-2)$$

The propagation constant β for any guided mode must satisfy:

$$n_1 k \geq \beta \geq n_0 k \quad (2-3)$$

where k is the wave number:

$$k = \frac{2\pi}{\lambda} \quad (2-4)$$

with λ being the wavelength of the light in free space. (In the first part of this work $\lambda = .6328 \mu\text{m}$). Defining the parameters:

$$u = a(k n_1^2 - \beta^2)^{\frac{1}{2}} \quad (2-5)$$

$$w = a(\beta^2 - k n_0^2)^{\frac{1}{2}} \quad (2-6)$$

where a is the core radius, allows us to express the mode field expression by a Bessel function J in the core and a modified Hankel function K in the cladding.

With a third parameter, the normalised frequency v :

$$v = (u^2 + w^2)^{\frac{1}{2}} = a k (n_1^2 - n_0^2)^{\frac{1}{2}} \quad (2-7)$$

and after matching the field at the core/cladding interface taking into account the weak guidance, propagating modes can be constructed.

They are polarised linearly, are essentially transverse electromagnetic and are known as LP modes.

For a step index fibre the field is [41]

$$\text{in the core: } E_y = E_\ell \frac{J_\ell(ur/a)}{J_\ell(u)} \cos \ell \phi e^{j(\omega t - \beta z)} \quad (2-8)$$

$$\text{in the cladding: } E_y = E_\ell \frac{K_\ell(wr/a)}{K_\ell(w)} \cos \ell \phi e^{j(\omega t - \beta z)} \quad (2-9)$$

using cylindrical coordinates (r, ϕ, z) (fig. 2-3a) and with E_ℓ equal to the electric field at the interface.

$$\ell \in [0, \infty] \cap \mathbb{N}$$

ω is the radian frequency

The longitudinal components are given by [41]: in the core:

$$E_z = \frac{-jE_\ell}{2ka} \left(\frac{u}{n_1} \frac{J_{\ell+1}(ur/a)}{J_\ell(u)} \sin(\ell+1)\phi + \frac{u}{n_1} \frac{J_{\ell-1}(ur/a)}{J_\ell(u)} \sin(\ell-1)\phi \right) e^{j(\omega t - \beta z)} \quad (2-10)$$

$$H_z = \frac{-jE_\ell}{2kZ_0 a} \left(u \frac{J_{\ell+1}(ur/a)}{J_\ell(u)} \cos(\ell+1)\phi - u \frac{J_{\ell-1}(ur/a)}{J_\ell(u)} \cos(\ell-1)\phi \right) e^{j(\omega t - \beta z)} \quad (2-11)$$

in the cladding:

$$E_z = \frac{-jE_\ell}{2ka} \left(\frac{w}{n_0} \frac{K_{\ell+1}(wr/a)}{K_\ell(w)} \sin(\ell+1)\phi - \frac{w}{n_0} \frac{K_{\ell-1}(wr/a)}{K_\ell(w)} \sin(\ell-1)\phi \right) e^{j(\omega t - \beta z)} \quad (2-12)$$

$$H_z = \frac{-jE_\ell}{2kZ_0 a} \left(w \frac{K_{\ell+1}(wr/a)}{K_\ell(w)} \cos(\ell+1)\phi + w \frac{K_{\ell-1}(wr/a)}{K_\ell(w)} \cos(\ell-1)\phi \right) e^{j(\omega t - \beta z)} \quad (2-13)$$

Z_0 being the plane wave impedance: $Z_0 = \sqrt{\frac{\mu}{\epsilon}}$

When $\Delta \ll 1$ these can be neglected when compared to the transverse components so they will not be taken into consideration.

Matching the fields yields the characteristic equation for LP modes (41).

$$u \frac{J_{\ell-1}(u)}{J_\ell(u)} = -w \frac{K_{\ell-1}(w)}{K_\ell(w)} \quad (2-14)$$

At this stage, dealing with multimode fibres, it is necessary to find simpler expressions. In order to seek further simplifications several methods can be investigated:

i) The replacement of the Bessel and modified Hankel functions by approximations [42].

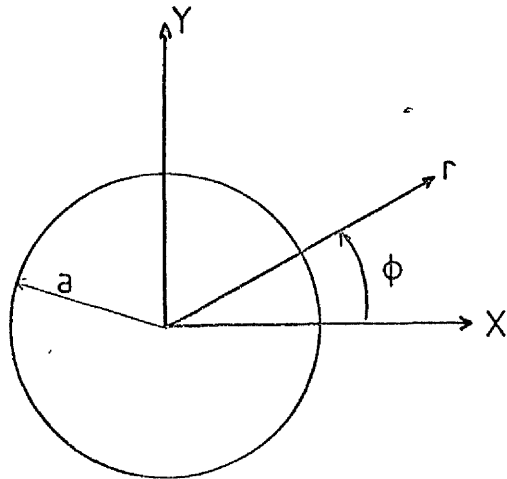


Fig.2.3.a

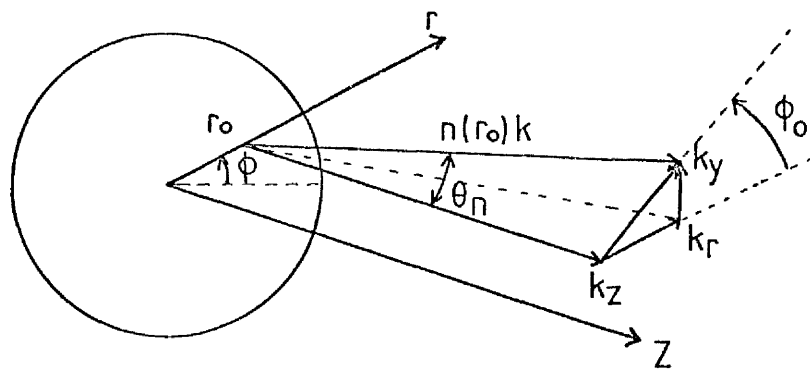


Fig.2.3.b

Fig.2.3 Wave Vector Components of Refracted Ray on Fibre Front Face

ii) The ray optics approach [43].

iii) The Wentzel Kramers Brillouin Jeffreys (WKBJ) technique of solving the wave equation.

The first method will be developed in the part of chapter dealing with the coupling.

The two last methods can be extended easily to graded index fibres and are valid for all the modes but the lowest order ones. The principles of the methods (ii) and (iii) are discussed below.

II-222 Ray analysis.

Assuming that fibres are ideal, the refractive index n depends only on r and thus the ray equation [40]:

$$\frac{d}{ds} n \frac{d\vec{r}}{ds} = \nabla n \quad (2-15)$$

can be written, in cylindrical coordinates:

$$\left. \begin{aligned} \frac{d}{dn} n_1 \frac{dr}{ds} - n_1 r \left(\frac{d\phi}{ds} \right)^2 &= \frac{dn_1}{dr} \\ n_1 \frac{dr}{ds} \frac{d\phi}{ds} + \frac{d}{ds} (n_1 r \frac{d\phi}{ds}) &= 0 \\ \frac{d}{ds} n_1 \frac{dz}{ds} &= 0 \end{aligned} \right\} (2-16)$$

where s is the geometrical path along the ray.

The incident ray can be described by its angle of incidence θ_o , the plane of incidence having the orientation $\phi = \phi_o$ and it impinges on the fibre at $z = 0$, $r = r_o$, $\phi = 0$ (fig. 2-36).

In the fibre the ray propagates with an initial angle θ_n given by Snell's Law:

$$n_1(r_o) \sin \theta_n = n_s \sin \theta_o \quad (2-17)$$

thus the wave number can be written

$$\left. \begin{aligned} k_r &= n_1(r_o) k \sin \theta_n \cos \phi_o \\ k_\phi &= n_1(r_o) k \sin \theta_n \sin \phi_o \\ k_z &= n_1(r_o) k \cos \theta_n \end{aligned} \right\} (2-18)$$

After some mathematical manipulations the general equations for the wave number are obtained:

$$k_r = [n^2 k^2 - n_1^2(r_0) k^2 \cos^2 \theta_n - n_1^2(r_0) k^2 \sin^2 \theta_n \sin^2 \phi_0 \frac{r_0^2}{r^2}]^{\frac{1}{2}}$$

$$k_\phi = \frac{r_0}{r} n_1(r_0) k \sin \theta_n \sin \phi_0 \quad (2-19)$$

$$k_z = n_1(r_0) k \cos \theta_n$$

The separation condition is verified:

$$k_r^2 + k_\phi^2 + k_z^2 = k^2 n_1^2 \quad (2-20)$$

It is possible to plot the projection of a ray path onto the fibre cross section, taking the case of $\phi_0 < \frac{\pi}{2}$ for example (fig. 2.4). As $\frac{dr}{dz} < 0$, the ray goes towards the centre of the fibre until $\frac{dr}{dz} = 0$. Then the ray goes towards the periphery until the next turning point and so on.

The turning points can be found by evaluating $\frac{dr}{dz}$ and finding its zeros [40].

$$\frac{dr}{dz} = n_1^2(r) k^2 - k_z^2 - k_\phi^2(r_0) \frac{r_0^2}{r^2} = 0 \quad (2-21)$$

By plotting $n_1^2 k^2 - k_z^2$ (square of the index profile) against $k_\phi^2(r_0) \frac{r_0^2}{r^2}$ we get the turning radius values (fig. 2-4).

It is obvious that the presence of turning points depends strongly upon the initial launching conditions, and for a given ϕ_0 , both r_0 and θ_n must be small enough to allow the occurrence of a turning point, the ray being then trapped in the fibre. This ray will form a mode only if it creates a standing wave in both transverse directions.

To fit around any circumference with an integer number ℓ of periods 2π , $k\phi$ must satisfy:

$$k_\phi r = \ell \quad (2-22)$$

which gives the initial values for the incident ray:

$$n(r_0) k r_0 \sin \theta_n \sin \phi_0 = \ell \quad (2-23)$$

Introducing the value of k_ϕ (2-22) in the value of k_r given by (2-19) and letting $k_z = \beta$ be the axial phase constant of the considered

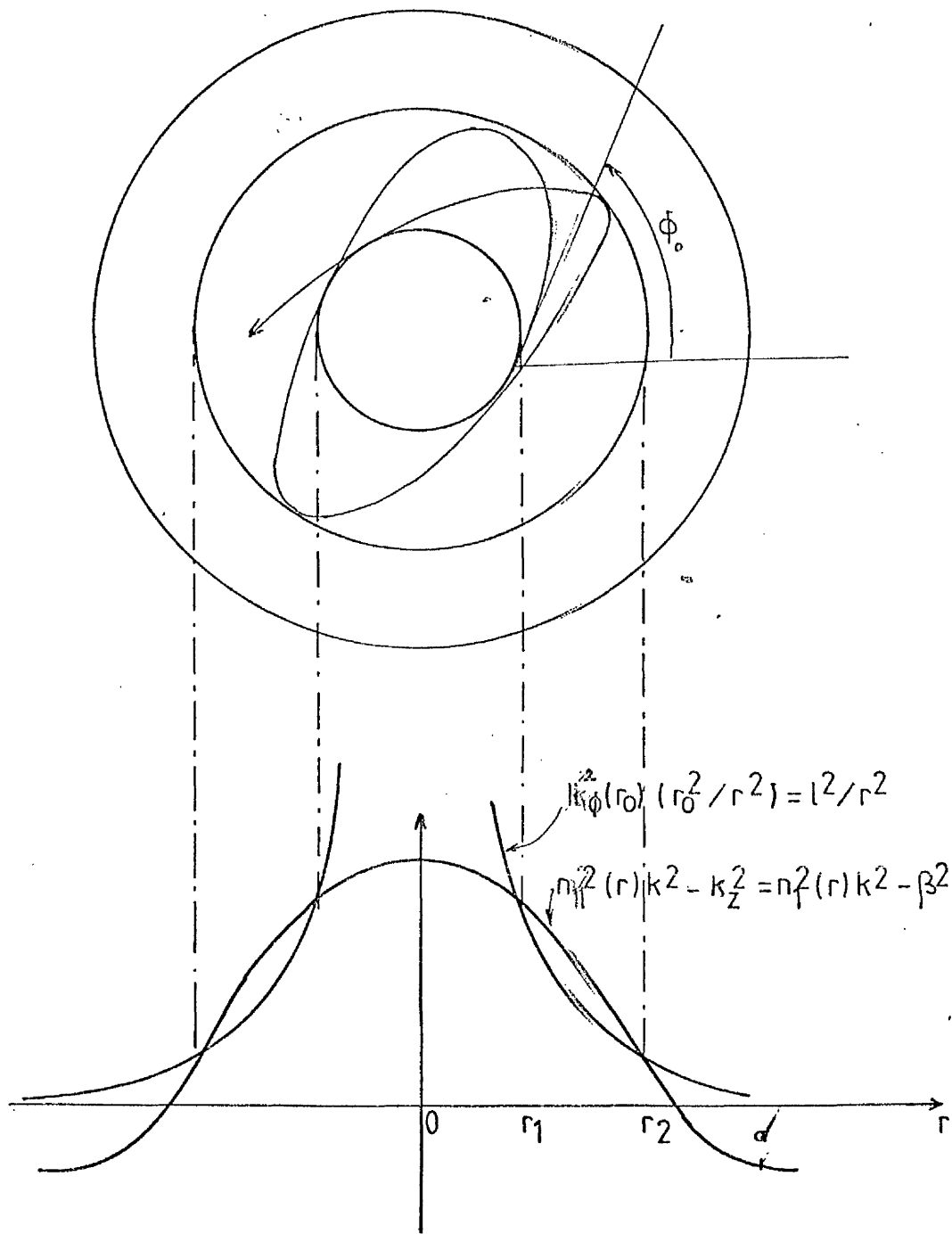


Fig.2.4. Cross-sectional Projection of a Ray in a Graded-index Fibre. (With Graphical Presentation of the Square of its Radial Wave Vector Component.)

mode yields:

$$k_r = (n_1^2(r) - \beta^2 - \ell^2/r^2)^{\frac{1}{2}} \quad (2-24)$$

The phase condition for a standing wave pattern in the radial direction with an integer number p of modes leads to the characteristic equation for modes of transverse order p and ℓ :

$$p\pi + \frac{\pi}{2} = \int_{r_1}^{r_2} (n_1^2(r)k^2 - \beta^2 - \frac{\ell^2}{r^2})^{\frac{1}{2}} dr \quad (2-25)$$

For large radial orders the phase shift at the caustic points $r_1, r_2, \frac{\pi}{2}$, can be neglected.

II-223 The WKBJ method. In cylindrical coordinates the wave equation becomes separable if n is a function of r only. The differential equation for the radial field dependence $E(r)$ can be then written [43]:

$$\frac{\partial^2 E}{\partial r^2} + \frac{1}{r} \frac{\partial E}{\partial r} + [k^2 n_1^2(r) - \beta^2 - \frac{\ell^2}{r^2}] E = 0 \quad (2.26)$$

Setting:

$$E = E_0 \exp [jkS(r)] \quad (2-27)$$

with $\frac{\partial E}{\partial r} = 0$ and replacing E by its approximation in 2-26 yields, with $S^1 = \frac{dS}{dr}$:

$$jkS^{11} + (jkS^1)^2 + jk \frac{S^1}{r} + (k^2 n_1^2 - \beta^2 - \frac{\ell^2}{r^2}) = 0 \quad (2-28)$$

Assuming that $n_1(r)$ varies slowly within a distance similar to the wavelength and expanding $S(r)$ in powers of λ (which thus converges rapidly):

$$S(r) = S_0 + \frac{1}{k} S_1 + \dots \quad (2-29)$$

After substitution of eq. (2.29) in eq. (2.28) and considering only the two first terms of the series we have for the two first terms of the expansion (2-29):

$$- (k S_0^1)^2 + k^2 n_1^2 - \frac{\ell^2}{r^2} = 0 \quad (2-30)$$

and

$$k S_0^{11} - S_2 k S_0^1 S_1^1 + jk S_0^1 / r = 0 \quad (2-31)$$

which give after integration:

$$S_0 = \pm \int^r (n_1^2(r) - \frac{\beta^2}{k^2} - \frac{\ell^2}{k^2 r^2})^{\frac{1}{2}} dr + Cste \quad (2-32)$$

$$S_1 = \frac{j}{4} L_n \left(r^2 n_1^2(r) - \frac{\beta^2 r^2}{k^2} - \frac{\ell^2}{k^2} \right) + C_{ste} \quad (2-33)$$

In order to obtain a complete solution, it is necessary to consider 3 regions in the guide. The tube where the actual propagation takes place (S_0 is real) and inside and outside the latter where S_0 is imaginary. The sign of (2-32) is chosen so that the field decays exponentially when r increases ($r > a$).

We then obtain:

$$r_1 < r < a \quad E_r = F_1 \left(\frac{2\pi}{r} \right)^{\frac{1}{2}} k_r^{-\frac{1}{2}} \cos \left[\int_{r_1}^r k_r(r^1) dr^1 \right] \quad (2-34)$$

$$r > a \quad = F_2 \left(\frac{\pi}{2r} \right)^{\frac{1}{2}} [(-k_r^2)^{\frac{1}{2}}]^{\frac{1}{2}} \exp \left[- \int_a^r (-k_r^2)^{\frac{1}{2}} dr^1 \right] \quad (2-35)$$

The constants F_1 and F_2 are chosen so that the solution fits with Debye approximations of the Bessel and modified Hankel functions.

For a multimode fibre we can assume that $F_2 = 0$, ignoring the evanescent field. In this case propagation occurs when:

$$\int_{r_1}^a k_r(r) dr = \left(p - \frac{1}{4} \right) \pi \quad (2-36)$$

and for high order modes the term $\frac{\pi}{4}$ can be omitted.

The same characteristic equation is thus obtained as in II-2.2.2.

II-23 The multimode fibre coupler Considering the advantages of multimode fibre link, a tap coupler is a very useful component. However the study of the coupling of thousands of modes is not an easy problem to solve. For this reason, here again, simplifying hypotheses are necessary.

Some authors [44],[45] considered the coupling between given mode pairs. Snyder [46] looked at the total power transition but Ogawa [47] give an even simpler solution for step index fibres whose cores are almost touching. Ogawa's theory applies quite well to the present problem since in the modified region the index profile is flattened - looking thus like a step index fibre - and the cladding is stripped so that the

cores are almost touching. We are thus going to consider Ogawa's approach to the problem.

II-2.3.1. The coupling coefficient

The expressions used here as a starting point are the ones derived by Snyder [44]. Considering the case depicted in fig. 2.5 of two almost identical fibres the coupling equations are:

$$d \frac{A(z)}{dz} + j \beta_A A(z) = - j B(z) C_{AB} \quad (2-37)$$

$$\text{and } d \frac{B(z)}{dz} + j \beta_B B(z) = - j A(z) C_{BA} \quad (2-38)$$

where A, B are the amplitudes of the modes.

The coupling coefficient is defined by:

$$C_{AB} = \frac{\omega}{2} \int_{\text{core B}} \epsilon_0 (n_1^2 - n_0^2) E_A E_B dS \quad (2-39)$$

where E_A , E_B are the normalised electric fields of fibres A, B and ϵ_0 is the vacuum value of the permittivity.

By is known (2-9) with E_ℓ given by (47):

$$\left. \begin{aligned} E_\ell &= \left(\frac{\mu}{\epsilon}\right)^{\frac{1}{4}} \left(\frac{2}{\pi n_1}\right)^{\frac{1}{2}} \frac{\mu K_\ell(\omega)}{a[\sqrt{K_{\ell-1}(\omega)} K_{\ell+1}(\omega)]} \quad \text{for } \ell \neq 0 \\ E_\ell &= \left(\frac{\mu}{\epsilon}\right)^{\frac{1}{4}} \left(\frac{1}{\pi n_1}\right)^{\frac{1}{2}} \frac{\mu K_0(\omega)}{av K_1(\omega)} \quad \text{for } \ell = 0 \end{aligned} \right\} (2-40)$$

where μ is the magnetic permeability.

These field expressions satisfy the eigenvalue equation (2-14).

The coupling coefficient between the mode p of fibre A and mode q of fibre B may be deduced, knowing the parameters of the two modes:

$$\begin{aligned} & \ell_1, \omega_1, q_1, r_1, \phi_1 \text{ and } \ell_2, \omega_2, q_2, r_2, \phi_2 \quad [47] \\ C_{ApBq} &= \frac{kn_1 a_2}{a_1} \frac{2\Delta u_1 u_2}{v_1 v_2} \left(w_2 K_{\ell_2+1}(w_2) I_{\ell_2+1}\left(w_1 \frac{a_2}{a_1}\right) + w_1 \frac{a_2}{a_1} K_{\ell_2}(w_2) I_{\ell_2+1}\left(w_1 \frac{a_2}{a_1}\right) \right) \\ & \times \frac{(-1)^{\ell_1 \ell_2} K_{\ell_1-\ell_2}\left(w_1 \frac{d}{a_1}\right) \cos(\ell_1-\ell_2)\alpha \pm (-1)^{\ell_1+\ell_2} K_{\ell_1+\ell_2}\left(w_1 \frac{d}{a_1}\right) \cos(\ell_1+\ell_2)\alpha}{\left[\frac{2}{u_2} + \left(w_1 \frac{a_2}{a_1}\right)^2 \left(K_{\ell_1-1}(w_1) K_{\ell_1+1}(w_1) K_{\ell_2+1}(w_2) K_{\ell_2-1}(w_2) \right)^{\frac{1}{2}} \right]} \quad (2-41) \end{aligned}$$

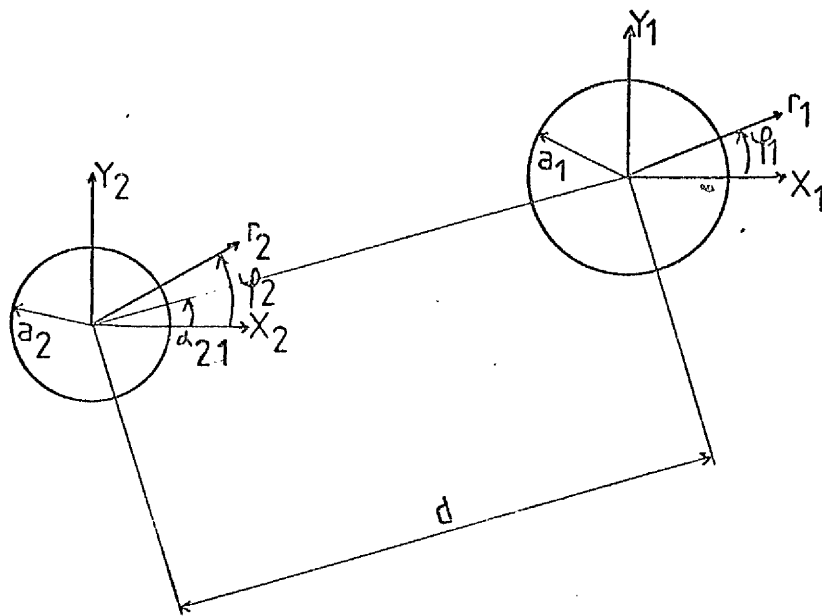


Fig.2.5 Geometry of the Coupling Set-up

Equation 2.41 leads to the general coupling equation involving all the modes carried by the two fibres.

$$\frac{d A_p(z)}{dz} + j\beta_{A_p} A_p(z) = -j \sum_{q=1}^N B_q(z) C_{A_p B_q} \quad (2-42)$$

$$\frac{d B_q(z)}{dz} + j\beta_{B_q} B_q(z) = -j \sum_{p=1}^N A_p(z) C_{B_q A_p}$$

with the coupling coefficient defined by 2-41 and where β_{A_p} and β_{B_q} are the z-direction propagation constants of the p^{th} and q^{th} modes in the fibres A and B respectively. ℓ_1 and ℓ_2 are the aximuthal order numbers of the modes in fibres A and B. Δ_1 and Δ_2 are the normalised index differences of fibres A and B.

The coupling coefficient can be written, with

$$\gamma_1 = \gamma_2 = 0 \quad \text{when} \quad \ell_1 = \ell_2 = 0$$

$$\gamma_1 = \gamma_2 = 1 \quad \text{when} \quad \ell_1 > 0 \quad \ell_2 > 0$$

$$|C_{A_p B_q}| = \frac{\delta_1 \delta_2}{2} \frac{\sqrt{2\Delta_1}}{a_1 v_1} u_1 u_2 \times$$

$$\left| \frac{K_{\ell_1 - \ell_2} (w_1 d/a_1) \cos (\ell_1 - \ell_2)\alpha \pm K_{\ell_1 + \ell_2} (w_1 d/a_1) \cos (\ell_1 + \ell_2)\alpha}{u_2^2 + w_1^2 \left(\frac{a_2}{a_1}\right)^2} \right|$$

$$\times \frac{(w_2) K_{\ell_2+1} (w_2) I_{\ell_2} (w_1 a_2/a_1) + w_1 a_2/a_1 K_{\ell_2} (w_1) I_{\ell_2+1} (w_1 a_2/a_1)}{[K_{\ell_1-1} (w_1) K_{\ell_1+1} (w_1) K_{\ell_2-1} (w_2) K_{\ell_2+1} (w_2)]^{1/2}} \quad (2-43)$$

II-2.3.2 Simplified coupling coefficient

The expression for the coupling coefficient may be further simplified by assuming that:

- the two fibres are absolutely similar
- only modes with the same propagation constants are coupled.
- The distance between two fibres is very close to $2a$.

The average coupling coefficient can be written, using the asymptotic expansion of the modified Bessel functions and assuming

that $\gamma = 1$ for all the modes (47):

$$|C_{A_1 B_1}| = \frac{\sqrt{2\Delta}}{a} \frac{u^2}{v^3} \frac{\sqrt{2w}}{\sqrt{\pi d/a}} e^{-w(d/a-2)} \quad (2-44)$$

$d/a \approx 2$.

This expression can still be simplified a little more by replacing u , v , w by simpler expressions. We assume that in the modified portion the fibre has a step index, thus according to Hunger [40]

$$v^2 = 2N \quad (2-45)$$

where N is the total number of modes. As before the modified region fibre is of graded index form, and assuming that N does not change significantly in this area, we have [40]:

$$N = \frac{k^2 a^2 (n_1^2 - n_0^2)}{4} \quad (2-46)$$

The cut-off value for the i^{th} mode is approximately:

$$u_{co} = (2i)^{\frac{1}{2}} \quad (2-47)$$

It is assumed that u can be replaced by u_{co}

$$u \approx u_{co} \quad (2-48)$$

which yields the simplified coupling coefficient:

$$|C_{A_1 B_1}| = \frac{2 \Delta^{\frac{1}{4}}}{\sqrt{\pi n_1 k a^3}} \frac{e^{(2-d/a)(2N-2i)^{\frac{1}{2}}}}{\sqrt{d/a}} \left(\frac{i}{N}\right) \left(1 - \frac{i}{N}\right)^{\frac{1}{4}} \quad (2-49)$$

Equation (2-49) simplifies even more if $d = 2a$:

$$|C_{A_1 B_1}| = \frac{\sqrt{2} \Delta^{\frac{1}{4}}}{\sqrt{\pi n_1 k a^3}} \left(\frac{i}{N}\right) \left(1 - \frac{i}{N}\right)^{\frac{1}{4}} \quad (2-50)$$

Fig. 2.6 shows a few curves where the coupling coefficient (in cm^{-1}) is plotted against the mode order i/N . The graph quite clearly shows the dramatic diminution of the coupling coefficient as the distance between the fibres increases.

II-233 Coupling efficiency. The power transfer from the fibre A (p^{th} mode) to the fibre B (q^{th} mode), when $A_p(z=0) = 1$ and $B_q(z=0) = 0$, is given by [47]:

$$|A_p(z)|^2 = 1 - K_{AB} \sin^2 \beta_{AB} z \quad (2-51)$$

$$|B_q(z)|^2 = K_{BA} \sin^2 \beta_{AB} z$$

COUPLING COEFFICIENT IN CM⁻¹

X10⁻¹

SELFOC FIBRES N1=1.542

DELTA N=0.02 A=30 μm

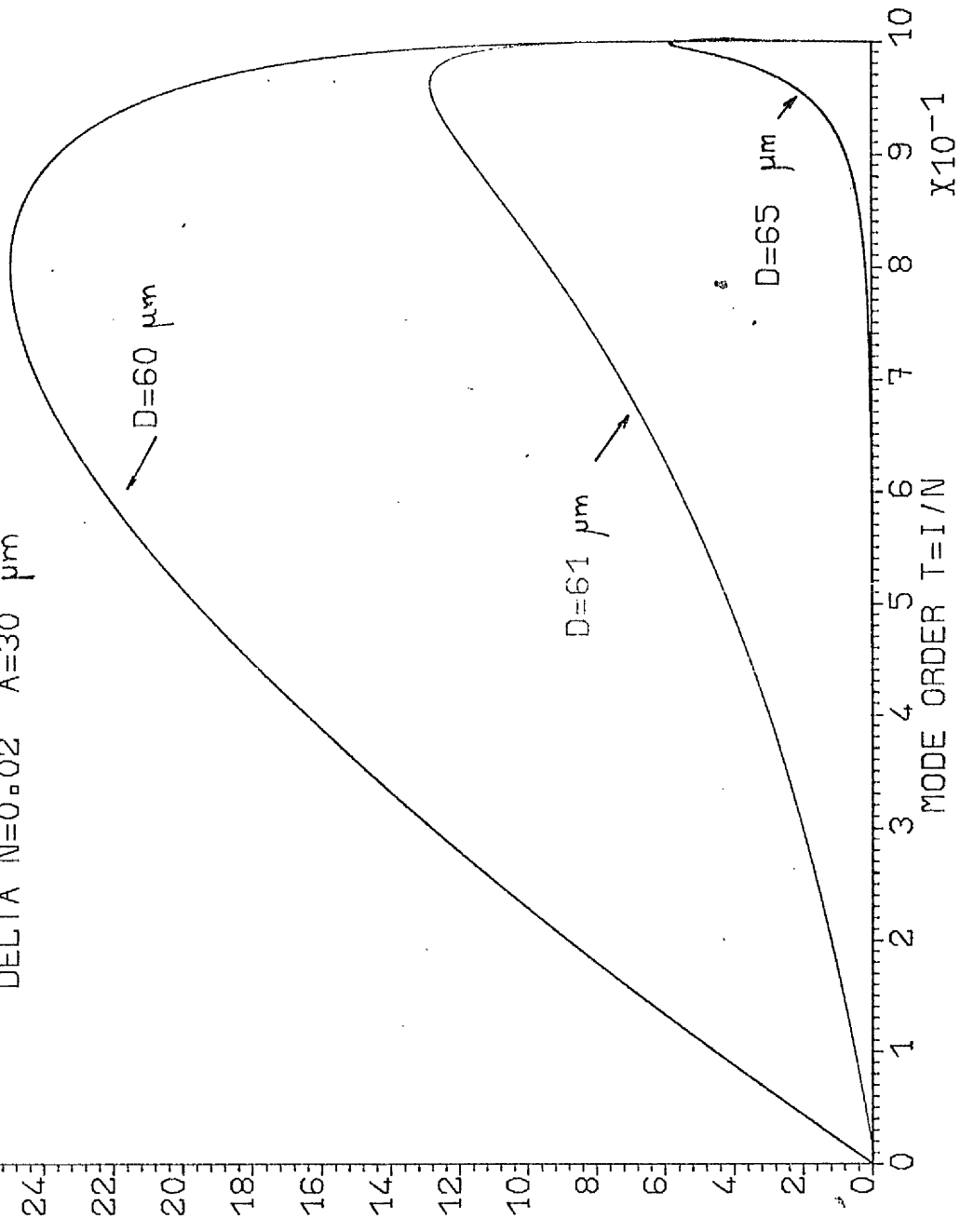


FIG:2.6: COUPLING COEFFICIENT VS MODE ORDER

where

$$K_{AB} = \left[1 + \frac{(\beta_{Ap} - \beta_{Bq})^2}{4|C_{ApBq} C_{BqAp}|} \right]^{-1} \quad (2-52)$$

$$K_{BA} = \frac{C_{BqAp}}{C_{ApBq}} K_{AB} \quad (2-53)$$

$$\beta_{AB} = \frac{|C_{ApBq}| |C_{BqAp}|}{K_{AB}} \quad (2-54)$$

and z is the coupling length.

The coupled power between the i^{th} mode of fibre A to the i^{th} of fibre B is then:

$$P_{AB}^i = \sin^2 (| \overline{C_{AiBi}} | z) \quad (2-55)$$

The total coupled power, if all the modes carry the same power in the fibre A, is

$$\eta = \frac{P_{AB}}{P_{\text{init.}}} \leq \frac{1}{N} \sum_{i=1}^N \sin^2 (| \overline{C_{AiBi}} | z) \quad (2-56)$$

There is an upper boundary since the coupling coefficient for some modes is almost zero.

With the high number of modes it is possible to assume that i is a continuous variable and thus we can write:

$$\eta = \frac{1}{N} \int_0^N \sin^2 (| \overline{C_{AiBi}} | z) di \quad (2-57)$$

Theoretical curves are plotted for three values of d/a in Fig. 2-7.

II-2.4 Conclusion. Theoretical curves were used to estimate the necessary fibre coupling length in order to design the coupling device. It is clearly visible from the graphs that the two fibres need to be very close to each other but, due to the irregularities in the fibre cross sections, and because the cores cannot be in physical contact, the average distance between the two axes was estimated to be $61 \mu\text{m}$ instead of the ideal of $60 \mu\text{m}$. The curves show also that if this separation is fairly large ($65 \mu\text{m}$) the coupling efficiency falls dramatically.

COUPLING EFFICIENCY

$\times 10^{-1}$

SELFOC FIBRES $N_1=1.542$ $N_0=1.511$ $A=30 \mu\text{m}$

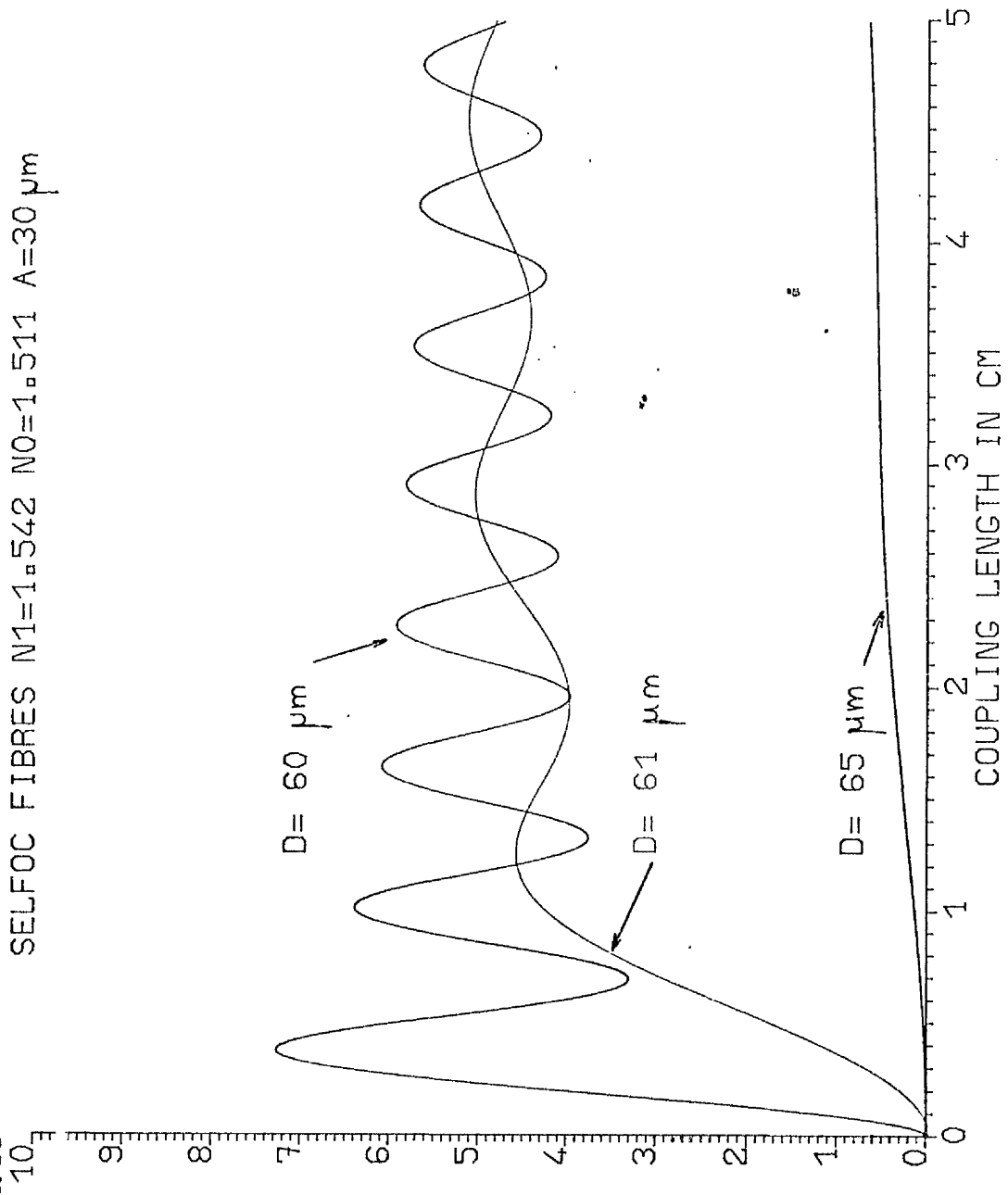


FIG:2.7: COUPLING COEFFICIENT VS COUPLING LENGTH

As the aim of the coupler is only to tap a small amount of the power, the coupling length chosen was taken just after the first minimum of the curve (as the modifying process induces two tapered regions) giving $L = 2.2$ cm, for the case where the two waveguides are separated by a gap of $1 \mu\text{m}$.

It must be emphasised that this theory is very simplified and implies some rather drastic approximations. However it explains the coupling phenomenon very clearly and gives very useful information for the dimensioning of the coupler.

It must be also stressed that, due to the simplifications, the theory overestimates the efficiency somewhat [47].

Finally it must be noted that, according to fig. 2.6, the exchange of power takes place essentially with the modes whose order is around 0.8. This means that the very low order modes will not be coupled and the very high order ones neither.

This can prove to be a very big disadvantage since the only part of the signal which will be tapped efficiently will be the one contained in the modes whose orders are ranging from .7 to 1 in the case where there is a gap of $1 \mu\text{m}$.

CHAPTER III

Fabrication and Measurements of Graded

Index Fibres.

II-3.1 Fabrication process of the fibres

At the beginning of this work Selfoc fibres were not available so it was necessary to manufacture graded index fibres. For this purpose several methods were investigated, chosen among the various types of process which had already been tried ([5] - [9], [52] - [54]), and the two methods tried which proved to be successful are discussed below.

II-3.1.1 Production of the raw fibre

a) the preform: The raw material consisted in rods of soda-lime glass whose diameters ranged from 4mm to 8mm.

Though the composition of the glass was not accurately known an estimation of it is given in II-1.1.5 for one type, for another it is as follows:

SiO ₂	67%
Na ₂ O	15.6%
CaO	.6%
BaO	2.0%
MgO	4.0%
Al ₂ O ₃	2.8%
B ₂ O ₃	1.5%

The physical properties of the latter type are as follows:

Strain point	:	472°C
Anneal point	:	512°C
Softening point:		696°C

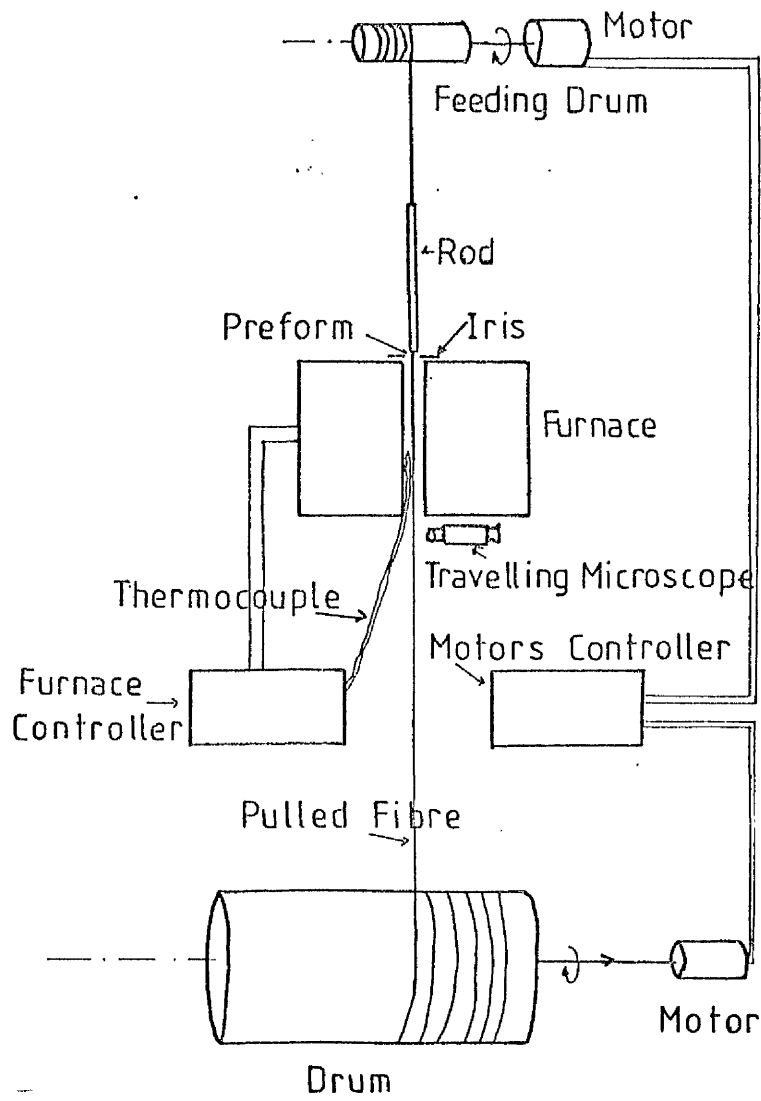
Refractive index at 633nm: 1.512

It can be seen that these compositions are not exactly ideal (II-1.1.5) especially with regard to the proportions of Al₂O₃ and CaO.

b) Fibre pulling: As the preforms are cylindrical it is very easy to pull from them cylindrical uncladded fibres. Fig. 3-1a shows a schematic diagram of the pulling machine used and fig. 3-2 shows the actual rig. The preform is thoroughly cleaned [37] with detergent and water in an ultra sonic cleaner, then rinsed with water, the remaining detergent being washed away with acetone before drying under a jet of pressurised nitrogen. The substrate is then clamped to the holder shown on fig. 3-16 which is held in a furnace whose temperature is accurately controlled at 800°C. Under the combined action of heat and weight, the preform increases its length slowly. When long enough the lower part of it is fixed to the take-up drum and the pulling begins. In order to have a fibre of constant cross section, a feed mechanism allows the preform to sink slowly into the furnace so that the quantity of heated glass remains as constant as possible. At the other end, the pulled fibre is wound on the take-up drum which provides the drawing force and stores the fibre neatly.

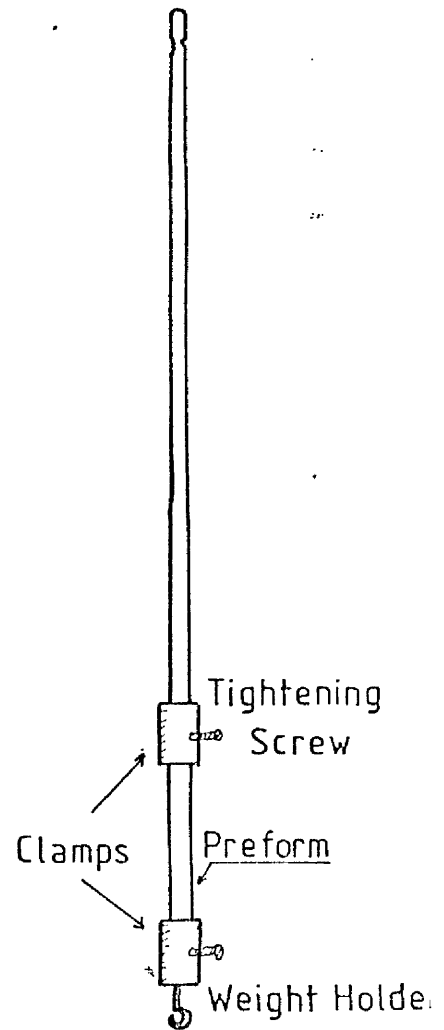
The temperature of the furnace being accurately controlled, the diameter of the substrate - checked with the travelling microscope - is governed by the ratio between the rate of introduction of the preform in the furnace and the rate of rotation of the take-up drum for a given diameter of the preform. With this device, long fibres (300m and over) were pulled with diameters varying between 25 μm and 600 μm .

c) Checking the fibres. Once pulled the fibres were checked and measured accurately. For this purpose a microscope, fitted with a calibrated graticule was used. It allowed a check on the regularity of the diameter, for possible faults and made the accurate measuring of the diameter easy. It was then feasible to select suitable lengths of substrate for manufacturing graded index fibres. Fig. 3-3 shows a typical fibre viewed through the microscope (magnification X20). The fibre diameter is 80 μm .



a) The Machine

Fig3.1 The Pulling Machine.



b) The Rod

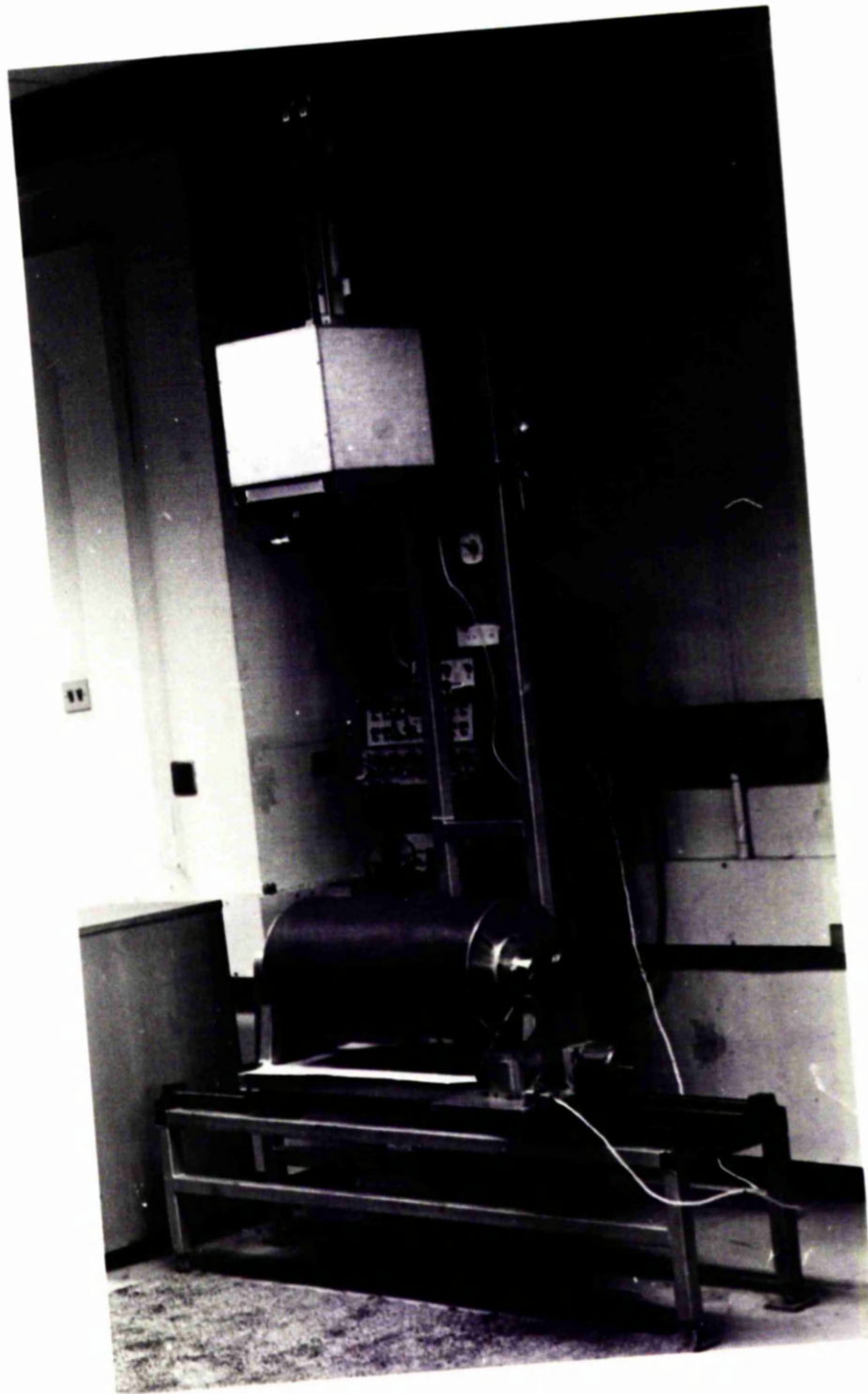


Figure 3.2: PHOTOGRAPH OF THE PULLING MACHINE.

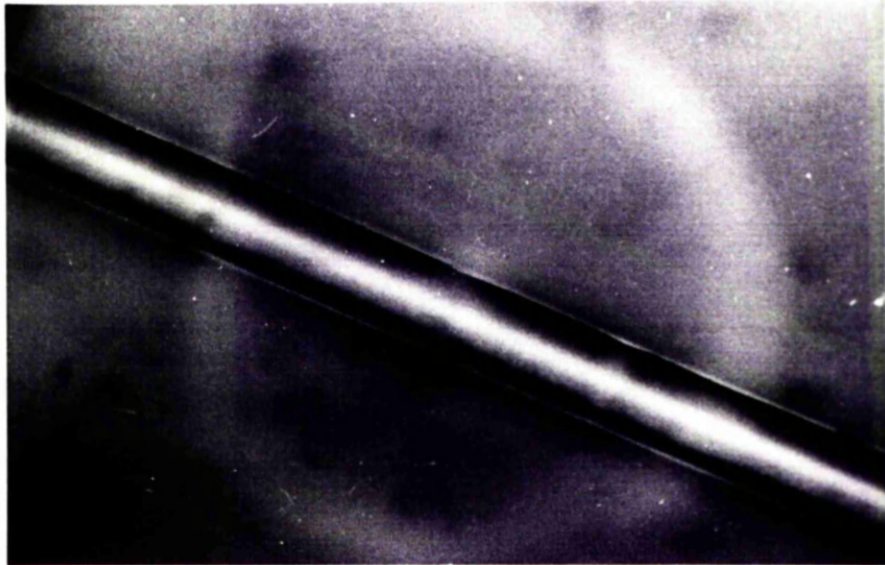


Figure 3.3: FIBRE END VIEWED THROUGH A MICROSCOPE.
(X20:  :100 micron)

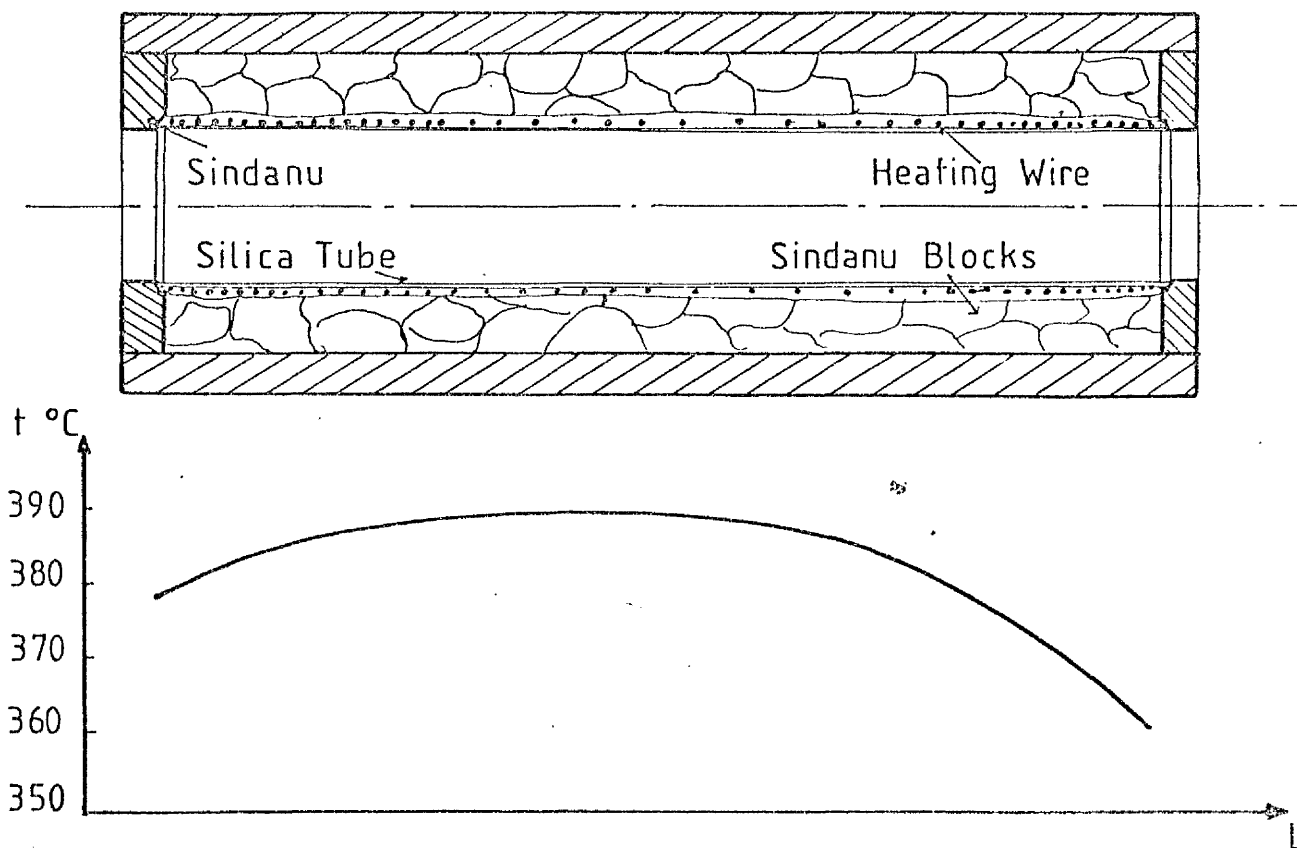
II-3.1.2. Production of graded index fibres by the two melt method.

A two melt system was used. The first one was a dilute melt consisting of 0.3g silver nitrate and 88g sodium nitrate. The fibre was immersed in it for several hours (the diffusion time depends on the fibre diameter) which is long enough for the silver ions to saturate the silica network. The second bath was a melt of pure sodium nitrate and the treated fibre is dipped in it until the ionic concentration in the periphery returns to its former value.

a) The furnace design. The furnace was made up with a quartz tube (low expansion coefficient) around which a resistance wire was wound, in such a way that the temperature profile along the furnace was as flat as possible. The furnace was controlled around a set point with a precision of $\pm 1.5^{\circ}\text{C}$. This was not too good ([49], [50]) but did not significantly affect the repeatability since the diffusion times were quite long and the average temperature had, in the long term, a precision of less than 0.1°C .

The containers, or boats, for the melt were as depicted in fig. 3.4-c. Quartz would have been an ideal material to make the boats from because it is unaffected by either of the melts but, during cooling, the melts induced stresses which tended to break the quartz. It was thus decided to make the boats in stainless steel. It was not very good since reactions took place at the stainless steel/melt interface and a more suitable material will have to be found. The containers were fitted with a hollow tube in the bottom to take the thermocouples and the ends of the boats were shaped to support the rods which held the fibres (fig. 3-4c). These rods were fitted with clamps for this purpose, but, as the clamping action tended to smash the fibres, they were abandoned and the fibres just placed in the melt. Two boats were made - one for each type of melt - so that there was not cross-contamination of the melts.

a) The Furnace



b) Temperature Profile

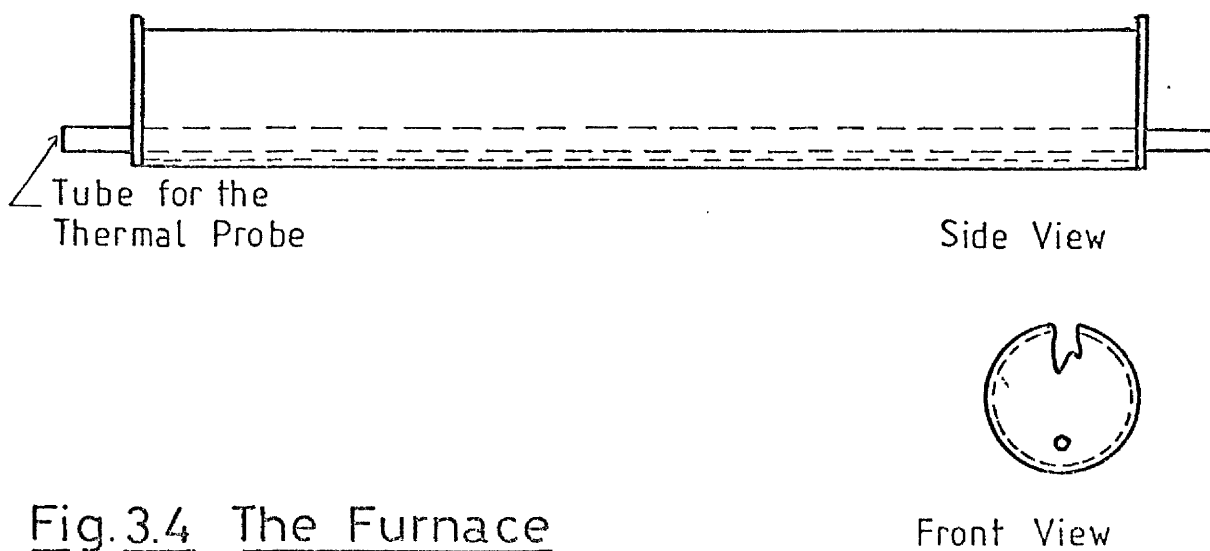


Fig.3.4 The Furnace

b) The melts Two melts are used and the method was derived from the one described by Giallorenzi et al. [51]. Following Stewart [20], dilute melts were used for the following reasons:

- i) if a fibre is dipped in a pure silver nitrate melt, it is liable to split (through a diameter) due to the stresses induced during the diffusion,
- ii) the index change is smaller,
- iii) the repeatability is improved,
- iv) there is less tendency for reduction of silver ions since Ag^+ concentration is lower,
- v) the cost of the melt is reduced.

The only disadvantage is the elevation of the processing temperature (silver nitrate melts at 207°C and the very dilute melt at 308°C), since high temperatures makes the reduction of silver more probable. Different degrees of dilution were tried, going from a mole ratio of 1.76×10^{-3} to a mole ratio of 2.24×10^{-3} .

To achieve melting of the mixture throughout the length of the bath, a temperature of over 350°C was necessary at the centre of the furnace. At first, the set point was 390°C as it was the highest possible (over 395°C decomposition occurs in the melt) giving the shortest diffusion time possible.

It worked very well for the first batch of fibres but, with a second batch, even at 370°C , reactions took place (reduction of silver), and the fibres were deeply stained. The reasons for this change lay in the contamination of the boats due to the reaction between the silver nitrate and the walls of the container.

c) Results. Several graded index fibres were made with this process and proved to be satisfactory. The diameter of these varied between $23.5 \mu\text{m}$ and $445 \mu\text{m}$. Required diffusion times were estimated with the help of a

computer program (II-1.2.2).

After exchange, the graded index fibres were again checked with the microscope in order to find out any irregularities that had developed. It was found that inhomogeneities were frequent when clamps were used to hold the fibres in the bath and that these points were always very weak.

d) Conclusion. Even if fibres were obtained satisfactorily with this process, it had several disadvantages as follows:

- i) The furnace temperature profile along its length is not flat enough (due to heat losses at each end).
- ii) Due to the dimensions of the boats, it was not possible to make long lengths of fibre.

Considering these two facts, several other methods were investigated and one was found interesting though delicate.

II-3.1.3. The repulling method.

The method used to manufacture the Selfoc fibres was employed [52]. First a rather large fibre (more than $250\ \mu\text{m}$) was completely diffused with silver ions from a dilute melt so that the refractive index was uniformly raised throughout. It was then placed in a soda-lime capillary tube (bore $500\ \mu\text{m}$) and both of them were pulled together. During the pulling, because of the high temperature involved, the silver ions tended to migrate in the capillary tube, depleting the periphery of the core (fig. 3-5). In this way a graded concentration profile - and thus a graded index profile - was created in the core of the fibre.

When the staining of the core could be avoided, this method was successful and had the following advantages over the previous method:

- i) very long fibres could be made,
- ii) the manufacturing time of a fibre is shorter,
- iii) The core could be very small allowing the fabrication of fibres carrying only a few modes,

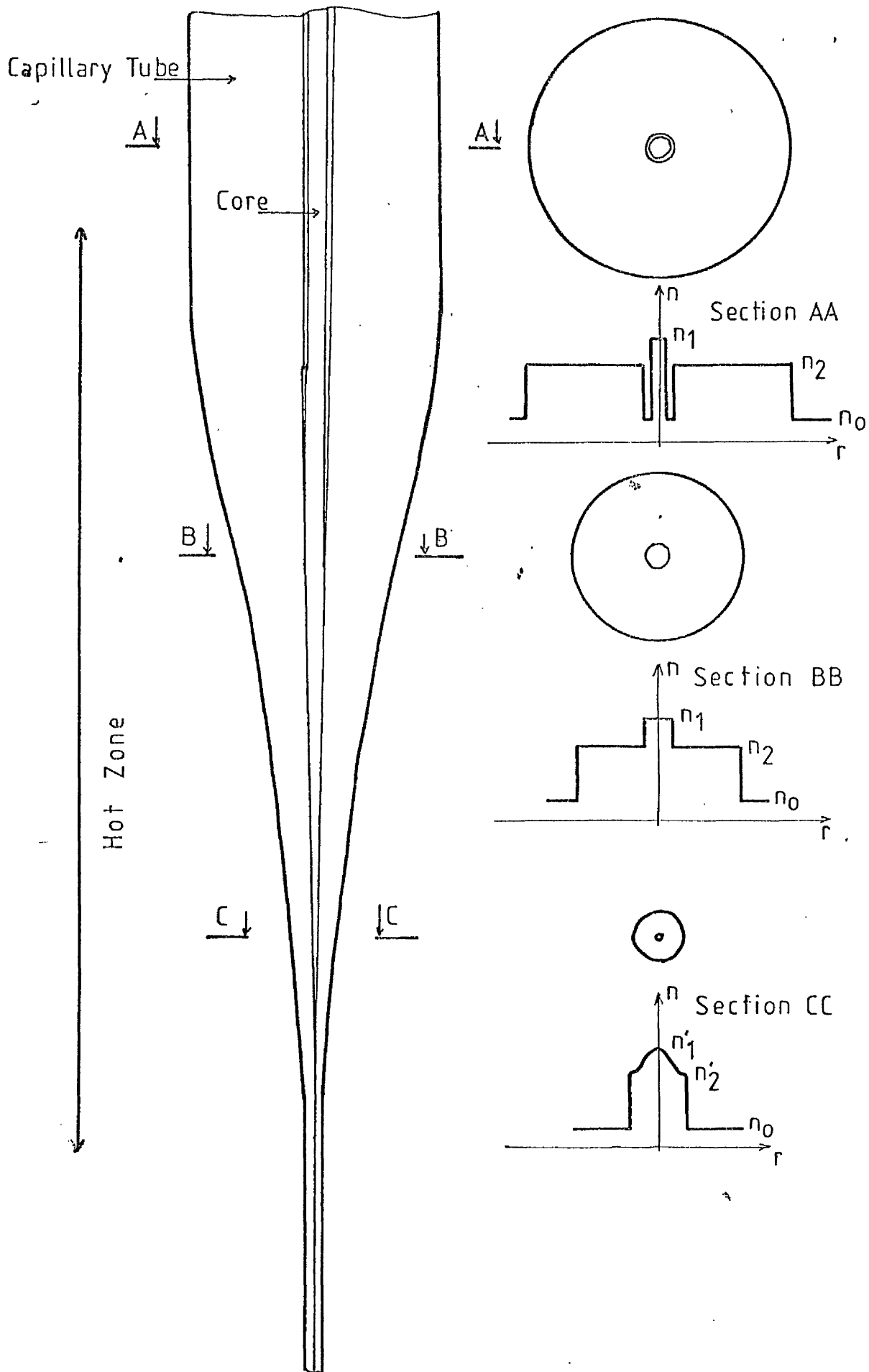


Fig.3.5 Pulling of a Capillary Tube

iv) The fibres were stronger.

Though this method has not been thoroughly developed it gave fairly good results (fig. 3-10, 3-11). However the dimensions of the cladding makes the local modification of the index very time-consuming and the flattened index profile would have a very low value due to the large silver ion depletion.

So, in spite of the advantages presented by this method, it was not frequently used. By the time the method had been developed, Selfoc fibres had become available and were used instead.

III-3.1.4. Selfoc fibres

a) Fabrication process. The Selfoc fibres are made using an ion-exchange process to produce a parabolic - shaped graded index. The first fibres were made by placing a rod containing Tl^+ in a bath of KNO_3 at $500^\circ C$ before pulling them into a fibre. Another method was then developed [52] in which the process was continuous and the ion exchange occurred during the pulling process itself. Selfoc fibres are now made [3], using sodium borosilicate glass, the core being doped with TlO_2 melted in a double crucible (fig. 3-6) so that both the core and the cladding flow together while the sodium and thallium ions are exchanged at the interface, thus achieving a graded index profile.

b) Properties of the fibres. The fibres made with such a process have losses as low as 5 dB/Km at $0.830 \mu m$ with a parabolic index distribution which minimises pulse dispersion.

For this study Selfoc fibres of type GI 60 were used. They have the following characteristics [55], fig. (3-7):

core diameter: $2a = 60 \pm 3 \mu m$
core index: $n_1 = 1.542$
cladding diameter (external): $2b = 150 \pm 3 \mu m$
lossy jacket external diameter: $2c = 0.9 \pm 0.05 mm$

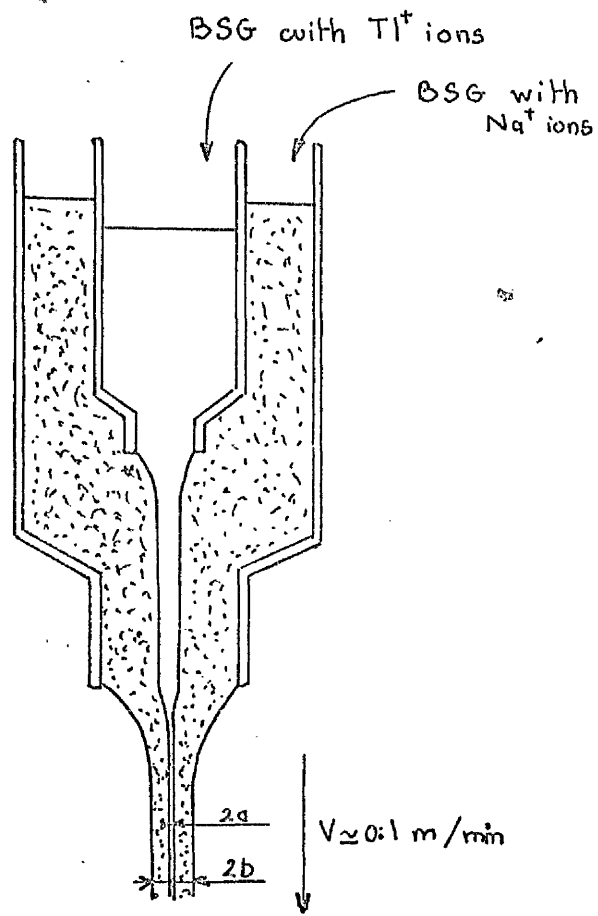
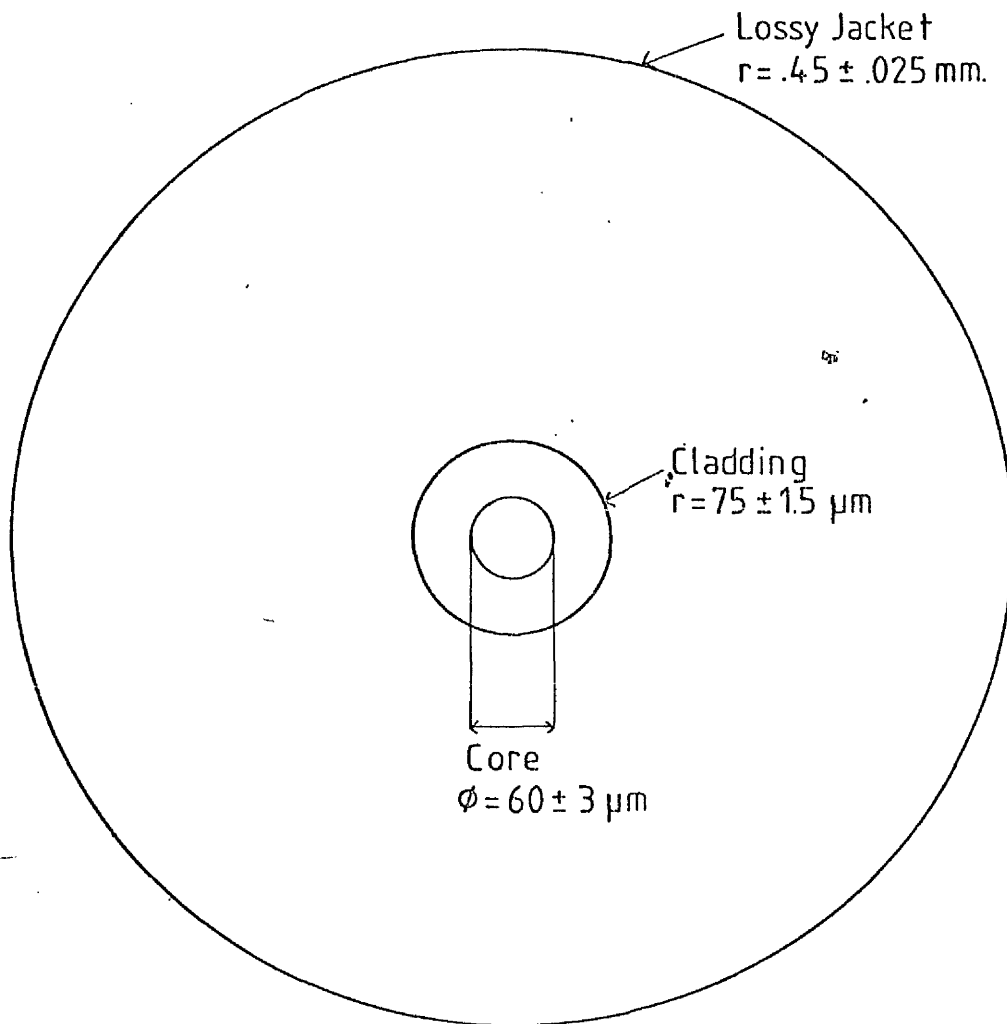


Fig.3.6 The Double Crucible Method



NA = .16

$N_1 = 1.542$

$N_0 = 1.511$

$\Delta n = .02$

$N = 2033 \text{ modes}$

Fig.3.7 Selfoc Fibre GI60

normalised index difference: $\Delta = 0.02$

numerical aperture: NA = 0.16

Fig. 3-8 depicts the baseband frequency response and spectral losses of the fibres as given in ref. [55].

II-3.2 Study of the index profile.

The aim of this work being to produce graded index fibres and to locally modify their index, it was necessary to know the index variation in the radial and axial directions. For this purpose several methods of measurements were investigated.

II-3.2.1. Indirect methods of measurements.

The refractive index profile of a given fibre may be determined indirectly by studying the mode propagation characteristics.

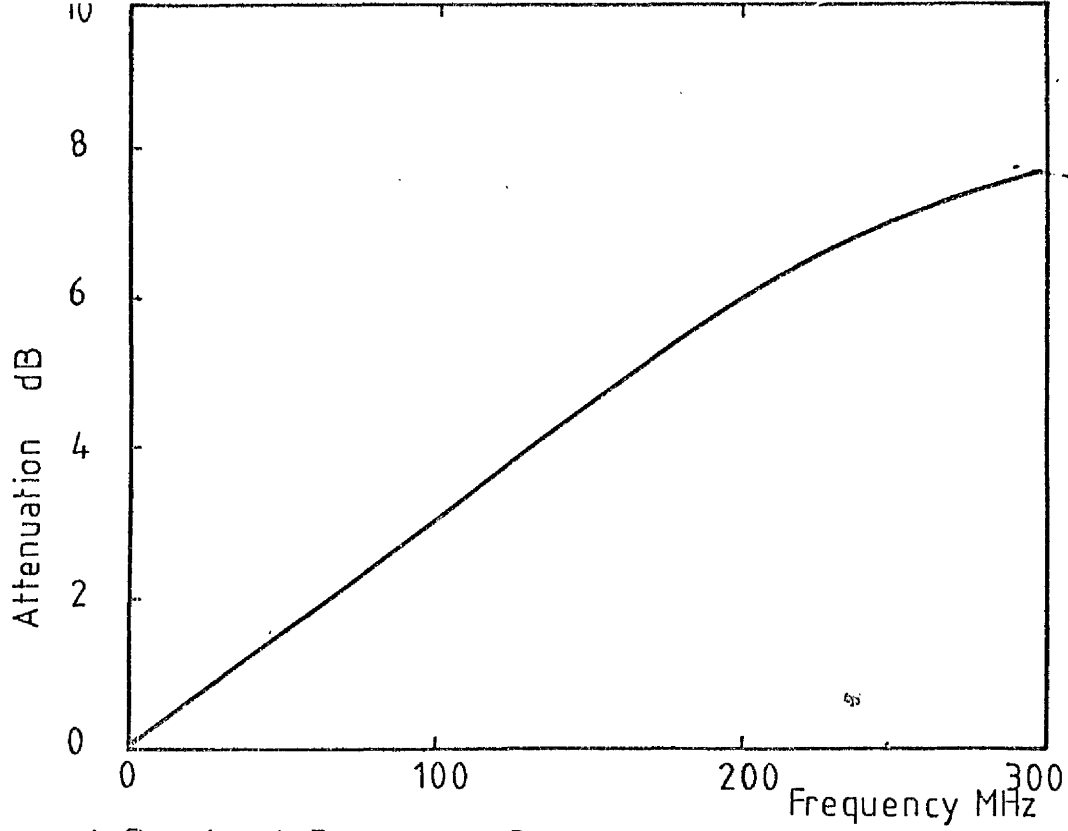
a) "Potting" fibres. The fibres made were very fragile so it was necessary to find a way to hold them during the measurements. For this they were potted in epoxy resin (fig. 3-9). This "substrate" was blackened with carbon powder. It was then easy to hold the fibre and to launch light in it. The end faces were lightly polished and equipped with a cover slide and a drop of index matching fluid.

In the resin, the fibre was either parallel to the axis of the cylinder (fig. 3-9a) or tilted so that one end touches the wall of the cylinder (fig. 3-9b). It was then possible to polish the fibre into a taper allowing coupling to a thin film or anything else.

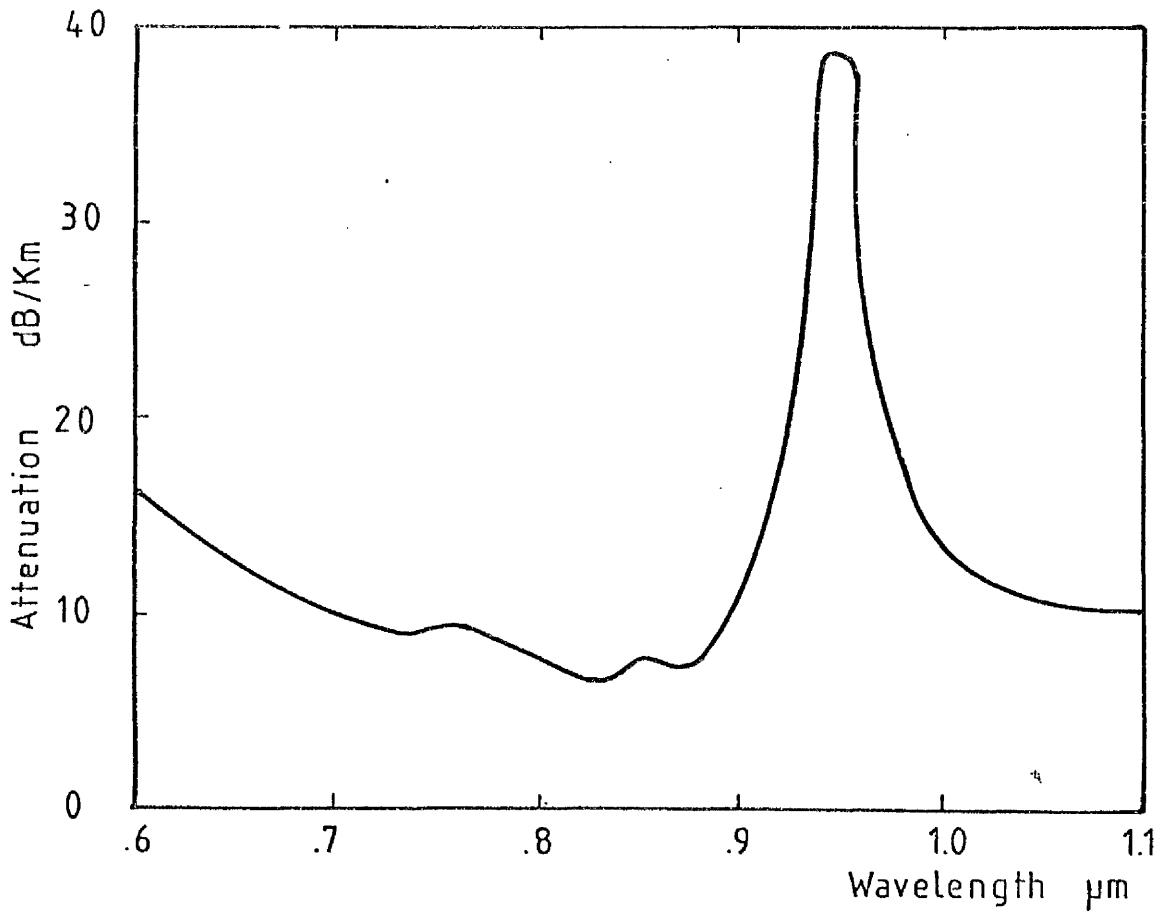
Though handy this method was abandoned because:

- i) It can be very cumbersome to launch light in such a medium.
- ii) Only very small lengths (5 cm) could be made.
- iii) It was impossible to reuse, modify or retest the potted fibre by some other method.

b) End fire launching Dakin et al [56] suggest a method for launching light in glass fibres. Following this idea, two cells (fig. 3-12a) were made, one for each end of the fibre, and were fitted with an index



a) Baseband Frequency Response



b) Spectral Losses

Fig. 3.8 Characteristics of the GI60 Selfoc Fibre

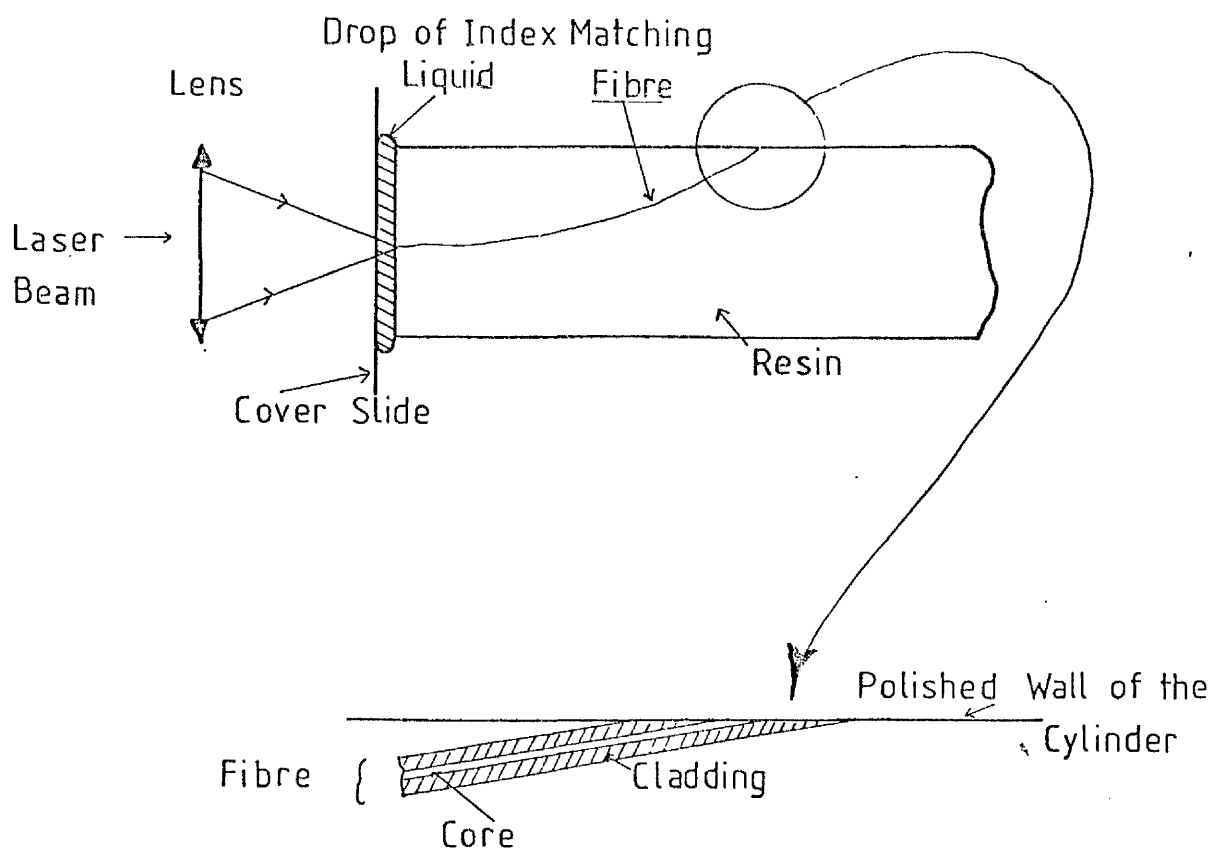
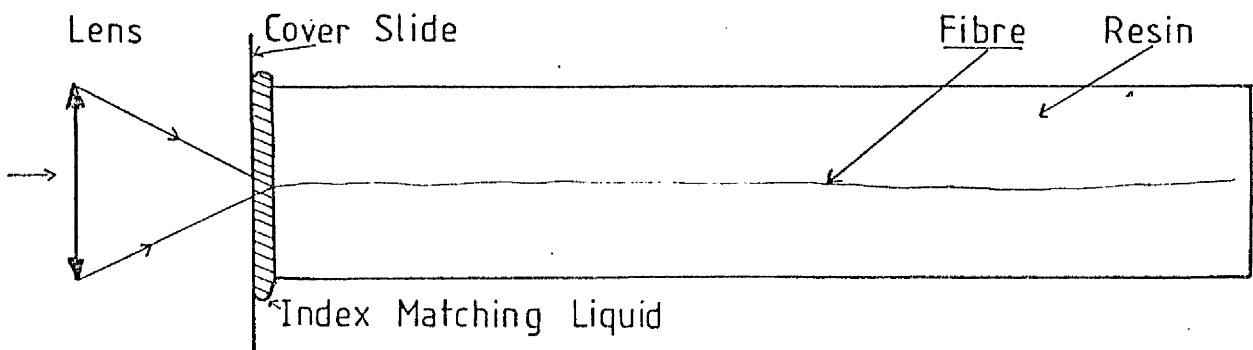


Fig. 3.9. Potted Fibres.

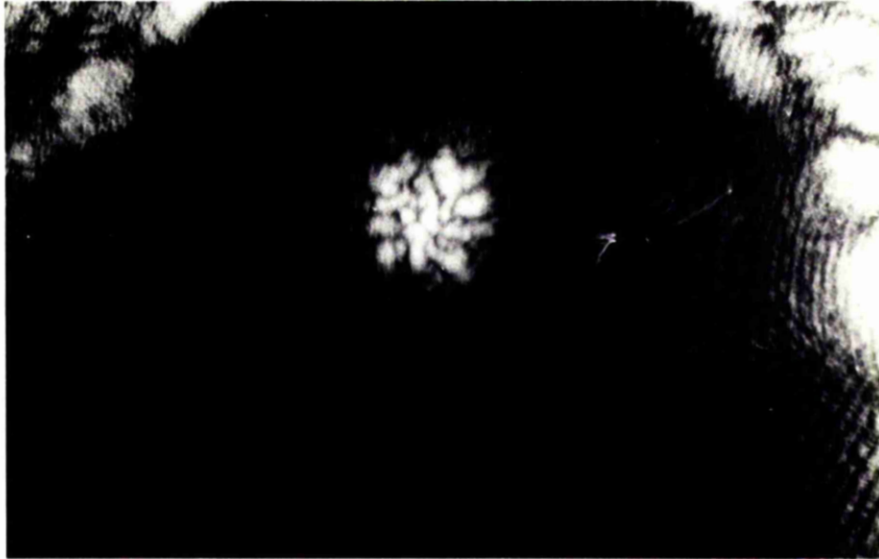


Figure 3.10: PULLED CAPILLARY TUBE: NEARFIELD
PATTERN. (X600)

matching liquid (methyl salicylate, $n = 1.538$). The apparatus is shown in fig. 3-12. Light from a helium - neon laser (5 mW, $\lambda = 632.8$ nm) was focussed on the end of the fibre with a microscope objective ($\times 20$). At the other end of the fibre, a travelling microscope enabled the near-field pattern to be observed (fig. 3-10), while the far-field pattern could be viewed using a ground glass screen (fig. 3-11). A photo-diode, with a chopper, was used to measure field intensities. The launching cell was mounted on a goniometer, allowing high and low order modes to be launched (fig. 3-12).

High order modes tend to travel near the periphery of the waveguide (fig. 2.2b) and, as the study of low order modes is more useful, a mode stripper was fitted along the fibre (fig. 3-12b). It consisted of a cell filled with an index matching liquid of high refractive index (e.g. quinoline or α -monobromo naphthalene) which "caught" the high order modes and left the low order ones, near the centre of the fibre, unaffected.

For efficient end-fire launching the faces of the fibres must be carefully cut. The cutting was done by inducing a stress in the fibre by stretching over a cylinder (normal to its axis) and then to scratch the top of it with a diamond. This method is both simple and effective.

End fire launching was used for several fibres but it did not prove to be very efficient for selecting a few of the very numerous modes.

The apparatus depicted in fig 3-12 was used to measure the numerical aperture of the waveguides. The results obtained (fig. 3-13) are in good agreement with the theory which gives the expression [40]:

$$NA_{MAX} = (n_1^2 - n_0^2)^{\frac{1}{2}} \quad (3-1)$$

The shape of the curves obtained is related to the index profile as it is clearly visible when figures 3-13 and 3-14 are compared but the method was not considered to be accurate enough for the present purposes.



Figure 3.11: PULLED CAPILLARY TUBE: FARFIELD PATTERN.

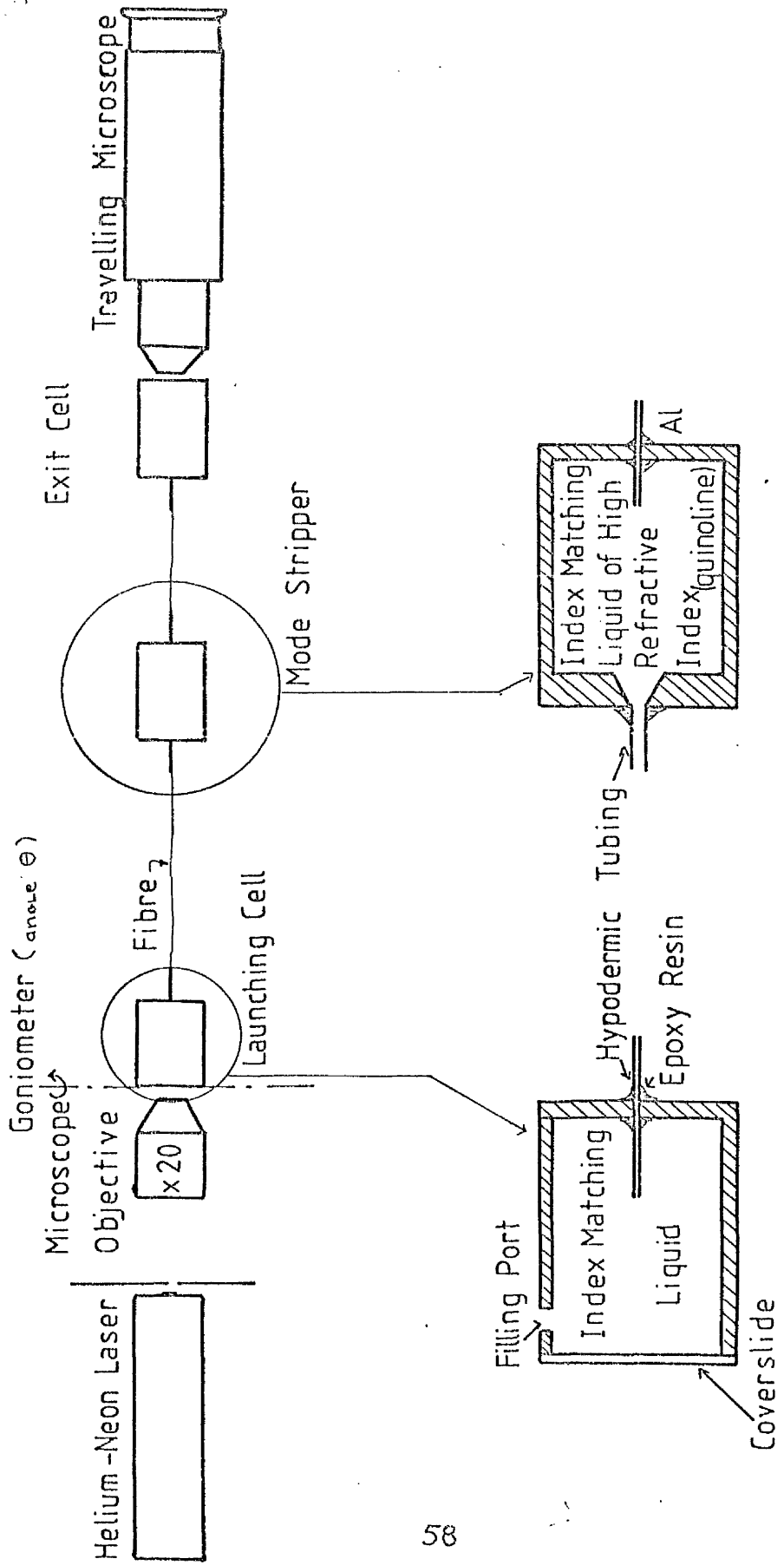
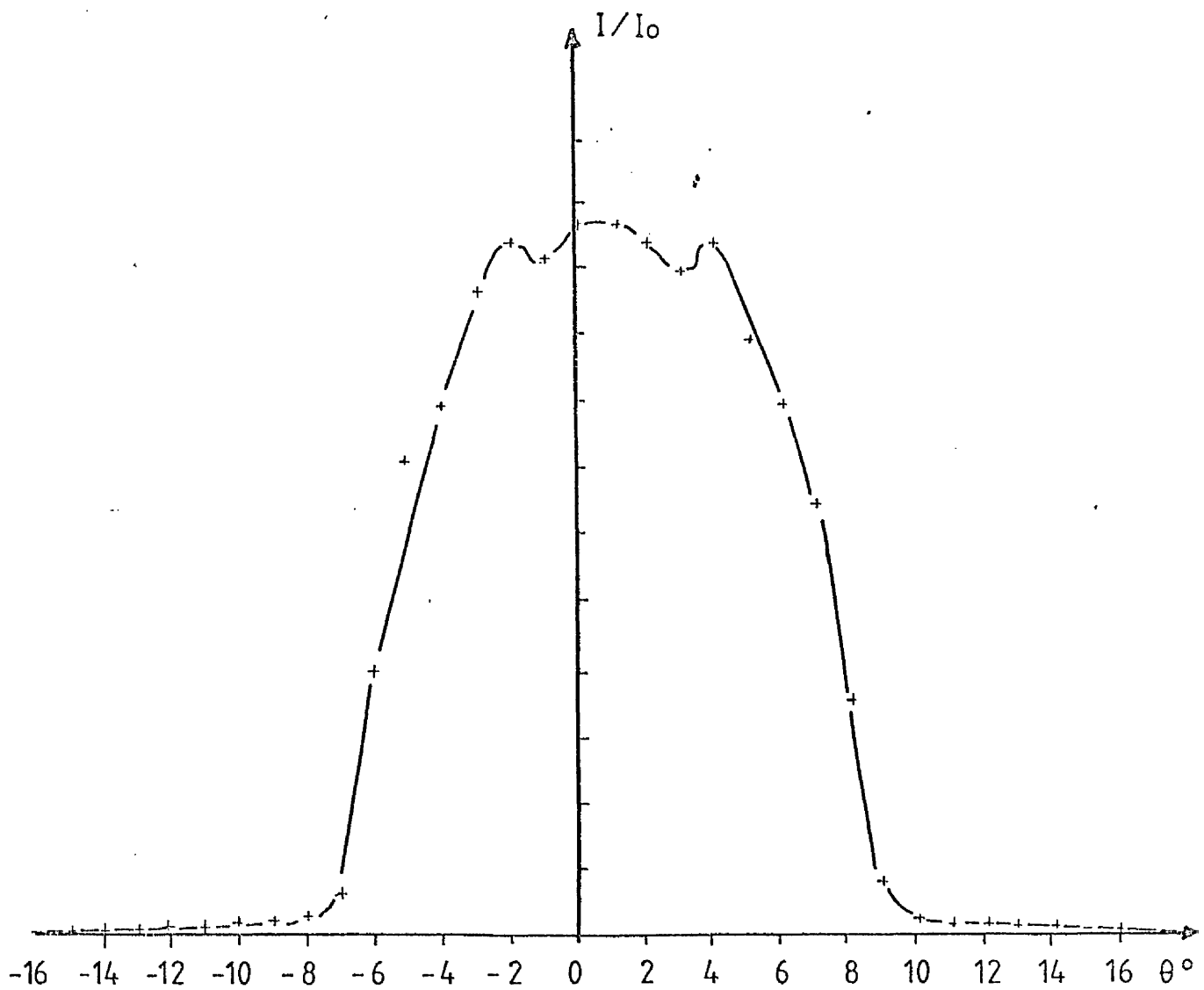


Fig.3.12. Fibre Examination Set-up

Fig.3.13 Numerical Aperture of a Graded Index Fibre.(20)



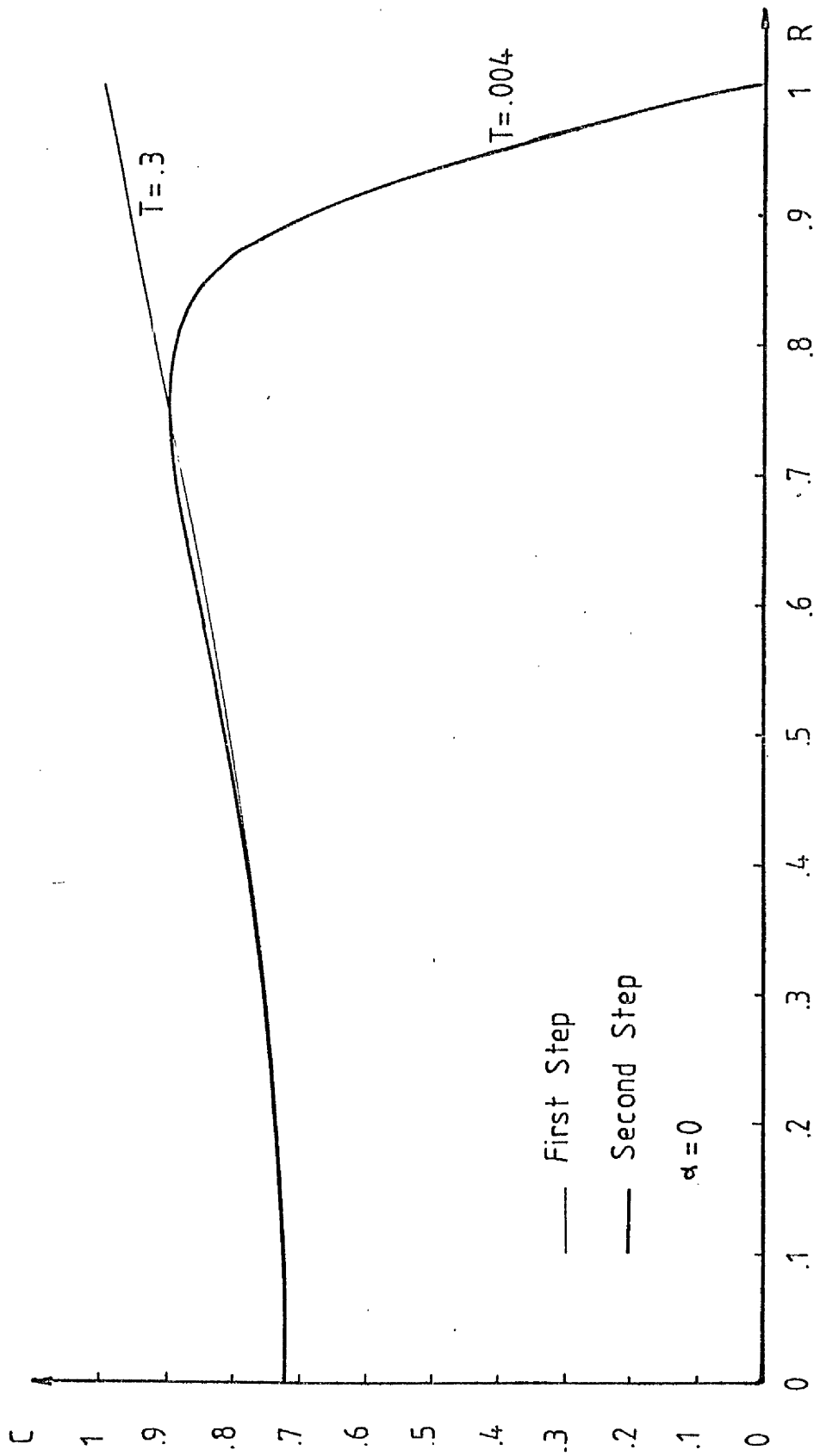


Fig.3.14 Computed Profile of Fibre 20

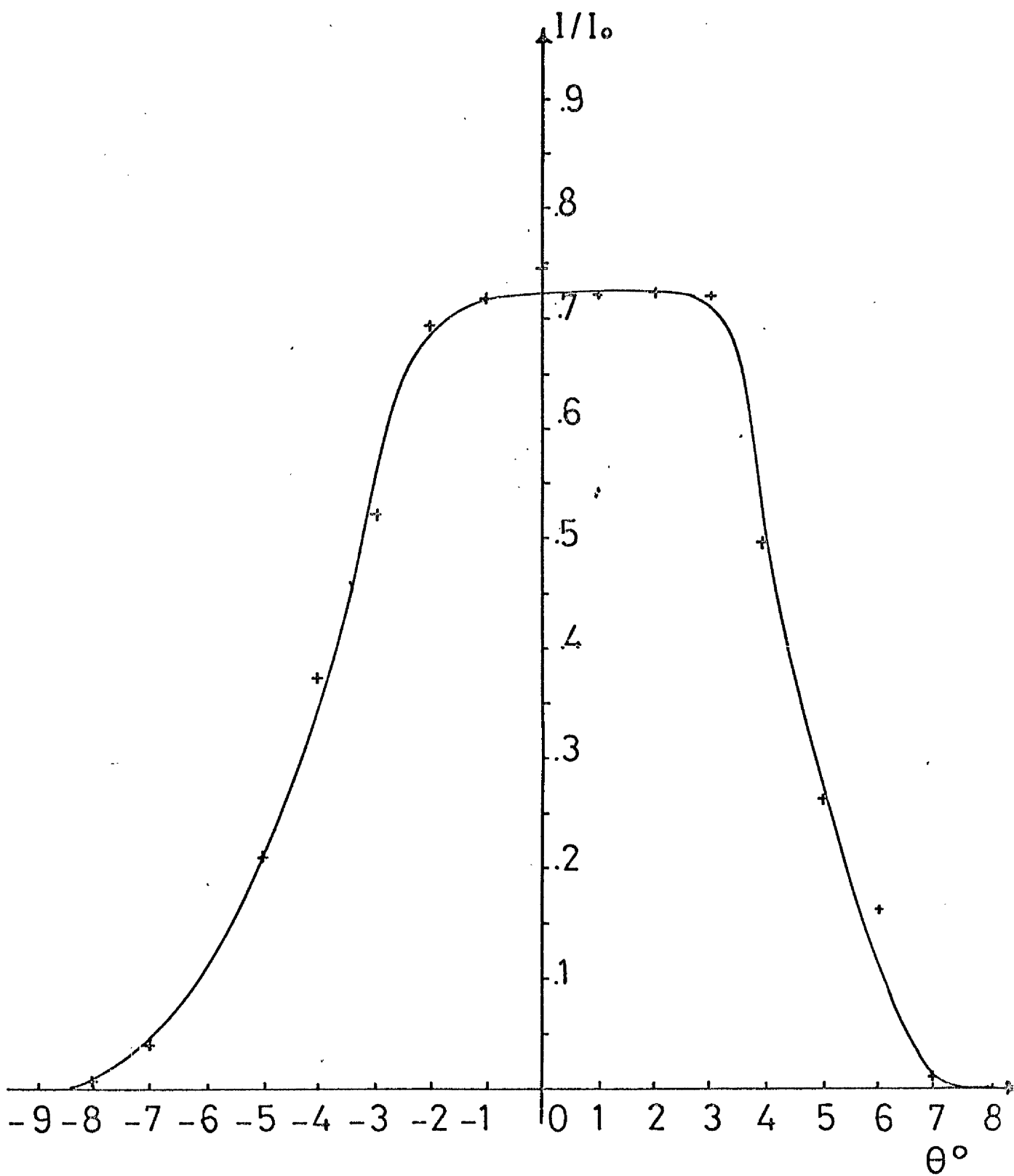


Fig.3.15 Radiation Pattern of a Step-index Fibre.

c) Prism launching.

The idea was to use a prism so that only meridional rays are launched. However, to be efficient, it required the flattening of the index profile in the launching region so that the light will go through the cladding to the fibre core. It was then possible to launch low order modes [57]. For this, one end of the fibre was repulled with a small furnace (fig. 3-16b) down to a diameter of a few microns. Thus the first order modes only were launched and the index was flattened by the heat of the furnace in the launching region. The waveguide was then held against a prism by a rubber pad pressed by the screw of the prism holder (fig. 3-16a). Light from a helium-neon laser (5 mW, $\lambda = 632.8$ nm) was launched into the fibre, through the prism in a conventional method.

However, an unsuspected problem arose. During the repulling, severe staining of the heated part of the fibre occurred and in this region the waveguide was completely opaque. Several temperatures (ranging from 500°C to 900°C) and several pulling speeds were tried without any improvement. There are several explanations for this phenomenon as such staining occurs frequently, silver nitrate being a very powerful oxidising agent. The problem here was that staining did not always occur. For example it did not happen in the process described in II-3.1.3 in spite of similar experimental conditions. This is due to the thickness of the cladding which reduces the temperature in the centre of the fibre and, mainly, because the core, being in a capillary, is protected from any outside pollution.

d) Conclusion All methods described proved to have some big disadvantages and the study of propagation characteristics did not appear to be very adequate for obtaining refractive index profiles. For this reason direct methods were investigated.

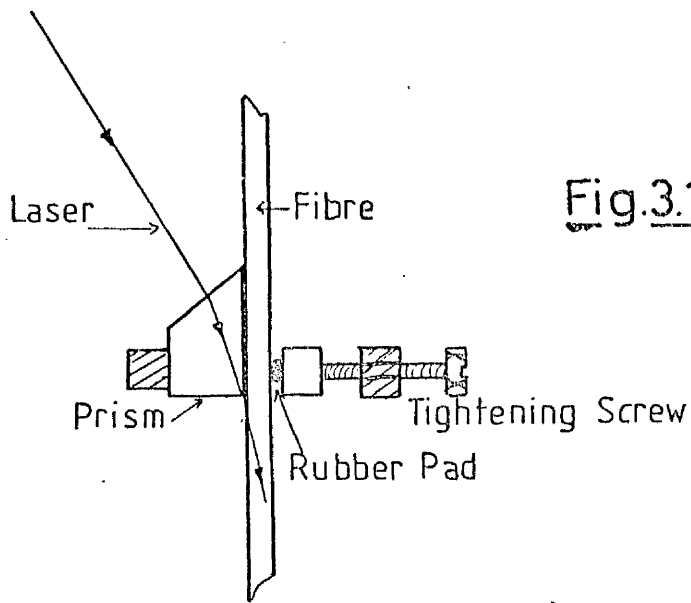


Fig.3.16.a. Prism Launching Method

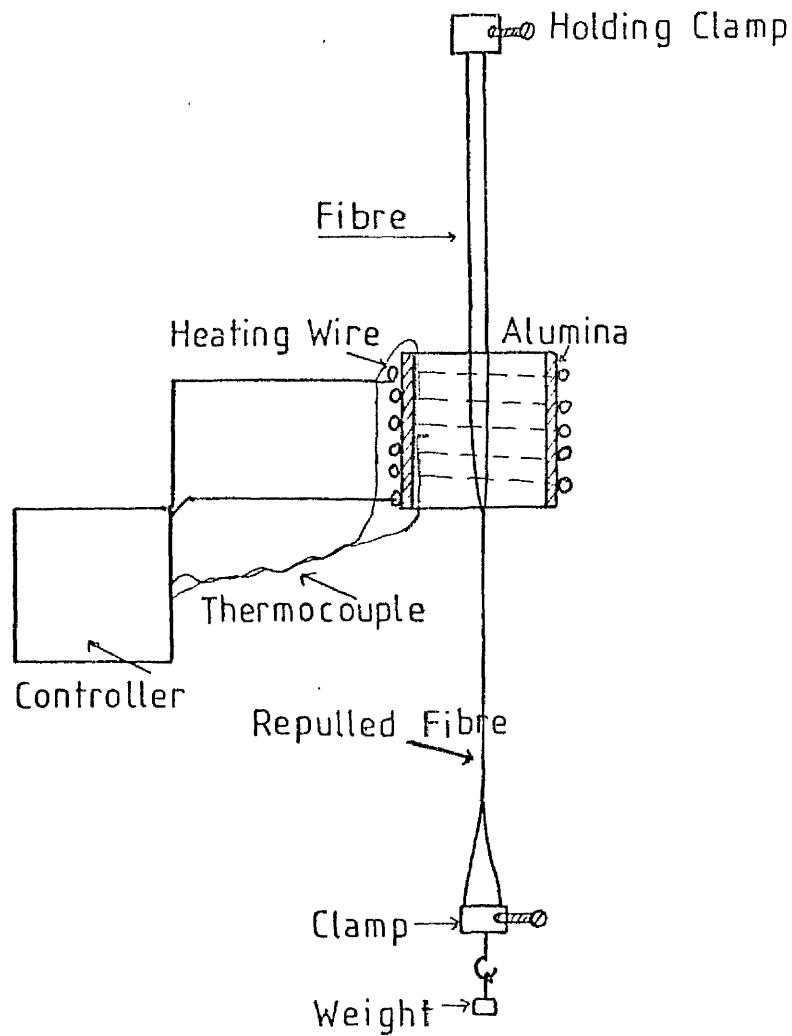


Fig.3.16.b. Repulling Apparatus

II-3.2.2. Direct methods of profile measurements.

II-3.2.2.1 Interferometric measurements

As Martin [58] suggested, it is possible to have a good knowledge of the refractive index profile by using an interferometric method. With this technique, the refractive index variation can be seen directly, as a fringe profile. Two types of interferometers were used: a Michelson interferometer mounted on a microscope and a Mach Zehnder system. To prepare samples, a length of fibre was held by glueing it in a piece of capillary tube (fig. 3-17). A slice was then cut out and polished down to a given thickness.

a) The Michelson interferometer. In this case the sample needs to be aluminised on one side. The interferometer used was fitted on a microscope and the sample illuminated with sodium light (λ) (fig. 3-18a). In the Michelson system, since light passes through the sample twice, the index change $\Delta n(x,y)$ is related to the number of fringe displacements $N(x,y)$ by the relation:

$$\Delta n(x,y) = \frac{\lambda_0}{2t} N(x,y) \quad (3-2)$$

where λ_0 is the wavelength of the light used ($\lambda_0 = 589.6$ nm), t is the sample thickness.

The system, though efficient, had some disadvantages:

- i) its accuracy depends strongly on the flatness of the sample and problems arise if the edges are rounded [58].
- ii) any distortion of the optics might seriously affect the results.
- iii) the reflective coating quality might also affect the results.

In order to suppress this last disadvantage the following system was tried.

b) The Mach Zehnder interferometer. Details of this apparatus are given in fig. 3-18b. The light source is a helium neon laser ($\lambda_1 = 632.8$ nm). For this method the sample is not aluminized and the

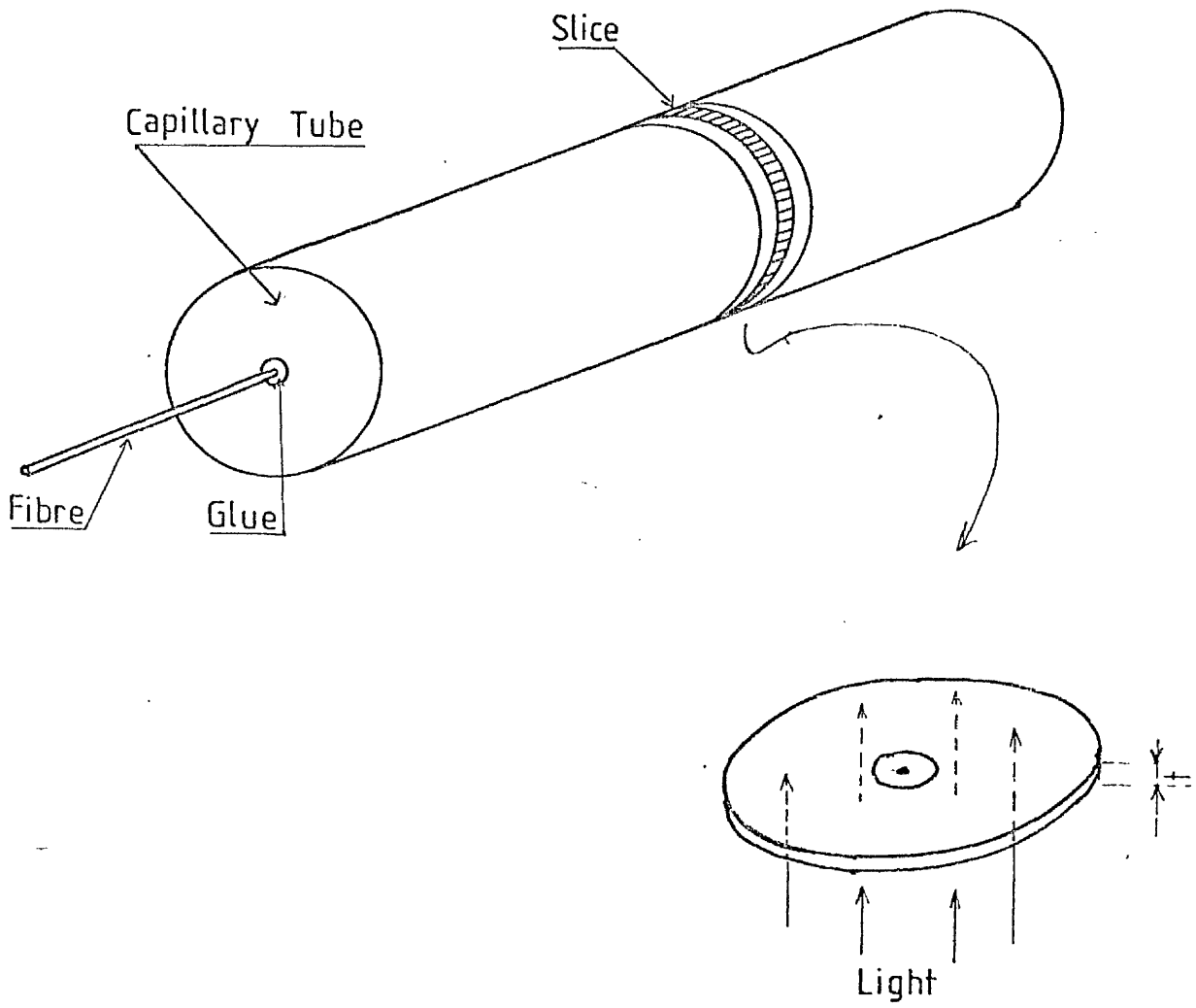
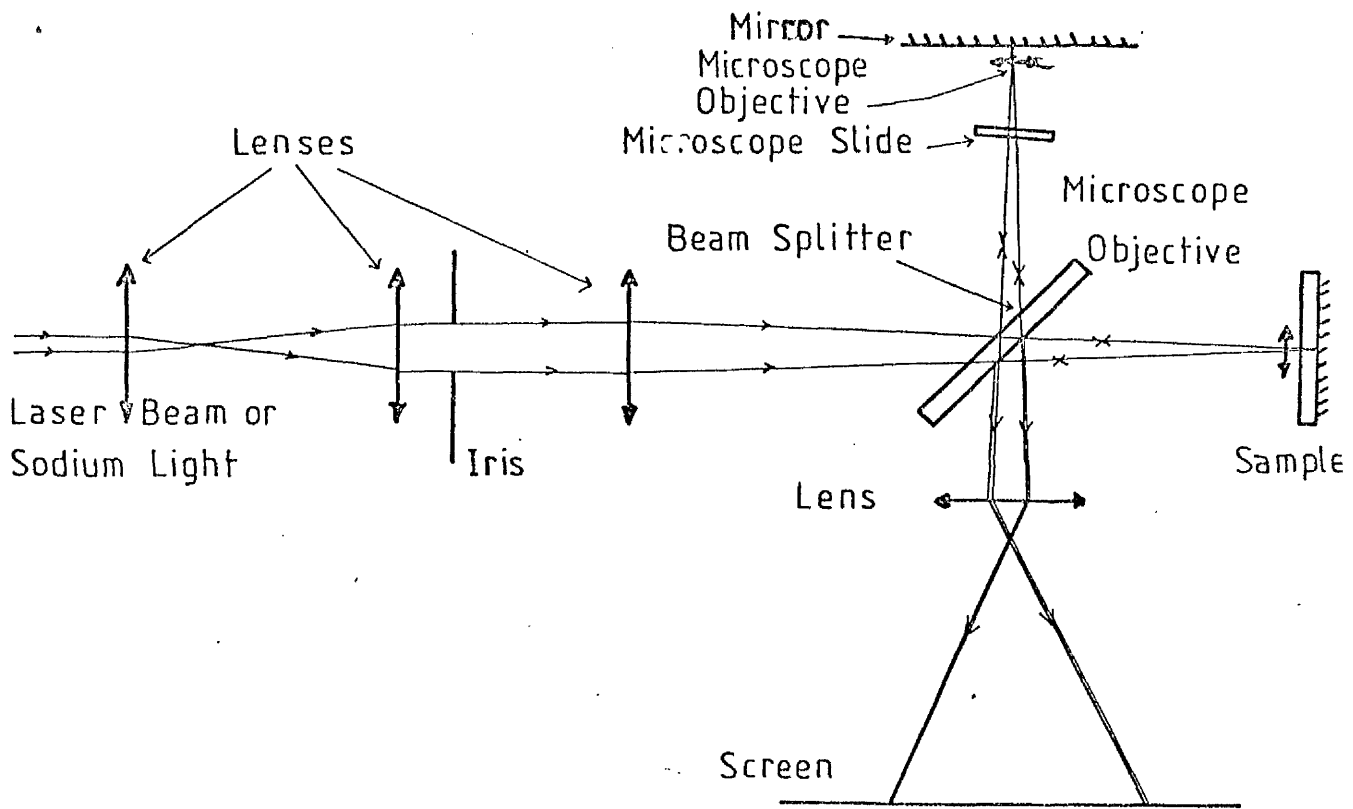
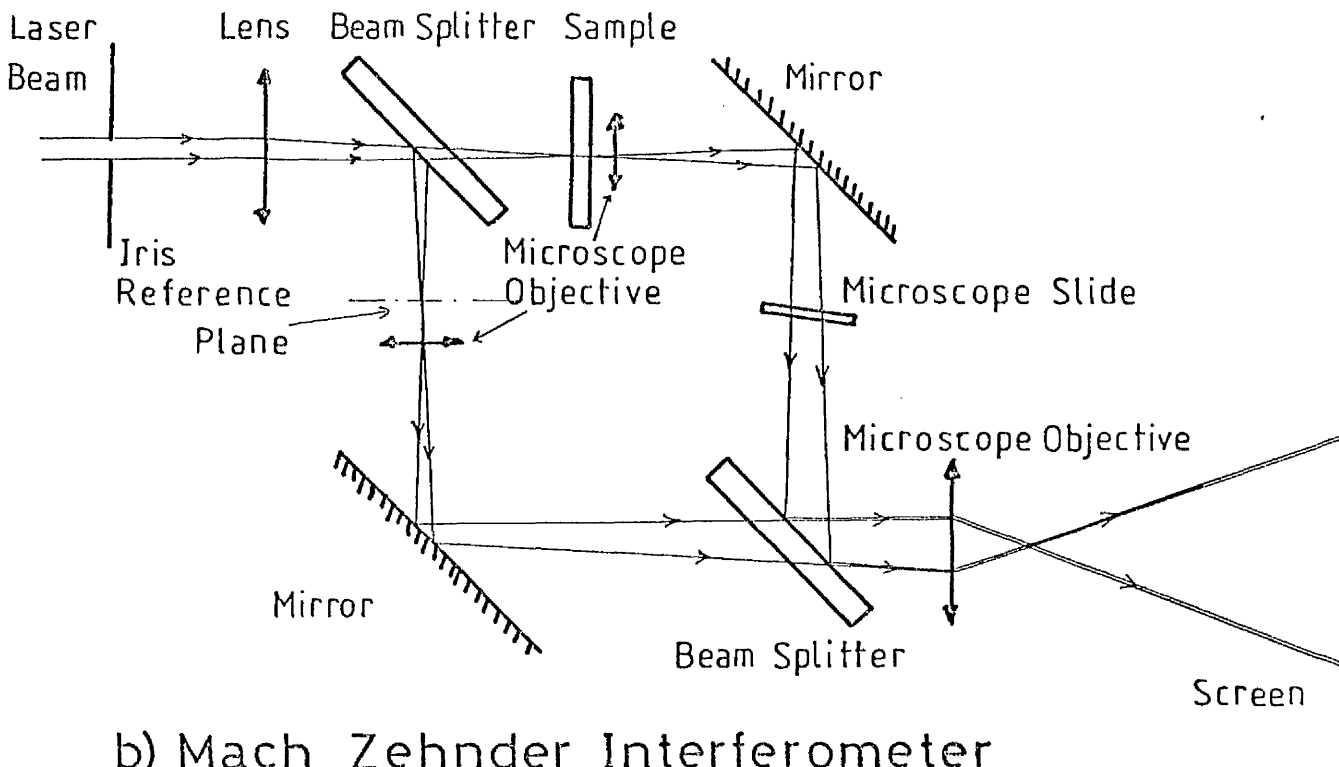


Fig. 3.17 Slicing a Fibre



a) Michelson Interferometer



b) Mach Zehnder Interferometer

Fig. 3.18 The Interferometers

light goes through it only once, reducing slightly the influence of poor flatness of the sample. In this case the index change is given by:

$$\Delta n(x,y) = \frac{\lambda_1}{t} N(x,y) \quad (3-3)$$

c) Conclusion. The Mach-Zehnder interferometer proved to be more accurate than the Michelson interferometer because it needed no aluminisation of the sample and because the imperfections in the sample preparation had a smaller influence. However the system still had disadvantages such as:

- i) The fibre is destroyed and it is impossible to see the variation of the profile along the z axis and even to know exactly what part of the fibre is in the sample.
- ii) The polishing of the sample is very delicate since the portion of fibre has a tendency to fall out of the capillary tube during the operation.
- iii) This method is very time consuming and the sample preparation can take up to a month.

To cope with the last problem another way was tried of holding the fibre in the sample. For this the fibres were potted in resin and then sliced with a microtome before a being given light polishing. This method was not very satisfactory since the microtome broke the fibres instead of cutting them neatly and, in addition, the polishing was rather difficult due to the difference in hardness between the resin and the fibre.

Consequently, another method for determining the index profile was necessary.

II-3.2.2.2. Index profile from refracted light from fibre

a) Introduction. The main features decided for the apparatus were the following:

- i) non destructive.
- ii) rapid so that the fibres could be tested at once without extensive sample preparation.
- iii) simple so that the method gives directly the profile without computation or corrections.
- iv) gives the maximum of information (e.g. Numerical aperture, dimensions, shape of the core).
- v) suitable for all types of round fibres.

Many techniques already exist for measuring index profiles but most of them do not fulfil these requirements. The micro method presented by Tracy [59] is not adapted for fibres and is not accurate enough; reflectivity measurements [60] need a very good end surface of the fibre and are very sensitive to its degradation; the device using the scattering pattern method for a normally incident laser beam [61] is only valid for a fibre whose core and index variation are small; interference microscopy with an automatic computer video analysis system ([62],[63],[64]) needs much equipment; the near field scanning method ([65],[66]) depends on the determination of the leaky rays contribution and needs computing. The method suggested by Stewart ([67],[68],[69]) seemed to be the most suitable as it is the one which satisfies most of the conditions given above.

The system works by measuring the light refracted by the front end of the fibre. This method is somewhat similar to the near-field scanning method but avoids the problem of leaky rays. It can give, as will be shown, the refractive index profile directly, across the whole diameter of the fibre, without any special preparation of the waveguide. It is suitable for any round fibre and is not destructive. Additionally it can give further information concerning the waveguide, such as numerical aperture, core and clad radii, core centrality and ellipticity.

b) Principle and description of the method. If a beam of light is focused on one end of the fibre immersed in index matching liquid with a microscope objective whose numerical aperture is bigger than that of the waveguide, the light tends to be divided in two; part of it is ducted along the fibre and the rest is refracted in a hollow cone. The leaky rays, being situated in the inside of the cone, are easily removable by placing a disc intercepting the inner part of the core (fig. 3-19a) before the light reaches the photo-diode.

The apparatus was set up as shown in fig. 3-20.

i) The light was provided by a polarised helium-neon laser (6.87mW, $\lambda = 632.8$ nm). The reflectivity of light is strongly dependent of the angle and polarisation so a quarter wave plate was fitted after the laser to change the vertical polarisation to circular and, in order to prevent reflected light going back into the laser, a polariser was placed between the laser and the quarter wave plate.

ii) The microscope objectives (magnification X3 and X6) were placed to expand the beam so that it was almost uniform over the X20 microscope objective, the latter focusing the light on the fibre end. A special filter surrounded by a white screen was made with a pinhole and was situated at the point of focus of the X3 microscope objective. The microscope objectives could be translated along any of the 3 axis.

iii) The cell is shown on fig. 3-19. It was made of aluminium, the front window being a microscope coverslide fitted with a hypodermic tube in its centre but this had to be abandoned because of its fragility. Another type of cell was made with a rear window of perspex, but unfortunately most of the index matching fluids attack perspex so finally the rear window was made from an ordinary slide glued with epoxy. The index matching liquid of the cell must have a slightly higher index than that of the cladding. The translating stage allowed

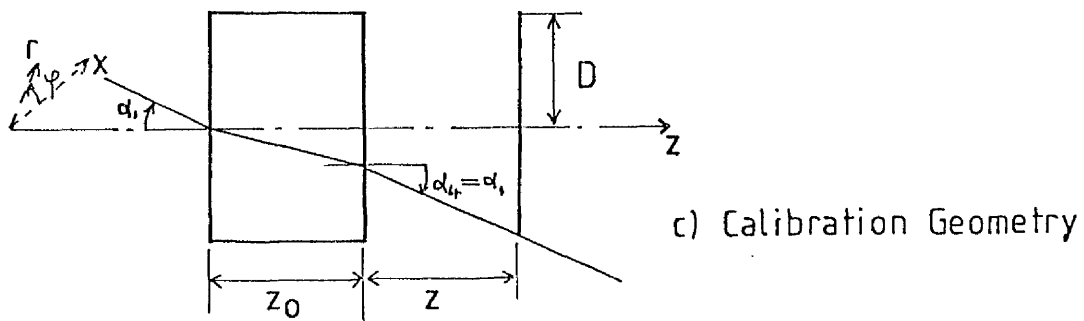
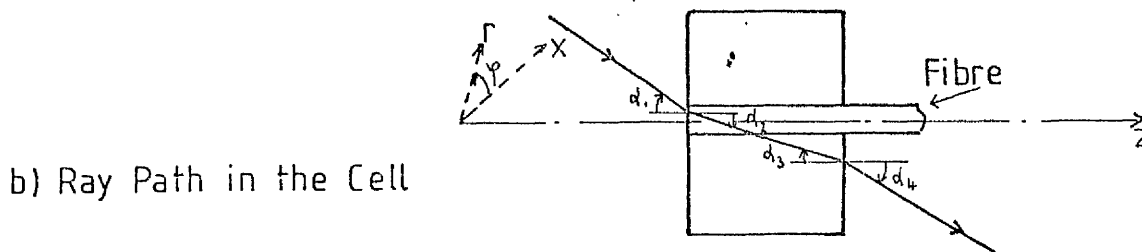
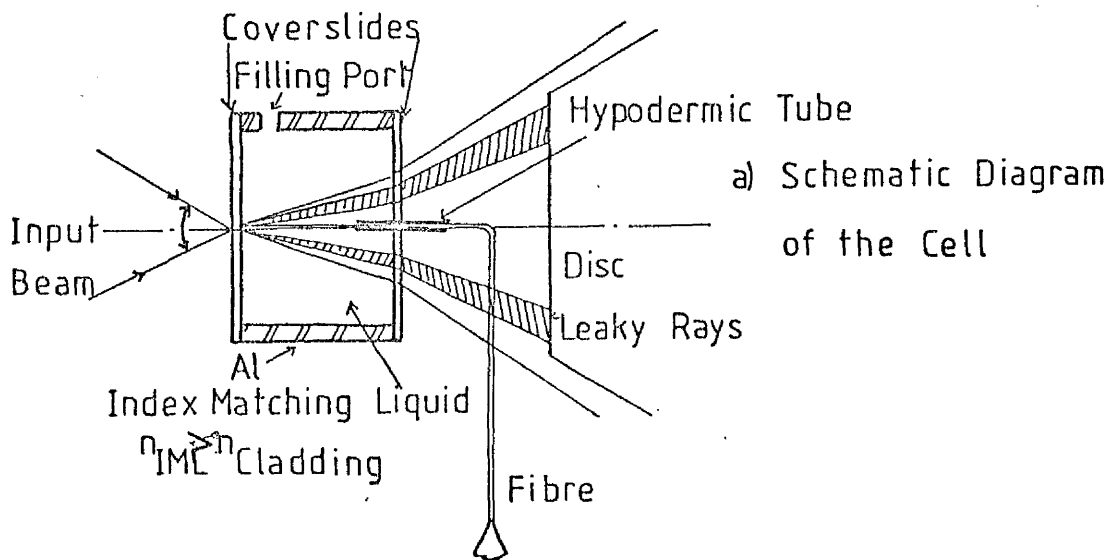


Fig. 3.19. The Launching Cell.

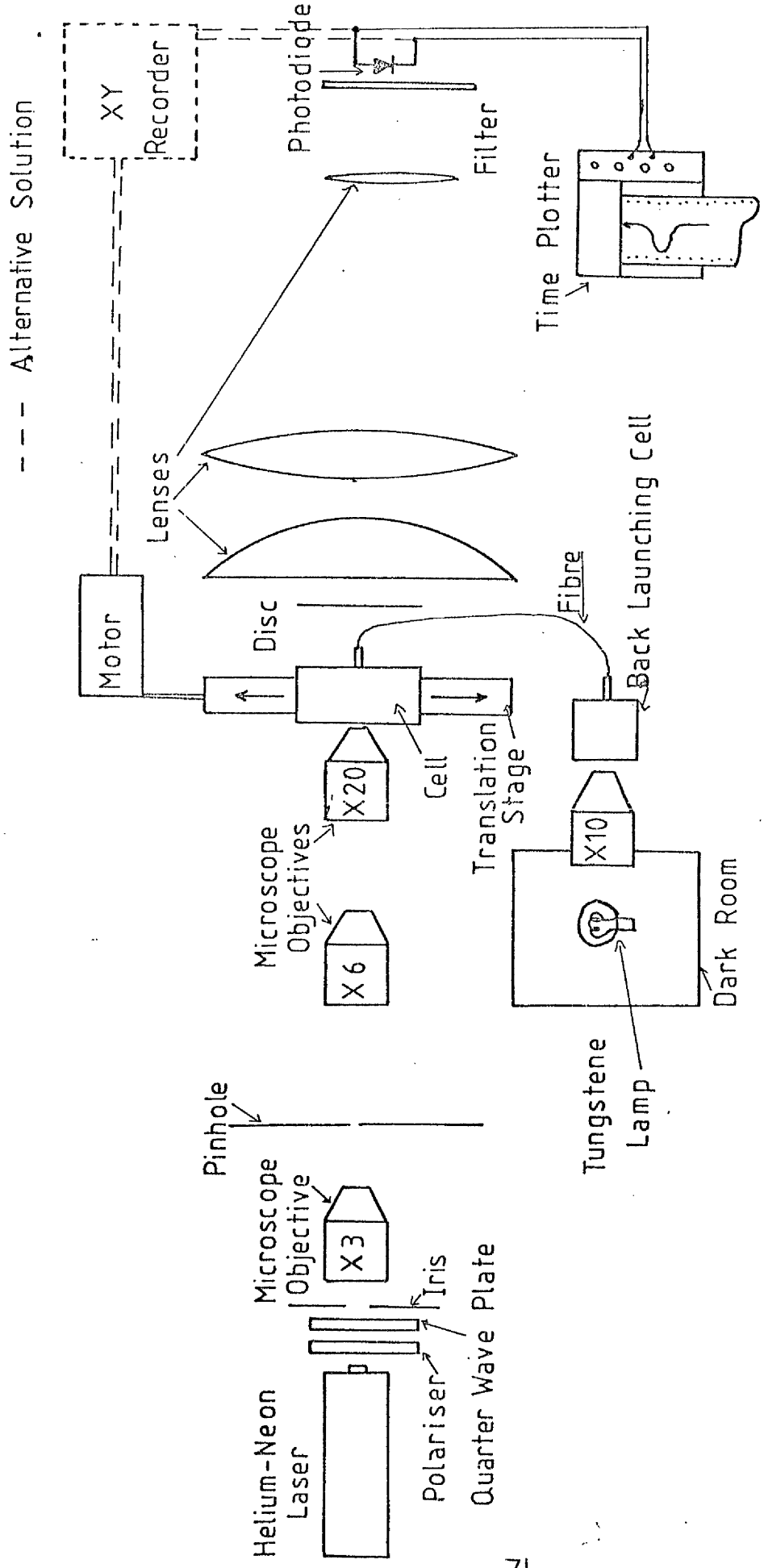


Fig.3.20. Index Profile Drawing Set-up

the fibre to be scanned along its diameter.

iv) The disc stopping the leaky rays was held by three large glass fibres and could be moved along the axis of the set up. The three lenses focused the refracted light onto a photo-diode connected to a chart recorder.

A filter was placed just before the detector in order to suppress the ambient light.

v) At the other end, the fibre, held in a cell [56], was illuminated by a tungsten lamp through a X10 microscope objective. The lamp was in a "blackbox" to prevent light leakage. The purpose of this back-launching was to produce an image of the fibre end (enlarged 120 times) so that it is possible to focus the laser beam very accurately on the fibre and to know the shape of the latter. It is now possible to see the reason for the three microscope objectives.

The X3 and X5 objectives expended the beam, the X6 and X20 gave a magnified image of the fibre on the screen/pinhole, while the X20 focused the light on the waveguide. It should be noted that the cell and the fibre end must be exactly normal to the beam and parallel to the translation movement (within the field depth of the X20 objective).

c) Theory of the refracted light method. Consider a cell as shown on fig. 3-19b. Since the fibre, the cell and the beam are circularly symmetric, the component of the wave number along the z axis is constant. The wave number in vacuo is:

$$k_0 = \frac{2\pi}{\lambda_0} \quad (3-4)$$

In the fibre:

$$\frac{\beta}{k_0} = n(r) \cos \alpha_2 \quad (3-5)$$

In the index matching liquid:

$$\frac{\beta}{k_0} = n_{IML} \cos \alpha_3 \quad (3-6)$$

Applying Snell's law to the ends of the cell

$$n(r) \sin \alpha_2 = \sin \alpha_1 \quad (3-7)$$

$$\sin \alpha_4 = n_{\text{IML}} \sin \alpha_3 \quad (3-8)$$

Taking the square of (3-7) - (3-8) and using (3-5) - (3-6), it is possible to eliminate α_2 and α_3 leading to:

$$n^2(r) = n_{\text{IML}}^2 + \sin^2 \alpha_1 - \sin^2 \alpha_4 \quad (3-9)$$

During a measurement n_{IML} , $\sin^2 \alpha_4$ are fixed [69] so there is a direct relation between $n^2(r)$ and $\sin^2 \alpha_1$. The photo-diode measures all the power transmitted in the cone above an angle defined by the disc or α_{40} - which corresponds to an angle α_{10} defined by eq. (3-9) and thus to the total power in the input beam $P(\alpha_1)$.

Assuming that the intensity is constant across the width of the input beam and that there are no angle-dependent losses we can write:

$$P(\alpha_1) = P_0 \frac{\tan^2 \alpha_{1M} - \tan^2 \alpha_1}{\tan^2 \alpha_{1M}} \quad (3-10)$$

where α_{1M} is the numerical aperture of the microscope objective (fig. 3-19a). Of course, in fact the reflection losses depends on the angle so the field is arranged in order to decrease slightly towards the edges in order to reduce the dependance of $P(\alpha_1)$ on α_1 from $\tan^2 \alpha$ to approximately $\sin^2 \alpha_1$ (over small angles \tan^2 and \sin^2 are very close). This is only necessary over the range of α_1 used during the measurements.

From (3-9) it is seen that during a scan, for a given α_4 :

$$n^2(r)_{\text{max}} - n^2(r)_{\text{min}} = (\text{N.A.})^2 = \sin^2 \alpha_{1\text{max}} - \sin^2 \alpha_{1\text{min}} \quad (3-11)$$

So if we test a fibre whose numerical aperture is, say 0.3 we have a variation of α_1 of roughly 3° . For this variation it is necessary to have $P(\alpha_1)$ as linearly dependent as possible on $\sin^2 \alpha_1$ which is linearly dependent on $n^2(r)$ and hence on $n(r)$ since the index variation is small over the fibre.

Consequently the detected power gives directly the index at the focused spot.

In order to calibrate the cell, it is viewed when empty (fig. 3-19c). Without a fibre $\alpha_1 = \alpha_4$ and hence:

$$R = \frac{z}{\cos \alpha_1} \sin \alpha_1 + \frac{\sin \alpha_1}{n_{IML}} \frac{z_0}{\left(1 - \frac{\sin^2 \alpha_1}{n_{IML}^2}\right)^{\frac{1}{2}}} \quad (3-12)$$

where R is the disc radius.

Consequently:

$$z = \left(\frac{R}{\sin \alpha_1} - \frac{z_0}{\sqrt{n_{IML}^2 - \sin^2 \alpha_1}} \right) \cos \alpha_1 \quad (3-13)$$

The power transmitted beyond the disc as it is scanned along the z-axis is plotted, which gives, from (3-13) the relation between $P(\alpha_1)$ and $\sin^2 \alpha_1$, while $\sin^2 \alpha_1$ leads to $n^2(r)$ through (3-9).

The numerical aperture of the fibre can also be found from:

$$N.A. = (n_1^2 - n_0^2)^{\frac{1}{2}} = \sqrt{\sin^2 \alpha_1(o) - \sin^2 \alpha_1(b)} \quad (3-14)$$

where $\alpha_1(o)$ is the value of α_1 for $r = 0$ and $\alpha_1(b)$ for $r = b$.

We can draw a profile, then take the fibre away and place the disc in the two positions giving the power received when the spot was on the centre of the core and on the cladding. Noting the two corresponding values of z, we have access to the two values of $\sin^2 \alpha_1$ (eq 3-13) which leads to the numerical aperture (eq 3-14).

The leaky mode contribution has been studied [70] and it has been shown that the maximum angle in the input cone from which light can be launched into leaky modes is given by:

$$\sin^2 \alpha_1 = \frac{n^2(r) - n^2(b)}{1 - (r/b)^2} \quad (3-15)$$

Considering equation (3-9) the minimum angle in the input cone which must be covered is given by:

$$\sin^2 \alpha_4 = (n_{IML}^2 - n^2(r)) + \text{Max} \left(\frac{n^2(r) - n^2(b)}{1 - (r/b)^2} \right) \quad (3-16)$$

In order to find the extremum of this function it is necessary to estimate the variation of $n(r)$.

Assuming that:

$$n(r) = n_{(o)} \left(1 - 2\Delta \left(\frac{r}{b}\right)^\alpha\right)^{\frac{1}{2}} \quad (3-17)$$

with

$$\Delta = \frac{n^2(o) - n^2(b)}{2n^2(o)}$$

then the minimum angle at which the disc must intercept the cone is given by:

$$\sin^2 \alpha_4 = (n_{IML}^2 - n^2(b)) + \frac{\alpha}{2} (N.A.)^2 \quad (3-18)$$

The first term gives the value of the internal angle of the hollow cone:

$$\text{Arc sin } (n_{IML}^2 - n^2(b))^{\frac{1}{2}} = \alpha_{4min} \quad (3-19)$$

To estimate α we can use the formula [71]:

$$\alpha = \frac{\log(0.5)}{\log(c/b)} \quad (3-20)$$

where c is the radius for which:

$$n(c) = \frac{n(o) + n(b)}{2} \quad (3-21)$$

These equations give the dimension of the cone and the contribution of the leaky rays, and thus allow the dimension of the disc to be determined.

d) Experimental results and conclusion. Experimental results obtained from three different types of fibres are shown in fig. 3-21. The recordings show clearly the refractive indices of the index matching fluid, of the cladding when there is one and of the core. Fig. 3-22 depicts a Selfoc fibre. However it seems that the method could be further improved.

The main problem is to reduce the vibrations which can induce a noise signal bigger than the useful one. To achieve this the apparatus should be installed on a vibration free table. The translation stage is also rather crude and does not allow for very precise measurements to be made. It would be a great improvement if it was also controlled by an electric micrometer able to delivery an input to an X-Y recorder. However the apparatus gave good results and has been used extensively in spite of

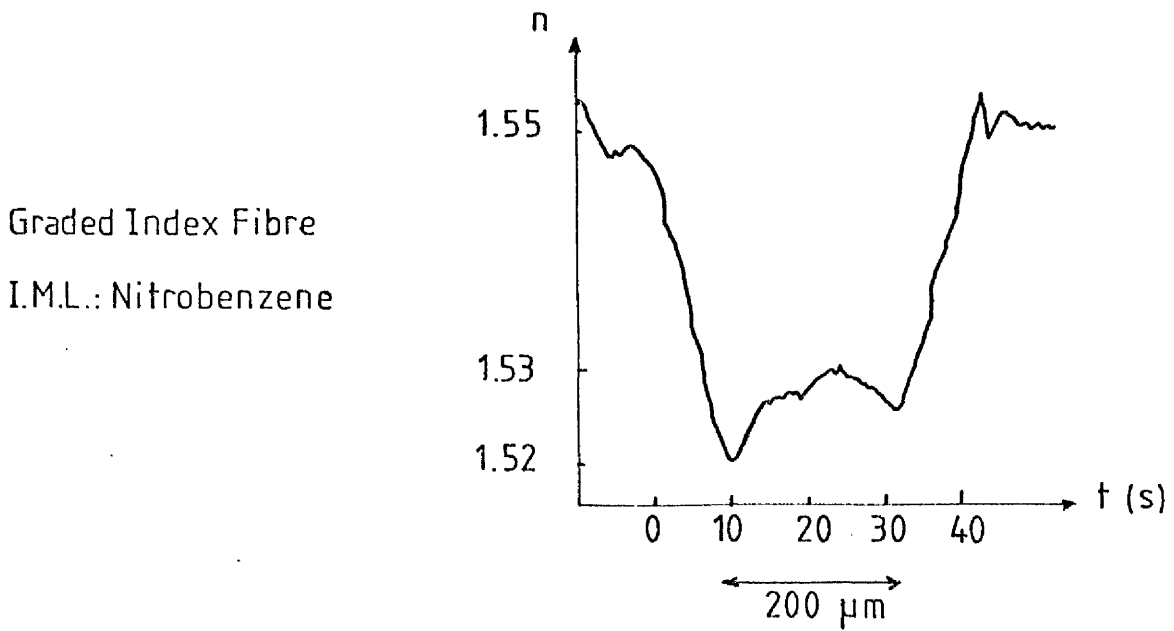
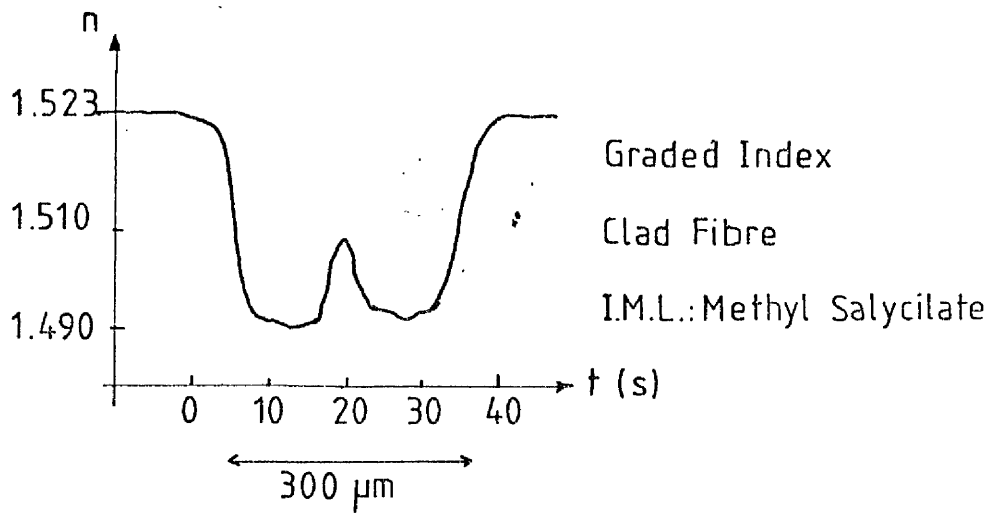
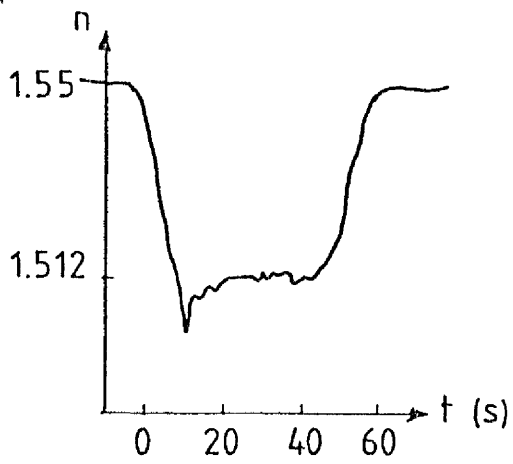


Fig.3.21. Some Profiles

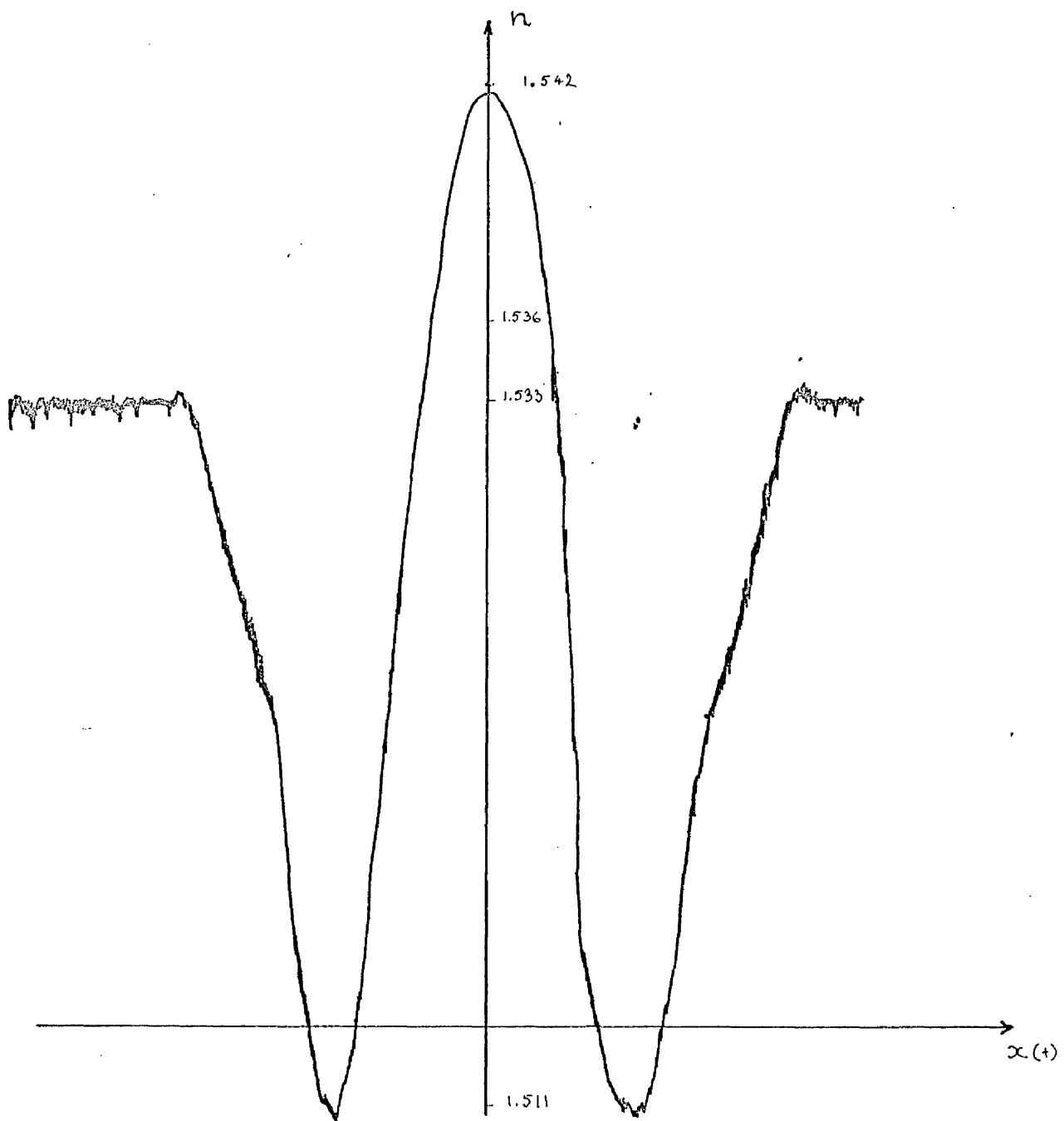


Fig.3.22 Measured Profile of a Selfoc Fibre
 $n_{iml} = 1.53$

its imperfections. It proved to be simple, needed no corrections and no extensive sample preparation was necessary. Moreover, it was only destructive when the evolution of the index profile along the z-axis of the fibre was studied as it required the cutting of the waveguide at regular intervals.

CHAPTER IV

Index Modification and Coupling

II-4.1 Introduction

Now that fibres can be made and tested, it is necessary to study the second part of the work, that is, the coupling of fibres. For this it is necessary to flatten the refractive index profile locally in the best way possible.

II-4.2 Principle of index modification

The first method tried to achieve such a modification was to rediffuse silver ions into a small portion of the guide. However this was abandoned for the following reasons:

- i) the process is long and cumbersome,
- ii) the fibre has to be dipped into the melt over a small length.

For this it was curved and this curvature is retained,

- iii) the variation of the refractive index profile along the axis is tapered in the wrong direction, i.e. towards the cladding, as shown on fig. 4-1a because of the diffusion process itself.

The following alternative was then tried. A small portion of the fibre was heated in a very small furnace (fig. 4.2). The heat allows the silver ions to migrate in the silica network so that they are equally distributed radially giving a flat profile. An important advantage of the method is that the flattening along the axis is tapered in the right position, i.e. towards the core (fig. 4-1b).

II-4.3 Index modification apparatus

II-4.3.1. Silver diffused fibres

The set up is described in fig. 4-2: A small furnace (2.5cm) heated up a portion of the fibre, which was supported by glass tubing. A controller delivered the power to the furnace for a given length of time. It was found that the temperature fluctuated a lot around the set point, mainly due to the very small thermal inertia of the furnace

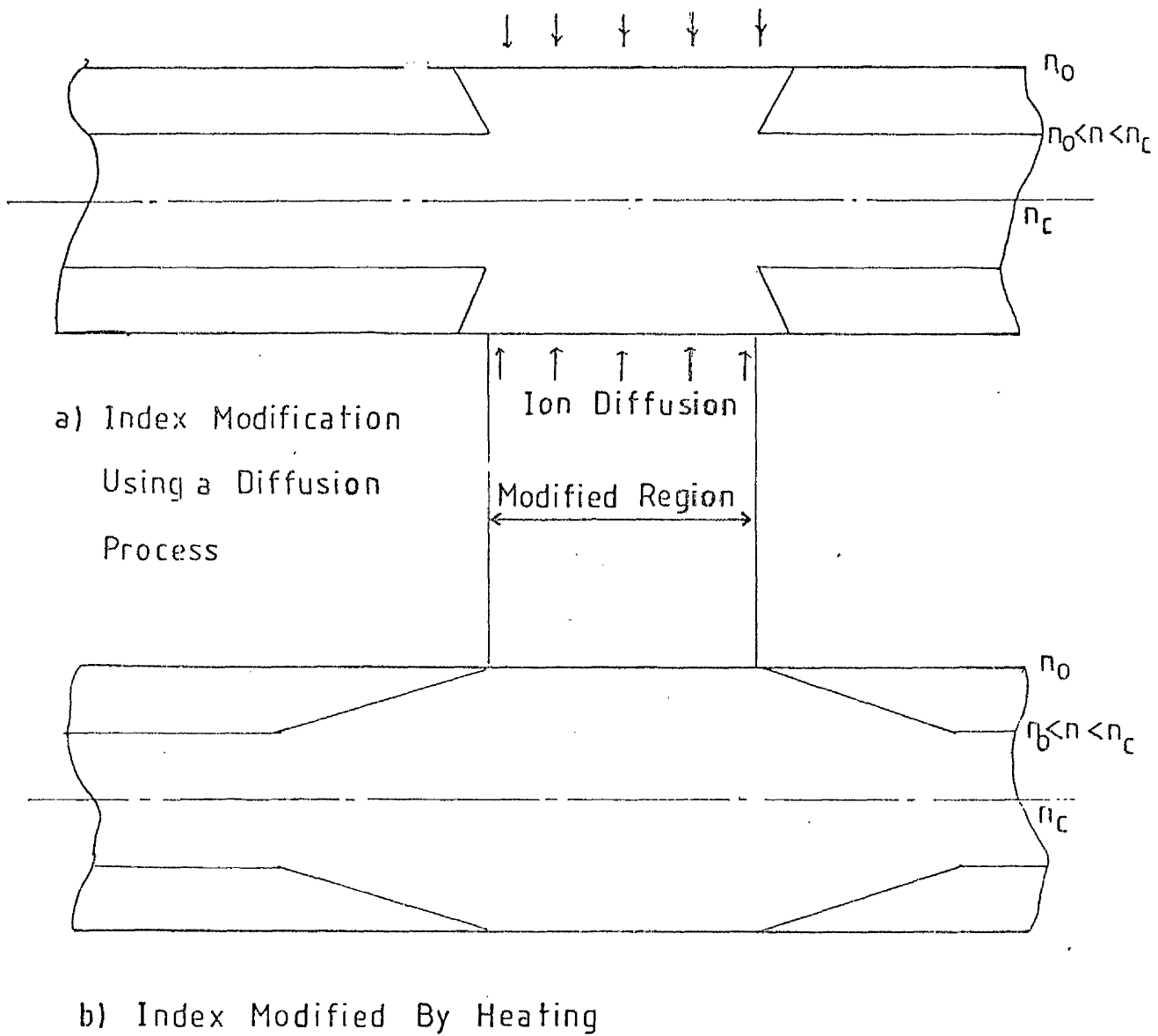


Fig.4.1 Index Modification of Fibres.

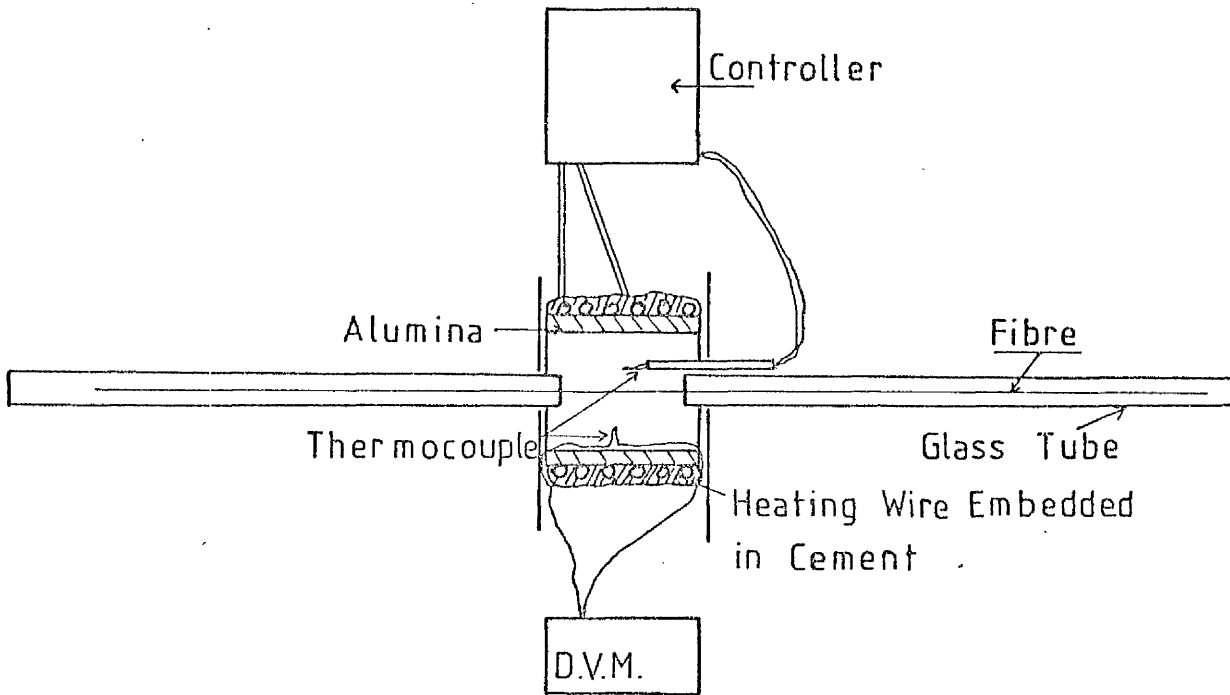


Fig.4.2.a. Index Modification: The Furnace

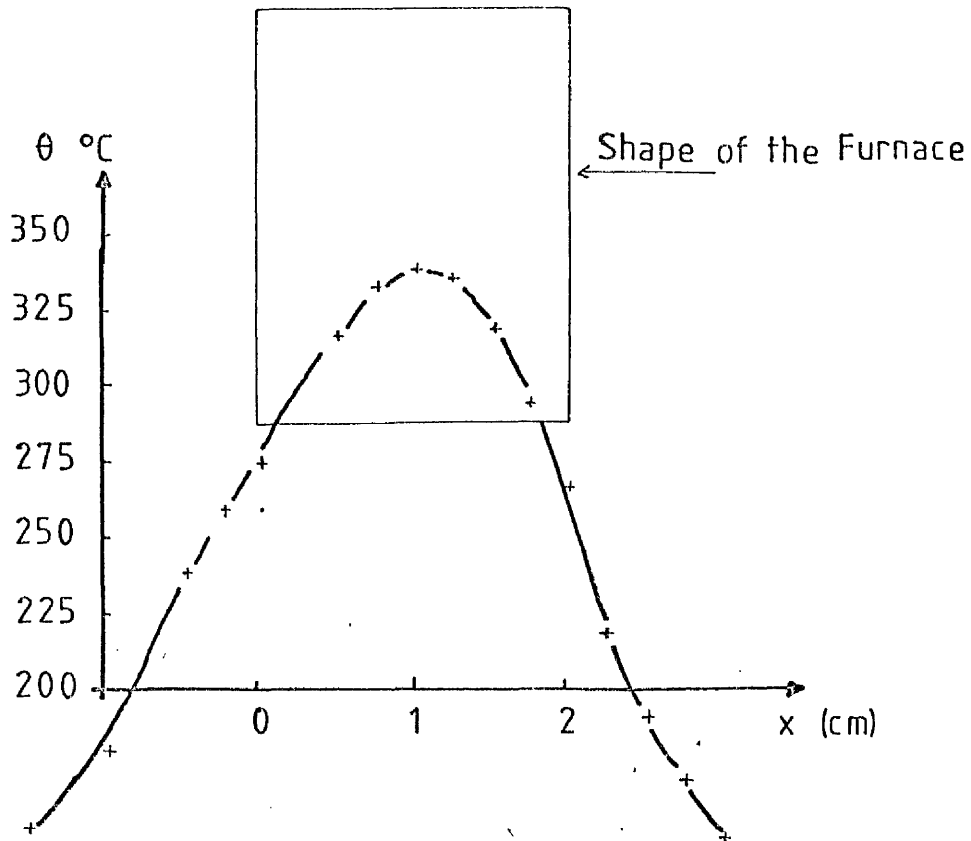


Fig.4.2.b. Temperature Profile of the Furnace

which was thus very draught-dependent. The problem was that it was rather difficult to isolate the furnace since it would have increased its size and thus the modified region of the fibre. To cope with this the temperature was set rather low (330°C) so that any surge in temperature would not damage the fibre. It must be remembered that fibres become opaque when overheated because of reactions with silver ions. Fig. 4-3 shows a fibre modified with this process. The region with a flat index is visible due to the light scattered.

However, this method has several disadvantages when it is applied to silver diffused fibres, the main one being that, in spite of all the precautions taken, several fibres were deeply stained. In addition the modified portion proved to be excessively fragile and, during the manipulation to clean or check the them, or to couple them, they would break.

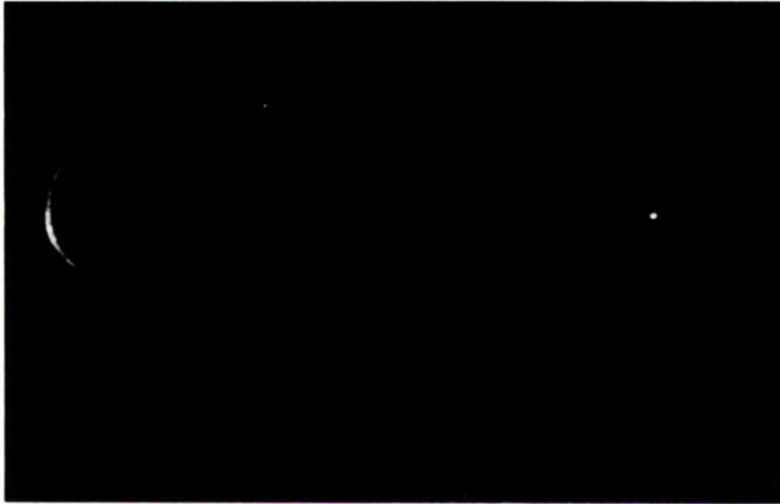
Finally the process, again, is very time consuming due to the low temperature at which the diffusion is done.

II-4.3.2. Selfoc fibres

For Selfoc fibres the same small furnace was used but it was baffled with mica to reduce the draughts and the set temperature ranged from 570°C to 610°C since there was no risk of staining.

Before being introduced in the furnace, the fibres needed to be stripped of their plastic jacketing. The best method appeared to consist in dipping them in concentrated Sulphuric acid for several hours (typically 5 hours) to etch most of the lossy jacket and cladding and then to dip them again in clean concentrated Sulphuric acid in order to remove any remnant. Afterwards the fibre was rinsed thoroughly in distilled water.

The fibres were then placed in the modifying furnace for times ranging from 9 to 52 hours. The fibres were not taken abruptly out of



Modified Region.

Figure 4.3: MODIFIED SILVER DIFFUSED FIBRE.

the furnace since this could cause an alteration of their characteristics due to a forced rapid cooling. Instead the temperature of the furnace was slowly brought to 385°C in two steps. The first one would typically bring the temperature to 550°C at the rate of 5°C per minute while the second would allow the temperature to reach 385°C at the rate of 2.5°C per minute. At this stage the furnace with the fibre inside would be allowed to cool down as its own since 385°C is below the annealing point [84]. Once modified, the fibres were cleaned in order to remove the black patches (non etched parts of the cladding now burnt) which appeared during heating in the furnace.

The modifying process proved to be rather successful with Selfoc fibres but they would still be very brittle in the modified area and very often showed distortions in this zone. In most cases the losses induced during the modification process could not be measured with the available equipment. Fig. 4-4 shows a photograph of the light scattered through a modified portion while fig. 4-5 gives the recording of the light output through the very same portion.

Fig. 4-6 shows a photograph of a monitor screen. A camera was aimed at the fibre and the system Hamamatsu C1000-03 was equipped with a device enabling the measurement of the light output along the viewed part of the fibre. This is indicated by the curve in the bottom of the picture. The modified portion is thus clearly visible by the amount of measured scattered light.

Fig. 4-7 depicts the various types of on-line patterns along such a modified fibre. It shows quite clearly that outside the modified portion only the very high order modes can be coupled out with the prism while within the modified portion lower order modes can also be tapped out.

Fig. 4-8 shows the evolution of the index profile in the modified region as measured with the apparatus described in II-3.2.2.2.

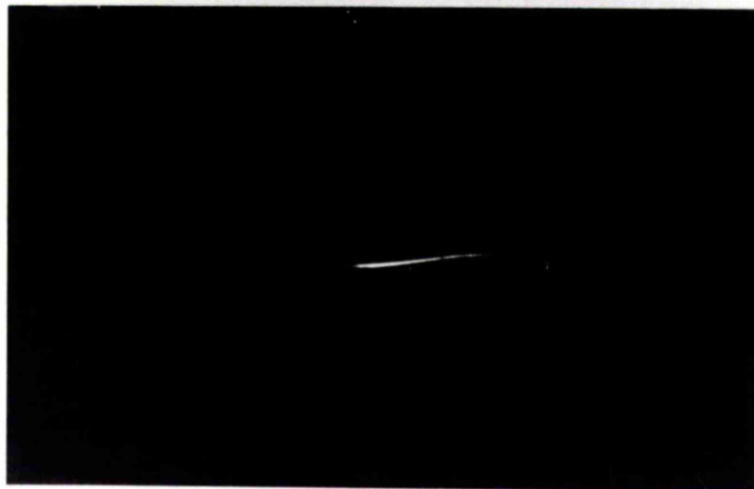


Figure 4.4: PHOTOGRAPHS OF THE MODIFIED REGION OF A SELFOC FIBRE.

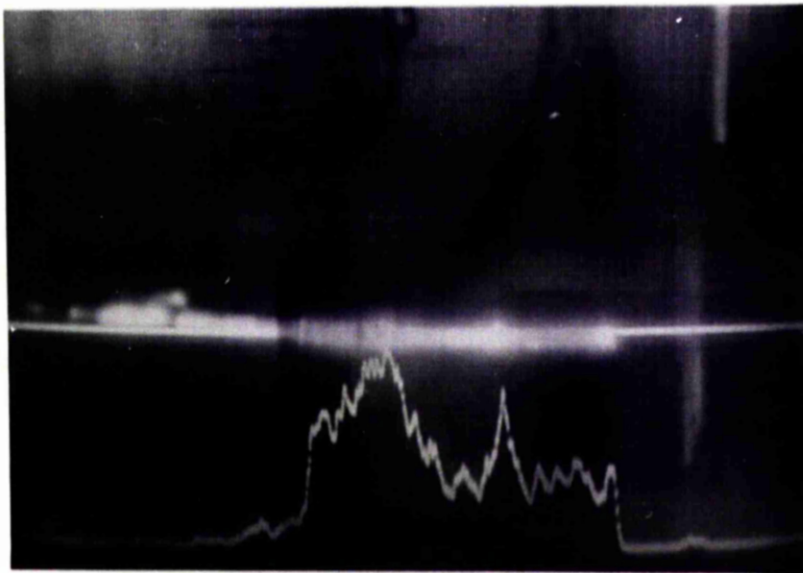


Figure 4.5: PHOTOGRAPH OF THE MONITOR SHOWING THE INTENSITY OF THE SCATTERED LIGHT.

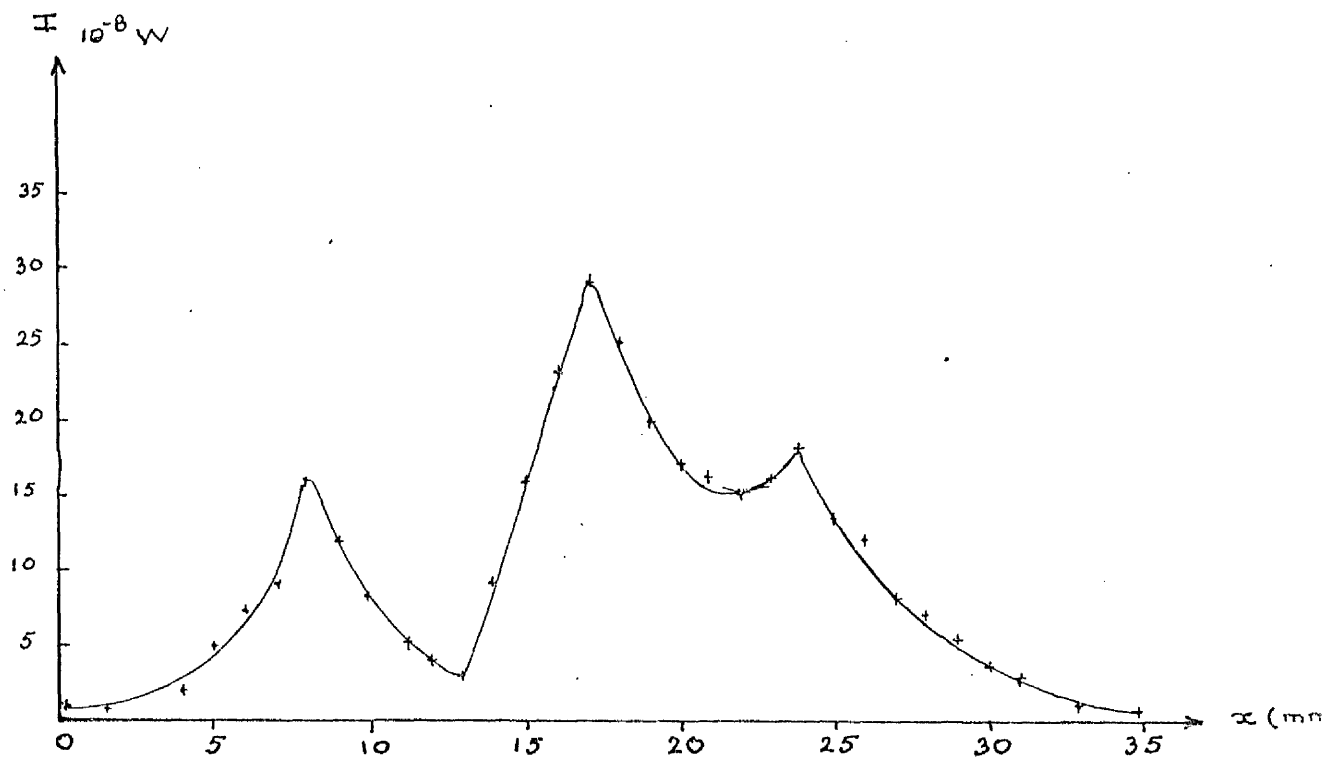


Figure 4.6: RECORDING OF THE LIGHT OUTPUT FROM THE MODIFIED REGION OF A SELFOC FIBRE.



A



B



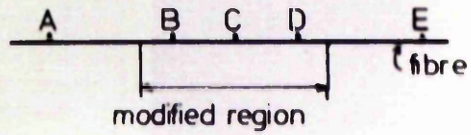
C



D

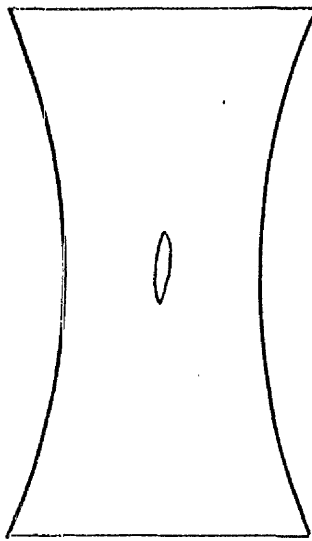


E

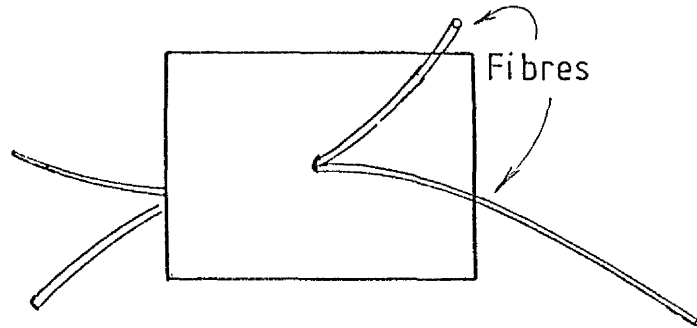


Prism position on the
photographs

Figure 4.7: M-LINES PATTERN ALONG A MODIFIED SELFOC FIBRE.



1) Expanded



2) In its Actual Shape, Clamping Two Fibres Together

RUBBER SYSTEM

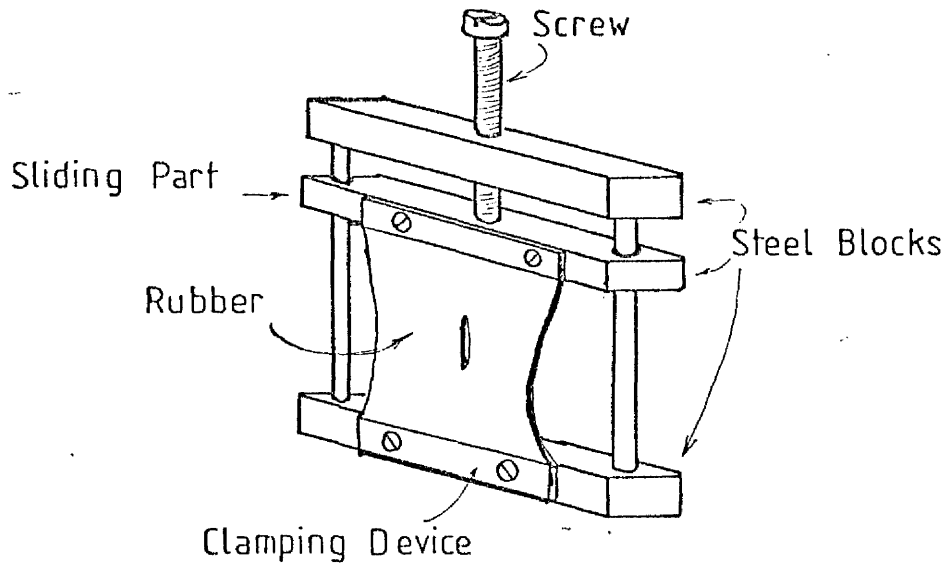


Fig.4.8 First Coupling Set-up

II-4.4 Coupling devices

In order to allow coupling between two fibres to occur, it is necessary to find a way to press them together, with the minimum risk of breaking them. To achieve this goal two methods were investigated.

II-4.4.1 Short coupling method

The first method consisted in making a very small hole (0.1mm) with an hypodermic needle in a piece of rubber (3mm x 50mm x 70mm). The rubber was then expanded by pulling two sides of it apart so that it was possible to insert the two fibres in the enlarged hole. They were fitted so that their modified regions coincided (fig. 4-8). Then the rubber was left to take its original shape, thus pressing the fibres together over a small length (fig. 4-8a).

The main disadvantage of this method is that it is not possible to use it when long coupling lengths are necessary which was the case here. In addition, it is rather difficult to make a suitably small hole, so another method was investigated.

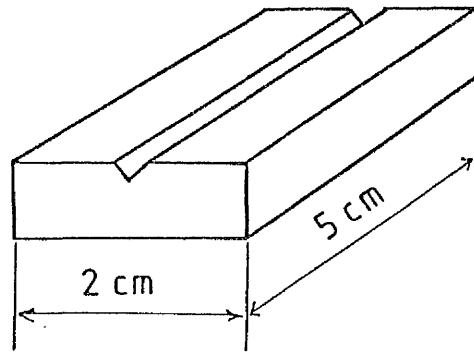
II-4.4.2 Coupling block method

In this case a more conventional method was used. A groove, wide enough to hold two fibres was cut in a brass block (fig. 4-9a), the block being fixed in a cramping device (fig. 4-10).

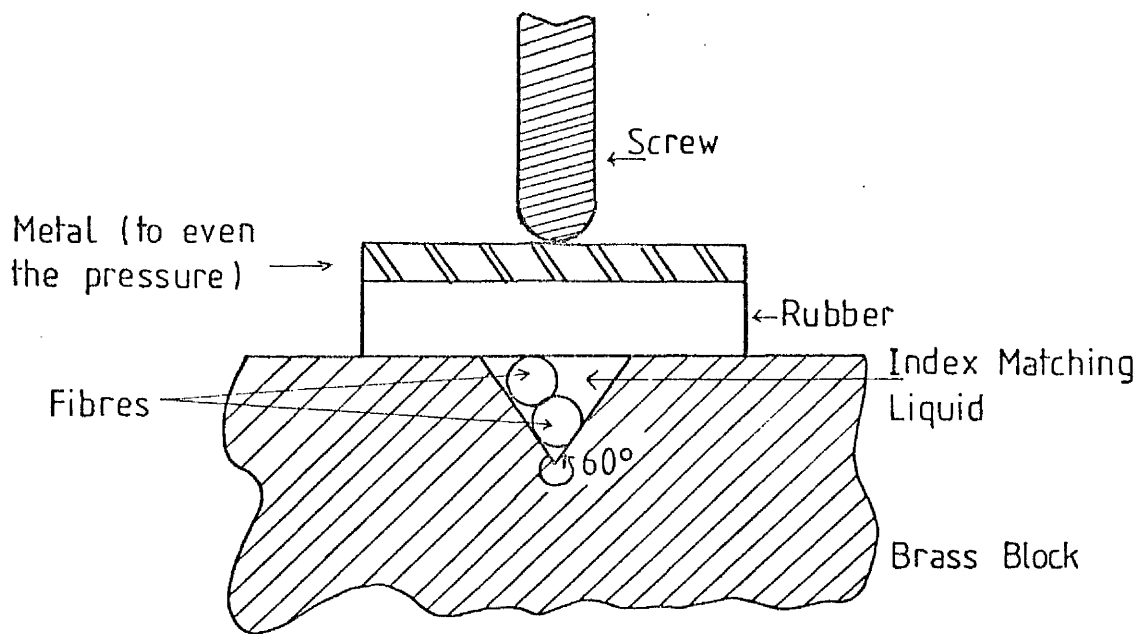
The two fibres to be coupled were then carefully placed into the groove, the modified areas in coincidence, with a drop of index matching liquid (Ethyl Salicylate, $n = 1.523$), before they were pressed together by means of a screw acting upon a steel plate (to even the pressure) and a rubber pad to avoid any damage to the fibres (fig. 4-9b).

The coupled length is given by the length of the steel plate (2.5cm) which was equal to the modified length of the fibres. This length was evaluated from the programme given in II-2.4.

Light from a helium neon laser ($\lambda = 632.8$ nm, $P = 6.87$ mW) was then launched into one of the fibres at the end of the other fibre with a



a) Brass Block



b) Detail of the Experimental Set-up

Fig.4.9 Coupling Device

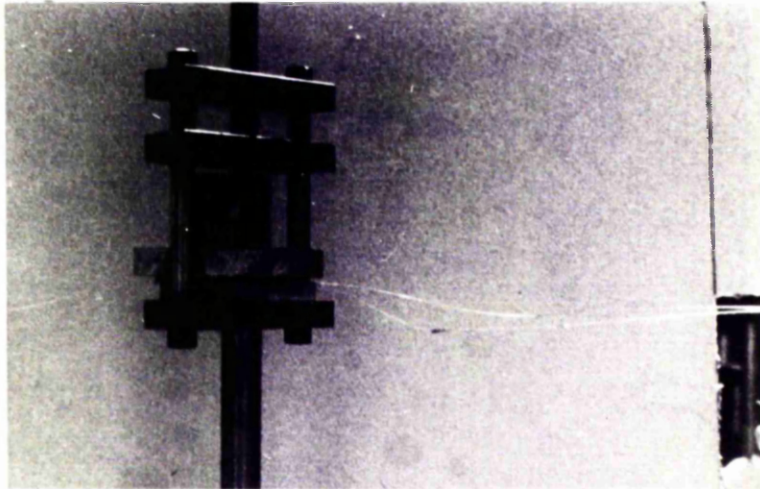


Figure 4.10: PHOTOGRAPH OF THE CLAMPING DEVICE.

photodiode. A travelling microscope could also be used in order to look at the nearfield pattern (fig. 4-11).

II-4.5 Results and Conclusion

The coupling efficiency of such a device can be evaluated with the two main characteristics which are:

$$\text{Coupling efficiency: } \eta = -10 \log \frac{P_2}{P_1} \quad (4-1)$$

$$\text{Directivity: } \delta = -10 \log \frac{P_3}{P_2} \quad (4-2)$$

These quantities were evaluated with the equipment shown in fig. 4-11. However, in most cases, the power contradirectionally coupled was too small to be accurately measured and only a rough estimation of it could be made.

The results for the efficiency ranged from 35 dB to 42 dB. For the directivity the results ranged from 40 to 50 dB. These results are below the theoretical predictions. This can be explained in two ways.

First, as stated in II-2.4, due to simplifications, the calculations overestimated the actual efficiency.

Secondly the fibres were stripped but no overall cladding was put round them once put together and thus a lot of power was lost, this being aggravated by the presence of index matching fluid. With these reasons in mind, the difference between theory and experiment can be understood.

The results were also in good agreement with the theory as regard to the fact that only high order modes were efficiently coupled. In fact it was noted that, after the modified region, the power tended to remain very near the periphery of the waveguides. This was greatly improved by the pseudo-annealing of the fibres after the modifying process (II-4.3.2.) simply because it allowed the index in the modified zone to remain close to its theoretical value (compaction effect).

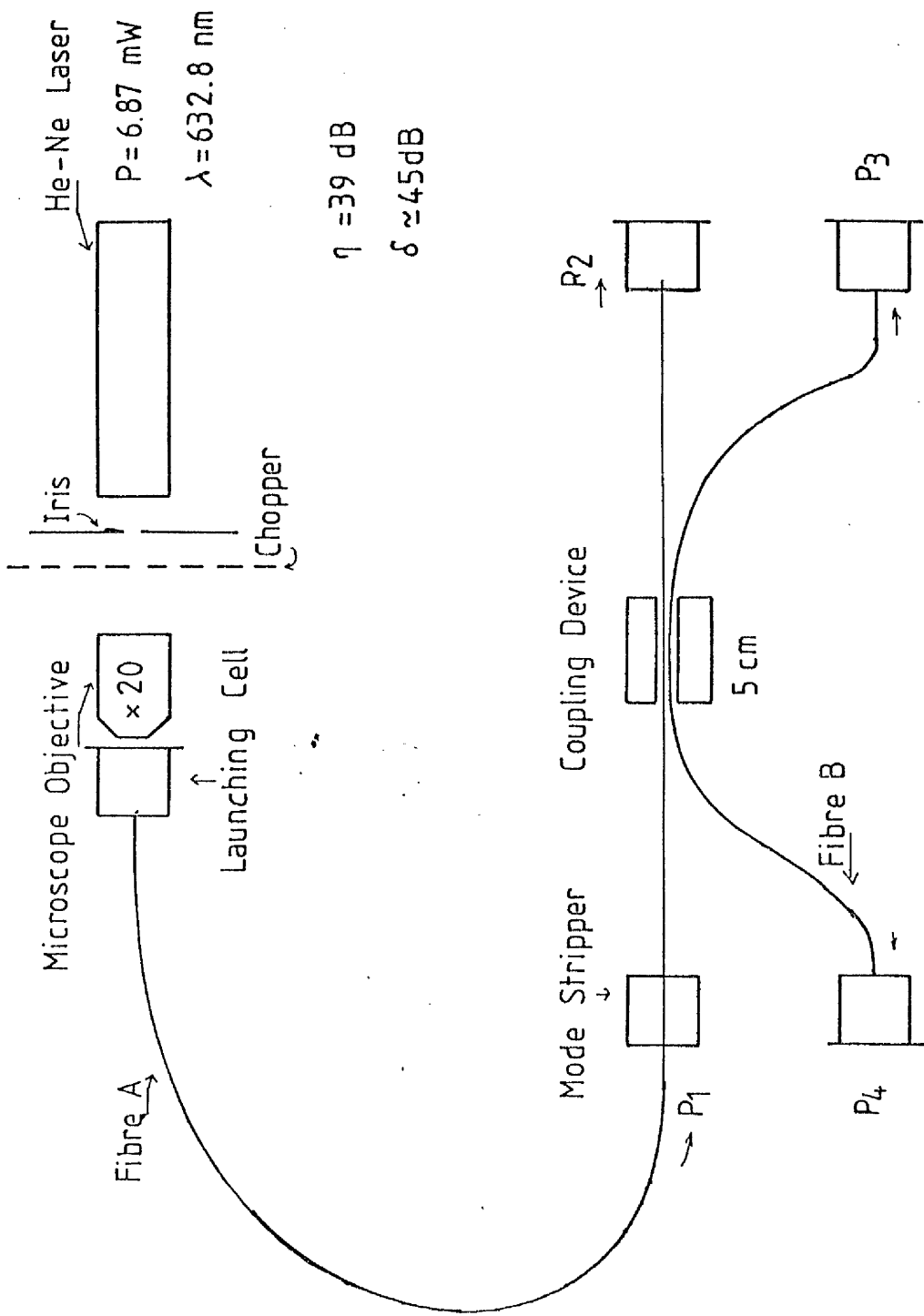


Fig.4.11 Apparatus Used to Measure the Coupling Efficiency

In conclusion the multimode fibre coupler proved to be an efficient way of tapping a relatively small amount of power from a "main" waveguide, this power being that contained in the high order modes.

It does not seem possible yet to couple power from the low order modes unless a means of having the cores actually touching each others is found and unless very large coupled lengths are achieved.

PART III

GRATING COUPLERS

CHAPTER I

INTRODUCTION

The linking of two integrated optical devices or connecting such devices to a fibre communication system requires a good coupler which, ideally, should be efficient, small, and able to work both from the integrated device to the fibre and vice-versa. Such devices are rather complex and it might be necessary to realise them in the laboratory with fibre ends protruding from the operational box in order to be coupled, with a conventional method, to the transmission fibres "on the field".

Two guides lying in close proximity are able to exchange power with high efficiency if the modes coupled are in synchronism. This study is concerned with contradirectional coupling between a single mode ribbon fibre and a thin film, the phase matching being achieved with help of a grating ([72],[73]).

Several other methods have already been proposed [74]. They are either based on end fire coupling where the fibre core is positioned at the end of the film or stripe ([15],[75]) or on evanescent wave coupling ([72],[76]), but all these methods require a very accurate alignment of flat and perpendicular end faces with matched modal fields.

Bulmer proposed [73] a way of avoiding these problems by using a grating coupler. However, the method used is based on directional coupling which may yield a low efficiency as the length of the coupling region (i.e. the grating) is critical. On top of this, the fibre used was a round one which brought problems as it needs to be stripped of its cladding and ~~the~~ its diameter to be reduced. An additional inefficiency resulted from the use of high order Bragg diffraction.

For these reasons it was decided to study the theory of a contradirectional coupler with a sandwich ribbon fibre. The advantages are that the power transfer is an exponential function of the coupling length instead of an oscillatory one and the sandwich ribbon fibre does not need a size reduction or a stripping of any cladding. Furthermore, in most cases, they can be made according to the desired specifications and tend to keep a polarisation along their length.

This method allows a high efficiency and can be used between fibres and films having a large effective index difference since the phase matching, as shown in section III - 3.2, is achieved by the grating when

$$|\beta_m + \beta_n| = \frac{2\pi}{\Lambda} \quad 5-1$$

where β_m and β_n are the film and fibre propagation coefficients and Λ is the grating pitch.

So, for any set of fibre and film, a given grating can be dimensioned to allow the coupling to take place.

PROPAGATION IN A SLAB AND IN A RECTANGULAR WAVEGUIDE

III 2.1. Introduction

In order to study and design a fibre/film coupler, it is necessary to know the guided mode characteristics in order to be able to phase match them. This chapter will thus be devoted to the evaluation of these parameters for homogeneous waveguides and for TE modes.

III 2.2. Slab waveguide

A complete expression of the modes for an asymmetric slab waveguide can be found once Maxwell's equations are solved for non conducting materials.

Using the notation $\nabla = \frac{\partial}{\partial x} \vec{e}_x + \frac{\partial}{\partial y} \vec{e}_y + \frac{\partial}{\partial z} \vec{e}_z$ (6-1)

where $\vec{e}_x, \vec{e}_y, \vec{e}_z$ are the unit vectors along the x, y and z axis, the equations can be written:

$$\begin{aligned} \nabla \times \vec{H} &= \epsilon_0 n^2 \frac{\partial E}{\partial r} \\ \nabla \times \vec{E} &= -\mu_0 \frac{\partial H}{\partial r} \end{aligned} \quad (6-2)$$

Assuming that there is no variation in the x direction:

$$\frac{\partial}{\partial x} = 0 \quad (6-3)$$

we can derive the expressions of the fields components which reduce to E_x, H_y, H_z , for TE modes, through the reduced wave equation

$$\frac{\partial^2 E_x}{\partial y^2} + (n^2 k^2 - \beta^2) E_x = 0 \quad (6-4)$$

with $k^2 = \epsilon_0 \mu_0 \omega^2 = \left(\frac{2\pi}{\lambda}\right)^2$ and after having matched the fields at the boundary and the vanishing conditions at $y = \pm \infty$ the field expressions are obtained [77].

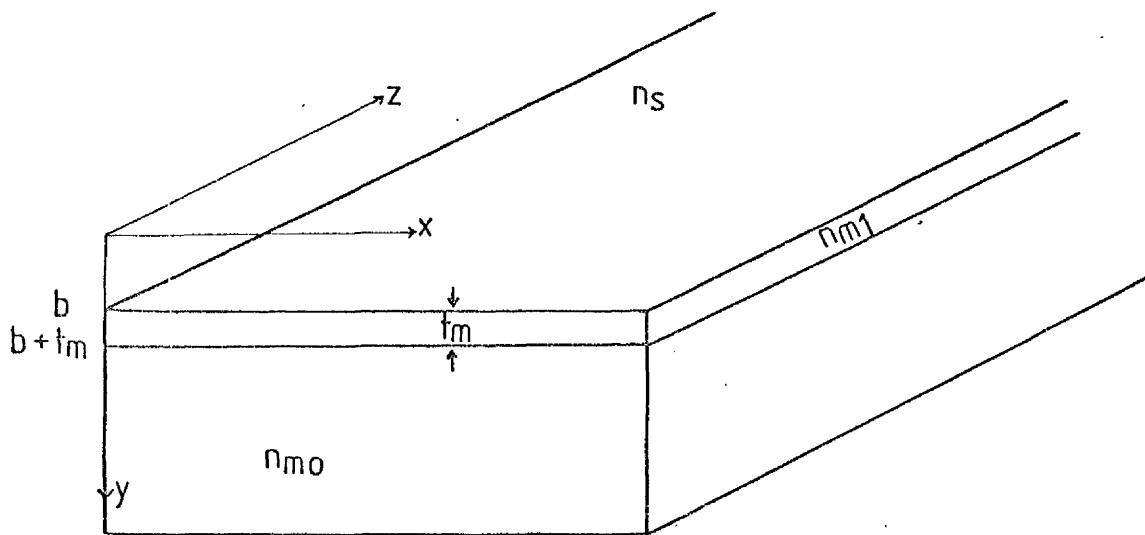


Fig.6.1 The Asymmetric Slab Waveguide

$$E_x = A_m e^{-\delta(y-b)} \quad \text{for } y \leq b \quad (6-5)$$

$$= A_m \left[\cos \kappa_m (b-y) - \frac{\delta_m}{\kappa_m} \sin \kappa_m (b-y) \right] \quad b \leq y \leq b+t_m$$

$$= A_m \left[\cos \kappa_m t_m - \frac{\delta_m}{\kappa_m} \sin \kappa_m t_m \right] e^{\gamma_m (t_m + b - y)} \quad b+t_m \leq y$$

$$\text{where } A_m = \frac{2\kappa_m \sqrt{\omega\mu_0 P_m}}{\sqrt{|\beta_m| \left(t_m + \frac{1}{\gamma_m} + \frac{1}{\delta_m} \right) (\kappa_m^2 + \delta_m^2)}} \quad (6-6)$$

$$\kappa_m = \sqrt{n_{m1}^2 k^2 - \beta_m^2} \quad (6-7)$$

$$\gamma_m = \sqrt{\beta_m^2 - n_o^2 k^2} \quad (6-8)$$

$$\delta_m = \sqrt{\beta_m^2 - n_s^2 k^2} \quad (6-9)$$

P_m is the power per unit length in the x direction for the mode:

$$\delta_{mn} P_m = \frac{\beta_m}{2\omega\mu_0} \int_{-\infty}^{+\infty} E_n(y) E_m^*(y) dy = \frac{\beta_m}{2\omega\mu_0} \int_{-\infty}^{+\infty} E_m^2(y) dy \quad (6-10)$$

$$H_y = -\frac{\beta_m}{\omega\mu_0} E_x \quad (6-11)$$

$$H_z = \frac{i}{\omega\mu_0} \frac{\partial E_x}{\partial y} \quad (6-12)$$

III 2.3. Stripe waveguide

The Sandwich ribbon (S.R.) fibre can be approximated to a strip waveguide as described on Fig. 6-2. Due to a more complex structure several approximations are necessary to evaluate the field in the different areas defined by the structure.

The assumptions made here are the ones used by Marcatili [78]. It is assumed that the mode propagating is far from cut-off which

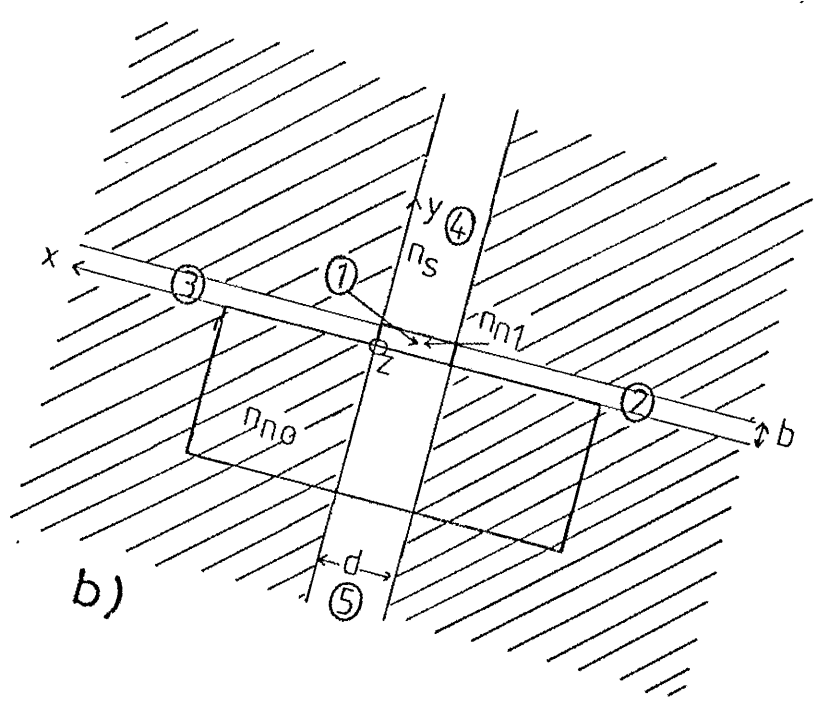
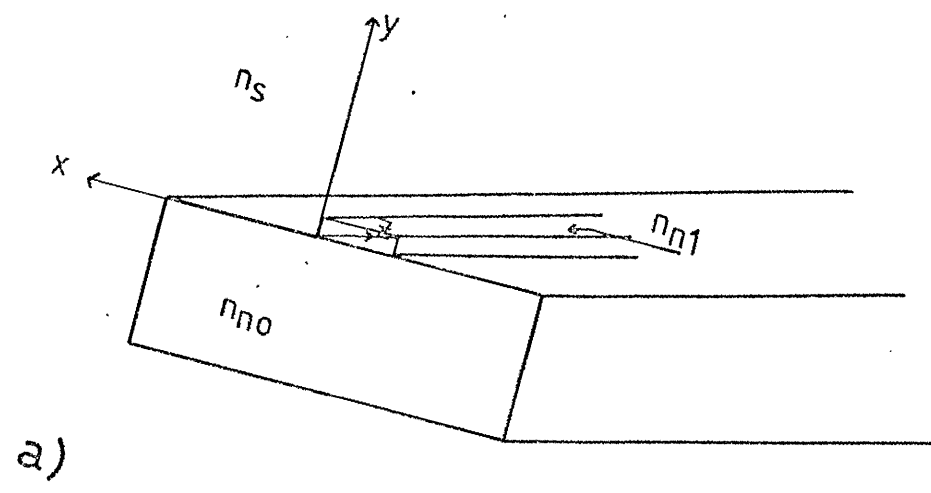


Fig.6.2 The Stripe Waveguide

means that the field is well confined in the region of the core and there is very little energy in the shaded areas of Fig 6-2b. Thus, these four regions are ignored in this analysis.

It is then possible to express the transverse field components in terms of the longitudinal components and Maxwell's equations (6-2) may be written:

$$E_x = - \frac{j}{n_j^2 k^2 - \beta_n^2} \left(\beta_n \frac{\partial E_z}{\partial x} + \omega \mu_0 \frac{\partial H_z}{\partial y} \right) \quad (6-13)$$

$$E_y = - \frac{j}{n_j^2 k^2 - \beta_n^2} \left(\beta_n \frac{\partial E_z}{\partial y} - \omega \mu_0 \frac{\partial H_z}{\partial x} \right) \quad (6-14)$$

$$H_x = - \frac{j}{n_j^2 k^2 - \beta_n^2} \left(\beta_n \frac{\partial H_z}{\partial x} - \omega n_j^2 \epsilon_0 \frac{\partial E_z}{\partial y} \right) \quad (6-15)$$

$$H_y = - \frac{j}{n_j^2 k^2 - \beta_n^2} \left(\beta_n \frac{\partial H_z}{\partial y} + \omega n_j^2 \epsilon_0 \frac{\partial E_z}{\partial x} \right) \quad (6-16)$$

where the subscript j assumes the values 1, 2, 3, 4, 5 for each of the five regions of the waveguide.

The waveguide can support two types of modes. One is polarized predominantly in the x direction and is call E_{pq}^x and the other is the y direction (E_{pq}^y). The amplitude coefficients will be adjusted so that the case of an E_{pq}^x mode is considered. Again omitting the factor $e^{j(\omega t - \beta_n z)}$ we have in region 1 and after some mathematical manipulations and matching of the field components at infinity:

$$-d \leq x \leq 0 \quad 0 \leq y \leq b$$

$$E_x^1 = \frac{jAn}{k_x \beta_n} (n_1^2 k^2 - k_x^2) \sin k_x (x + \xi) \cos k_y (y + \eta) \quad (6-17)$$

$$\text{with:} \quad n_1^2 k^2 - \beta_n^2 = k_x^2 + k_y^2 \quad (6-18)$$

$$\text{in region 2:} \quad x \leq -d \quad 0 \leq y \leq b$$

$$E_x^2 = jA_n \frac{(\gamma_2^2 + n_2^2 k^2)}{\gamma_2 \beta_n} \cos \kappa_x (\xi-d) \cos \kappa_y (y+\eta) \exp[\gamma_2(x+d)] \quad (6-19)$$

$$\text{with:} \quad n_2^2 k^2 - \beta_n^2 = \kappa_y^2 - \gamma_2^2 \quad (6-20)$$

$$\text{in region 3:} \quad 0 \leq x \quad 0 \leq y \leq b$$

$$E_x^3 = -jA_n \frac{\gamma_3^2 + n_3^2 k^2}{\gamma_3 \beta_n} \cos \kappa_x \xi \cos \kappa_y (y+\eta) \exp(-\gamma_3 x) \quad (6-21)$$

$$\text{with:} \quad n_3^2 k^2 - \beta_n^2 = \kappa_y^2 - \gamma_3^2 \quad (6-22)$$

$$\text{in region 4:} \quad -d \leq x \leq 0 \quad b \leq y$$

$$E_x^4 = jA_n \frac{n_1^2}{n_4^2} \frac{n_4^2 k^2 - \kappa_x^2}{\kappa_x \beta_n} \cos \kappa_y (b+\eta) \sin \kappa_x (x+\xi) \exp[-\gamma_4(y-b)] \quad (6-23)$$

$$\text{with:} \quad n_4^2 k^2 - \beta_n^2 = \kappa_x^2 - \gamma_4^2 \quad (6-24)$$

$$\text{and finally in region 5:} \quad -d \leq x \leq 0 \quad y \leq 0$$

$$E_x^5 = jA_n \frac{n_1^2}{n_5^2} \frac{n_5^2 k^2 - \kappa_x^2}{\kappa_x \beta_n} \cos \kappa_y \eta \sin \kappa_x (x+\xi) \exp \gamma_5 y \quad (6-25)$$

$$\text{with:} \quad n_5^2 k^2 - \beta_n^2 = \kappa_x^2 - \gamma_5^2 \quad (6-26)$$

It must be noted that E_x is only continuous due to the fact that κ_x^2 is neglected in comparison with $n^2 k^2$ and that E_y is only approximately zero in the regions 4 and 5.

Matching the field at the boundaries $x = 0$ and $x = -d$ yields:

$$\frac{n_1^2}{\kappa_x} \sin \kappa_x (\xi-d) - \frac{n_2^2}{\gamma_2} \cos \kappa_x (\xi-d) = 0 \quad (6-27)$$

$$\frac{n_1^2}{\kappa_x} \sin \kappa_x \xi + \frac{n_3^2}{\gamma_3} \cos \kappa_x \xi = 0 \quad (6-28)$$

The solution of these equations gives the eigenvalue equation:

$$\tan \kappa_x d = \frac{n_1^2 \kappa_x (n_3^2 \gamma_2 + n_2^2 \gamma_3)}{n_3^2 n_2^2 \kappa_x^2 - n_1^4 \gamma_1 \gamma_3} \quad (6-29)$$

The equation (6-28) yields the phase parameter ξ :

$$\tan \kappa_x \xi = -\frac{n_3^2 \kappa_x}{n_1^2 \gamma_3} \quad (6-30)$$

while γ_2 is given by (6-18) and (6-20) and γ_3 by (6-18) and (6-22):

$$\gamma_2 = \sqrt{(n_1^2 - n_2^2) k^2 - \kappa_x^2} \quad (6-31)$$

$$\gamma_3 = \sqrt{(n_1^2 - n_3^2) k^2 - \kappa_x^2} \quad (6-32)$$

Matching the field components at the boundaries $y = b$ and $y = 0$ yields:

$$\kappa_y \sin \kappa_y (b + \eta) - \gamma_4 \cos \kappa_y (b + \eta) = 0 \quad (6-33)$$

$$\kappa_y \sin \kappa_y \eta + \gamma_5 \cos \kappa_y \eta = 0 \quad (6-34)$$

Equation (6-34) gives:

$$\tan \kappa_y \eta = -\frac{\gamma_5}{\kappa_y} \quad (6-35)$$

and the vanishing system determinant of (6-33), (6-34) yields the eigenvalue equation:

$$\tan \kappa_y b = \kappa_y \frac{\gamma_4 + \gamma_5}{\kappa_y^2 - \gamma_4 \gamma_5} \quad (6-36)$$

with γ_4 given by (6-18) and (6-24) and γ_5 by (6-18) and (6-26):

$$\gamma_4 = \sqrt{(n_1^2 - n_4^2) k^2 - \kappa_y^2} \quad (6-37)$$

$$\gamma_5 = \sqrt{(n_1^2 - n_5^2) k^2 - \kappa_y^2} \quad (6-38)$$

The knowledge of κ_x and κ_y allows the evaluation of the propagation constant β_n from (6-18):

$$\beta_n = \sqrt{n_1^2 k^2 - (\kappa_x^2 + \kappa_y^2)} \quad (6-39)$$

Considering that the substrate thickness is infinite the Power contained in the mode is given by:

$$\delta_{nm} P_n = \frac{\beta_m}{2\omega\mu_0} \int_{-\infty}^{+\infty} \int_{-\infty}^{+\infty} |E_x|^2 dy dx \quad (6-40)$$

which after some computation gives in the case considered for $n_1 = n_{n_1}$, $n_2 = n_3 = n_4 = n_s$, $n_5 = n_{n_0}$:

$$P_n = \frac{A_n^2 \beta_n}{2\omega \mu_0} \left(\left(\frac{d}{2} + \frac{\sin 2\kappa_x (\xi-d) - \sin 2\kappa_x \xi}{4\kappa_x} \right) \left(\frac{\theta_1^2}{2\gamma_5} + \frac{\theta_3^2}{2} + \frac{\theta_5^2}{2\gamma_4} \right) + \left(\frac{b}{2} + \frac{\sin 2\kappa_y (b+\eta) - 2 \sin 2\kappa_y \eta}{4\kappa_y} \right) \left(\frac{\theta_2^2}{2\gamma_2} + \theta_3^2 \frac{\sin 2\kappa_x (\xi-d) - \sin 2\kappa_x \xi}{4\kappa_x} + \frac{\theta_4^2}{2\gamma_3} \right) \right) \quad (6-41)$$

with:

$$\theta_1 = j \frac{n_{n_1}^2}{n_{n_0}^2} \frac{n_{n_0}^2 k^2 - \kappa_x^2}{\kappa_x \beta} \cos \kappa_y \eta \quad (6-42)$$

$$\theta_2 = j \frac{\gamma_2^2 + n_s^2 k^2}{\gamma_2 \beta} \cos \kappa_x (\xi - d) \quad (6-43)$$

$$\theta_3 = j \frac{n_{n_1}^2 k^2 - \kappa_x^2}{\kappa_x \beta} \quad (6-44)$$

$$\theta_4 = -j \frac{\gamma_3^2 + n_s^2 k^2}{\gamma_3 \beta} \cos \kappa_x \xi \quad (6-45)$$

$$\theta_5 = j \frac{n_1^2}{n_s^2} \frac{n_s^2 k^2 - \kappa_x^2}{\kappa_x \beta} \cos \kappa_y (b + \eta) \quad (6-46)$$

and this completes the determination of the E_{pq}^x mode, the integers p and q being given by the order of the solutions of the eigenvalue equations (6-29) and (6-36).

CHAPTER III

COUPLING COEFFICIENT

III 3.1. Coupled mode theory

The aim of this study is to design a fibre-film coupler. The film and fibre modes are phase-matched by a periodic perturbation. But first, in order to understand the coupling mechanism, the general coupled mode equations must be derived.

If we consider two modes travelling in opposite directions in a loss-less medium, they can be described by [79]:

$$a(z) = A(z) e^{j(\omega t - \beta_a z)} \quad (7-1)$$

for the mode travelling in the forward direction and:

$$b(z) = B(z) e^{j(\omega t + \beta_b z)} \quad (7-2)$$

for the other one, A_i being the mode amplitude and varying slowly with z .

The coupled mode equations can be written:

$$\frac{\partial a}{\partial z} = -j \beta_a a + j c_{ab} b \quad (7-3)$$

$$\frac{\partial b}{\partial z} = j c_{ba} a + j \beta_b b \quad (7-4)$$

where c_{ab} and c_{ba} are the coupling coefficients between the modes.

Assuming that the coupling is uniform c_{ab} and c_{ba} are constant along the interaction length. Finally β_a and β_b are the mode propagation coefficients in the presence of coupling and are very close to their value for an isolated guide.

Substitution of equation (7-1), (7-2) in equation (7-3), (7-4) leads to:

$$\frac{\partial A}{\partial z} = j c_{ab} B e^{j(\beta_a + \beta_b)z} \quad (7-5)$$

$$\frac{\partial B}{\partial z} = j c_{ba} A e^{-j(\beta_a + \beta_b)z} \quad (7-6)$$

Conservation of total power can be then written:

$$\frac{d}{dz} (|A|^2 - |B|^2) = 0 \quad (7-7)$$

which is satisfied if:

$$c_{ab} = c_{ba}^* \quad (7-8)$$

If we consider an incident wave $a(z)$, it has an amplitude $A_0 = A(0)$ at $z \leq 0$ (Fig. 7-1) before the perturbed region and the other wave $b(z)$ has an amplitude $B(L) = B_0 = 0$ for $z \geq L$. With these boundary conditions, it is possible to solve equations (7-5), (7-6), the solution being:

$$A(z) = A(0) \frac{e^{j(\Delta z/2)} \times [\Delta \sinh(\frac{S}{2}(z-L)) + j S \cosh(\frac{S}{2}(z-L))]}{-\Delta \sinh(\frac{SL}{2}) + j S \cosh(\frac{SL}{2})} \quad (7-9)$$

$$B(z) = A(0) \frac{2j c_{ab} e^{-j(\Delta z/2)} \times \sinh(\frac{S}{2}(z-L))}{-\Delta \sinh(\frac{SL}{2}) + j S \cosh(\frac{SL}{2})} \quad (7-10)$$

$$\text{with: } \Delta = \beta_a + \beta_b \quad (7-11)$$

$$S = \sqrt{4|c_{ab}|^2 - \Delta^2} \quad (7-12)$$

If phase matching is achieved $\Delta = 0$ and we have:

$$A(z) = A(0) \times \frac{\cosh[|c_{ab}|(z-L)]}{\cosh(|c_{ab}|L)} \quad (7-13)$$

$$B(z) = A(0) \times \frac{c_{ab}}{|c_{ab}|} \times \frac{\sinh[|c_{ab}|(z-L)]}{\cosh(|c_{ab}|L)} \quad 7-14$$

Fig. (7-1) shows a plot of the transfer of power for this case. It depicts clearly the advantage of such a coupling device since the power transfer is exponential as regard to the coupling length while it is oscillatory for directional coupling [80].

III 3.2. Coupling by means of a grating (TE modes)

When a perturbation such as a grating is introduced the modes are affected and this can be expressed by a perturbation term ([81],[82])

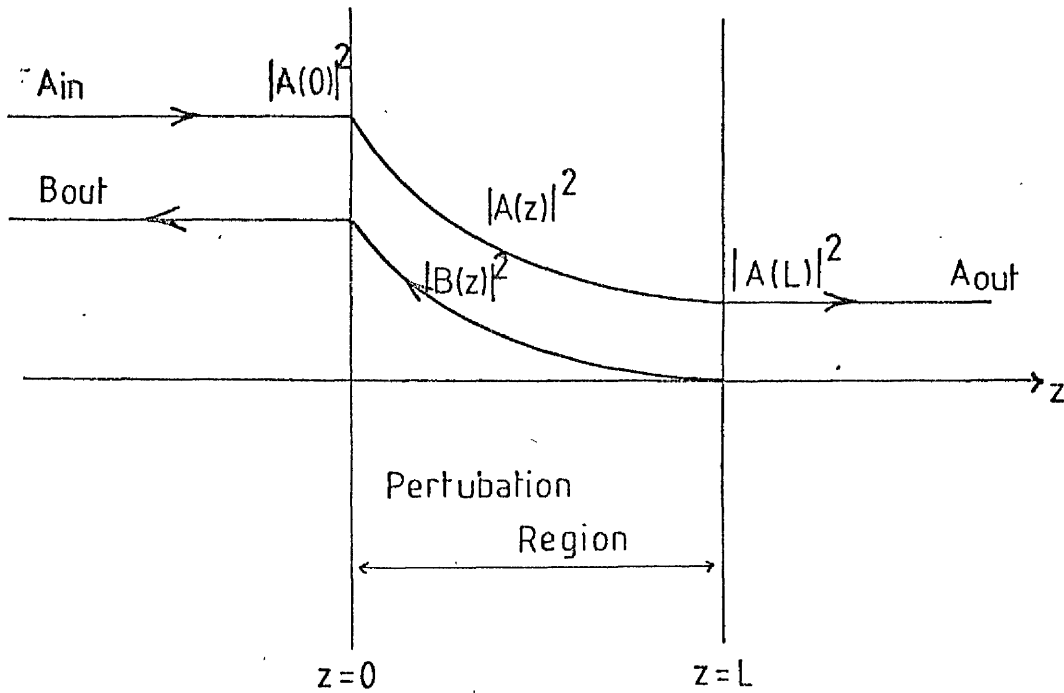


Fig.7.1 Transfer of Power from the Incident Wave to a Reflected Wave.

in the wave equation.

For two isolated guides, the transverse fields are:

$$E_m(y)e^{-j\beta_m z} \text{ and } E_n(y)e^{j\beta_n z}$$

if we consider the coordinate system depicted in Fig (6-2). When two structures are coupled, the electric field of the ensemble can be written:

$$E(y,z) = V_n(y) E_n(y,z) e^{j\beta_n z} + V_m E_m(y,z) e^{-j\beta_m z} \quad (7-15)$$

The perturbation (i.e. the grating) induces a change in the permittivity which can be expressed by:

$$\epsilon = \epsilon_0 [\epsilon(y) + \Delta\epsilon(y,z)] \quad (7-16)$$

$$\left(\frac{\partial^2}{\partial x^2} + \frac{\partial^2}{\partial y^2} + \frac{\partial^2}{\partial z^2} + k^2 \epsilon(y) \right) \vec{E}_1 = -k^2 \Delta\epsilon \vec{E}_0 \quad (7-17)$$

where $\vec{E} = \vec{E}_0 + \vec{E}_1$ \vec{E}_1 being the perturbation term and \vec{E}_0 the unperturbed term which is assumed to satisfy the wave equation.

To evaluate the coupling coefficient, it is useful to consider E_n as being the perturbation term E_1 and E_m as E_0 which yields:

$$\left[\frac{\partial^2}{\partial y^2} + \frac{\partial^2}{\partial z^2} + k^2 \epsilon(y) \right] V_n(z) E_n(y) e^{j\beta_n z} = -k^2 \Delta\epsilon(y,z) E_m(y) V_m(z) e^{-j\beta_m z} \quad (7-18)$$

The field of the isolated guides satisfies the unperturbed wave equation thus:

$$\left[\frac{\partial^2}{\partial y^2} + \frac{\partial^2}{\partial z^2} + k^2 \epsilon(y) \right] E_n(y) e^{j\beta_n z} = 0 \quad (7-19)$$

which gives after substitution of (7-19) in (7-18):

$$E_n(y) e^{j\beta_n z} \left[\frac{\partial^2 V_n(z)}{\partial z^2} + 2j\beta_n \frac{\partial V_n(z)}{\partial z} \right] = -k^2 \Delta\epsilon(y,z) E_m(y) V_m(z) e^{-j\beta_m z} \quad (7-20)$$

For weak coupling V_n varies slowly with z so:

$$\frac{\partial^2 V_n(z)}{\partial z^2} \ll 2j\beta_n \frac{\partial V_n(z)}{\partial z} \quad (7-21)$$

and $\frac{\partial^2 V_n(z)}{\partial z^2}$ can be neglected.

After multiplication of the two sides of (7-20) by $\frac{\beta_m}{2\omega\mu_0}$ $E_n^*(y) e^{-j\beta_n z}$ and integration over the whole cross section, equation (7-20) becomes:

$$\begin{aligned} \iint_{-\infty}^{\infty} E_n(y) E_n^*(y) \frac{\beta_m}{2\omega\mu_0} [2j\beta_n \frac{\partial V_n}{\partial z}] dy dx = & \quad (7-22) \\ \iint_{-\infty}^{\infty} -k^2 \Delta\epsilon V_m(z) E_m E_n^*(y) \frac{\beta_m}{2\omega\mu_0} e^{-j(\beta_m + \beta_n)z} dx dy & \end{aligned}$$

The orthogonality condition (6-40) can be written here:

$$\frac{\beta_m}{2\omega\mu_0} \iint_{-\infty}^{+\infty} E_n(y) E_m^*(y) dx dy = P_m \delta_{mn} \quad (7-23)$$

with $\delta_{mn} = 0$ if $m \neq n$
 $\delta_{mn} = 1$ if $m = n$

Hence:

$$2j\beta_m \frac{\partial V_n}{\partial z} P_n = - \frac{k^2 \beta_m}{2\omega\mu_0} e^{-j(\beta_m + \beta_n)z} V_m(z) \iint_{-\infty}^{+\infty} E_m(y) E_n^*(y) \Delta\epsilon dx dy \quad (7-24)$$

The dielectric variation $\Delta\epsilon$ produced by the grating can be represented by a Fourier series:

$$\Delta\epsilon = \sum_i D_1(y) e^{j\frac{2\pi iz}{\Lambda}} [u(y-b-d_1)-u(y-b-d_1-\delta)] x [u(z)-u(z-L)] x [u(x+d)-u(x)] \quad (7-25)$$

where the function $u(x)$ defines the spatial limits of the grating

- i) $u(x) = 0$ if $x < 0$
- ii) $u(x) = 1$ if $x \geq 0$
- iii) Λ is the grating periodicity,
- iv) d_1 is the gap width (see Fig.(7-3)),
- v) L is the grating length,
- vi) δ is the grating depth,
- vii) $D_1(y)$ are the Fourier coefficients of the grating.

For a sinusoidal grating etched on the film, the Fourier coefficients are reduced to one which is [83]:

$$D_1(y) = \frac{n_m^2 - n_s^2}{4} \quad (7-26)$$

It was decided to use sinusoidal gratings in order to avoid any trouble with the grating higher harmonics caused by random non-uniformity.

The phase matching equation for contradirectional coupling is:

$$|\beta_m + \beta_n| = \frac{2\pi}{\Lambda} \quad (5-1)$$

Considering a long grating which exactly phase matches the modes, the length term in (7-25) can be ignored.

Substituting (7-25), (7-26), (5-1) in (7-24) yields:

$$2j P \frac{\partial v_n}{\partial z} = -k^2 \frac{V_m(z)}{2\omega\mu_0} \int_{-d}^0 \int_{b+d_1}^{b+d_1+\delta} E_m(y) E_n^*(y) D_1(y) dy dx \quad (7-28)$$

Thus, from equations (7-5), (7-6):

$$\frac{\partial V_n}{\partial z} = \left(j \frac{k^2}{4\omega\mu_0 P_n} \int_{-d}^{b+d} \int_{b+d_1}^{b+d_1+\delta} \frac{n_{m1}^2 - n_s^2}{4} E_m(y) E_n^*(y) dy dx \right) V_m(z) = j c_{nm} V_m(z) \quad (7-29)$$

As, according to equation (7-8), $c_{nm} = c_{mn}^*$ we can derive the coupling coefficient:

$$c = \sqrt{c_{nm} c_{mn}} = \sqrt{c_{nm} c_{nm}^*} \quad (7-30)$$

which gives:

$$c = \frac{k^2}{4\mu_0 \omega \sqrt{P_n P_m}} \int_{-d}^0 \int_{b+d_1}^{b+d_1+\delta} \frac{n_{m1}^2 - n_s^2}{4} E_m(y) E_n^*(y) dy dx \quad (7-31)$$

For the case depicted in Fig (7-2), the coupling coefficient can be written, using the field expressions derived in chapter III-22 and III-23:

$$c = X_1 \frac{2}{\kappa_x (\delta_m - \gamma_4)} \sin \kappa_x d \cos \kappa_x (2\xi - d) [e^{(\delta_m - \gamma_4)d_1} - e^{(\delta_m - \gamma_4)(d_1 + \delta)}] \quad (7-32)$$

with:

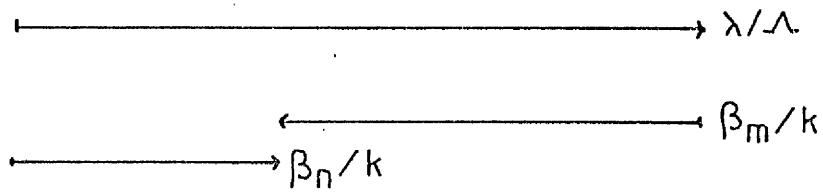
$$X_1 = \frac{k^2 A_m A_n}{4\mu_0 \omega \sqrt{P_n P_m}} \frac{n_{m1}^2 - n_s^2}{4} \frac{n_{n1}^2}{n_s^2} \frac{k^2 n_s^2 - \kappa_x^2}{\kappa_x \beta_n} \cos \kappa_y (b + \eta) \quad (7-33)$$

III 3.3 Numerical results

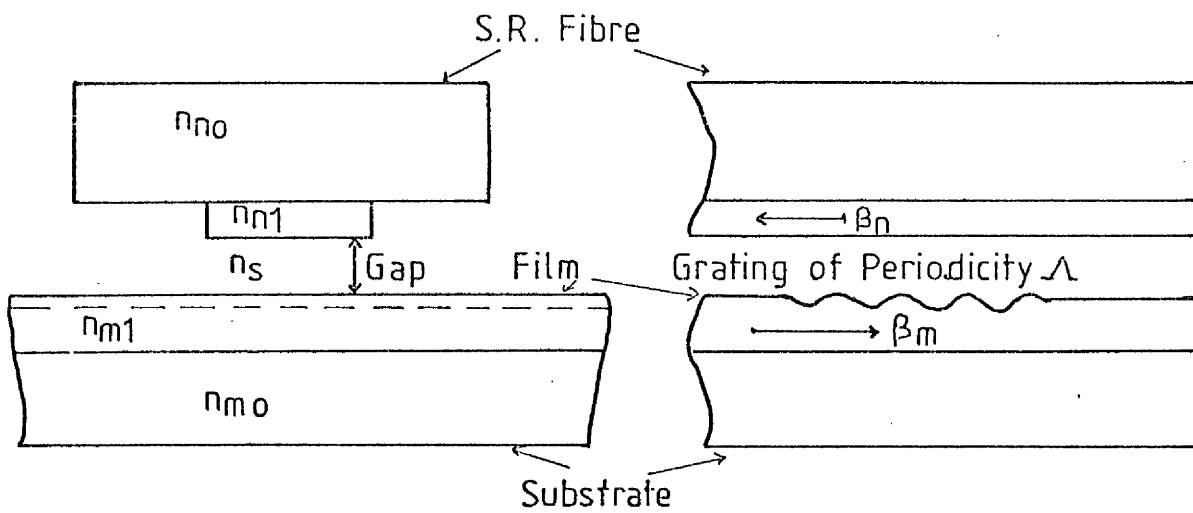
In order to evaluate the coupling coefficient in various cases and to estimate the influence of the different parameters a computing programme was written and this section is devoted to the analysis of its results.

III 3.3.1 Description of the model

All the different components of this model are supposed to be ideal. Thus the fibre core is assumed to have a perfect rectangular shape with uniform dimensions through its whole length. It is



a) Wave Vector Diagrams



b) Model for the Evaluation of the Coupling Coefficient

Fig.7.2 Contradirectional Grating Coupler

monomode but very close to the cut off of the second mode in order to satisfy the "far from cut-off" condition.

The grating is perfectly sinusoidal and its depth is constant through the whole coupling length. Its dimensions allow perfect phase matching.

Finally the input beam as well as the fibre are exactly perpendicular to the grating.

a) Fibre As it was possible to make a wide range of fibres, computation were made for various types.

The computations are made according to Marcatili's model [78]. Once the two glasses for a S.R. fibre are chosen, the dimensions of the core are calculated so that its width is 9 microns and the fibre carries only the E_{11}^x mode, being close to the cut-off thickness of the E_{21}^x mode.

The programme allows one to evaluate the corresponding propagation characteristics ($\beta_n, \kappa_x, \kappa_y$) which yield the field expression in the fibre.

b) Film The programme computes the propagation constant of TE modes in the waveguide for various thicknesses according to the expressions derived in III 2.2. The thickness expression was however corrected to take into account the change in the propagation constant due to the grating as Streifer proposes [83].

The wavelength of the launched beam is .6328 μm .

c) Grating It is assumed to be perfectly sinusoidal and is etched into the film over a length L, the coupling coefficient allowing one to work out the length necessary to achieve the best efficiency according to the expression of the coupling efficiency C [85]:

$$C = \tan h^2 (cL) \quad (7-34)$$

The grating periodicity is assumed to exactly satisfy the phase matching condition (5-1).

d) Coupler It is described on Fig (7-3). The fibre is pressed on the grating with a rubber pad. The gap, always present, is denoted by d_1 . It is assumed that d_1 is about 0.1 micron ($\approx \frac{\lambda}{6}$) which is reasonable [86]; however the influence of this parameter on the coupling efficiency is not very great as shown in III 3.3.2. The gap can be filled with either air or index matching fluid.

III 3.3.2. Computed results and conclusion

The results are given in the form of curves plotted by the computer. The curves give the coupling coefficient per centimeter or the coupling efficiency for a 4mm grating versus the film thickness.

Fig. 7-4 shows a typical curve depicting the first two modes of the slab waveguide. The maximum coupling coefficient is reached very soon after cut-off and then decreases. This is due to the fact that close to cut-off the power is not confined in the film and has a strong evanescent tail.

The grating depth has an influence on the coupling and this is clearly visible in Fig. 7-5. When the grating depth changes from 300 Å to 600 Å the coupling coefficient doubles. This proves that a higher efficiency is obtained with a deep grating.

As the gap dimension was only estimated, it was important to check its influence. Fig. 7-6 shows that the influence of this parameter is not drastic, especially when the thickness of the slab is not optimised to give the highest coupling coefficient.

It was also important to consider what type of fibres and what type of films would give the best efficiency. Fig. 7-7a and 7-7b show the efficiency achieved with some of the available fibres. They show clearly that, as expected, the higher the index difference in

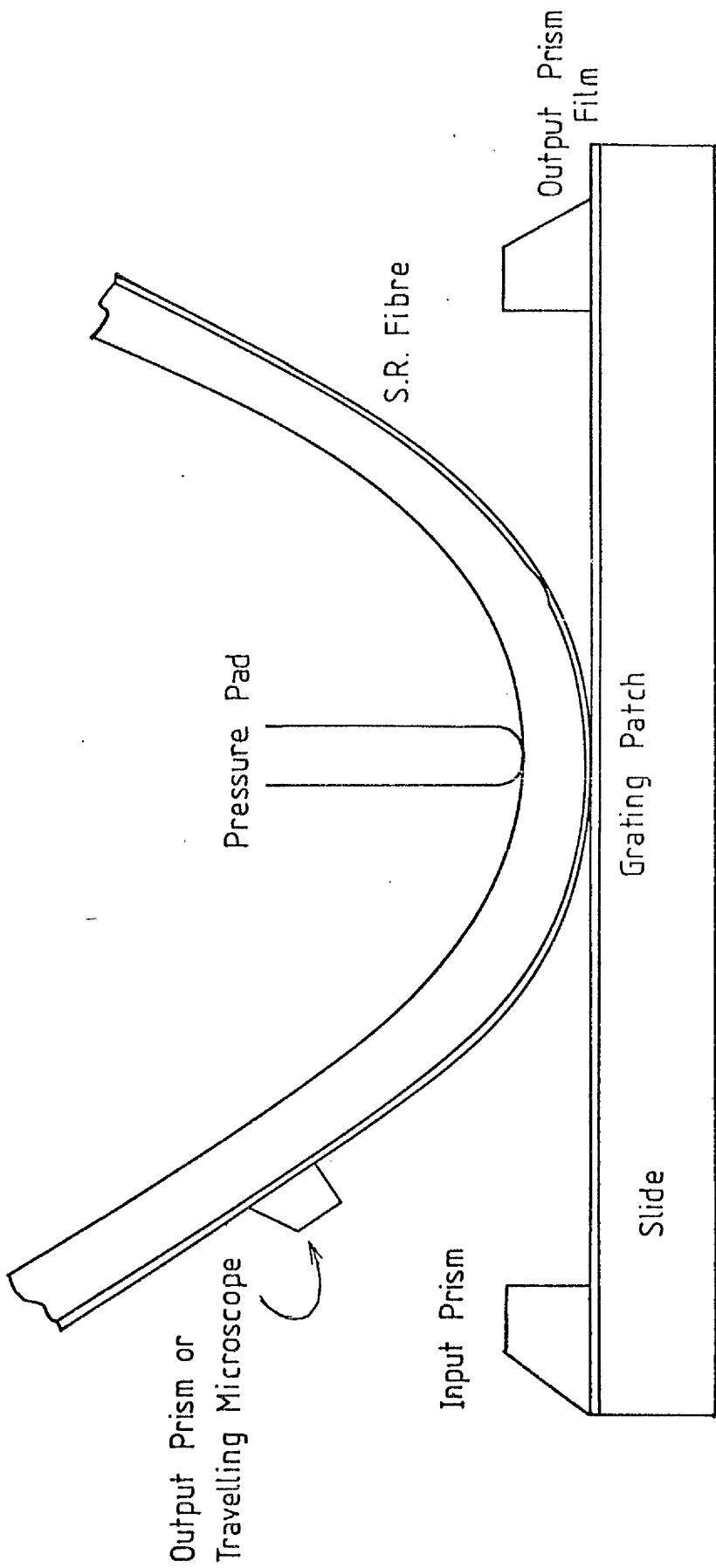


Fig.7.3 Coupling Device

7059/SILICA

LF3/LF8

COUPLING COEFFICIENT IN CM-1

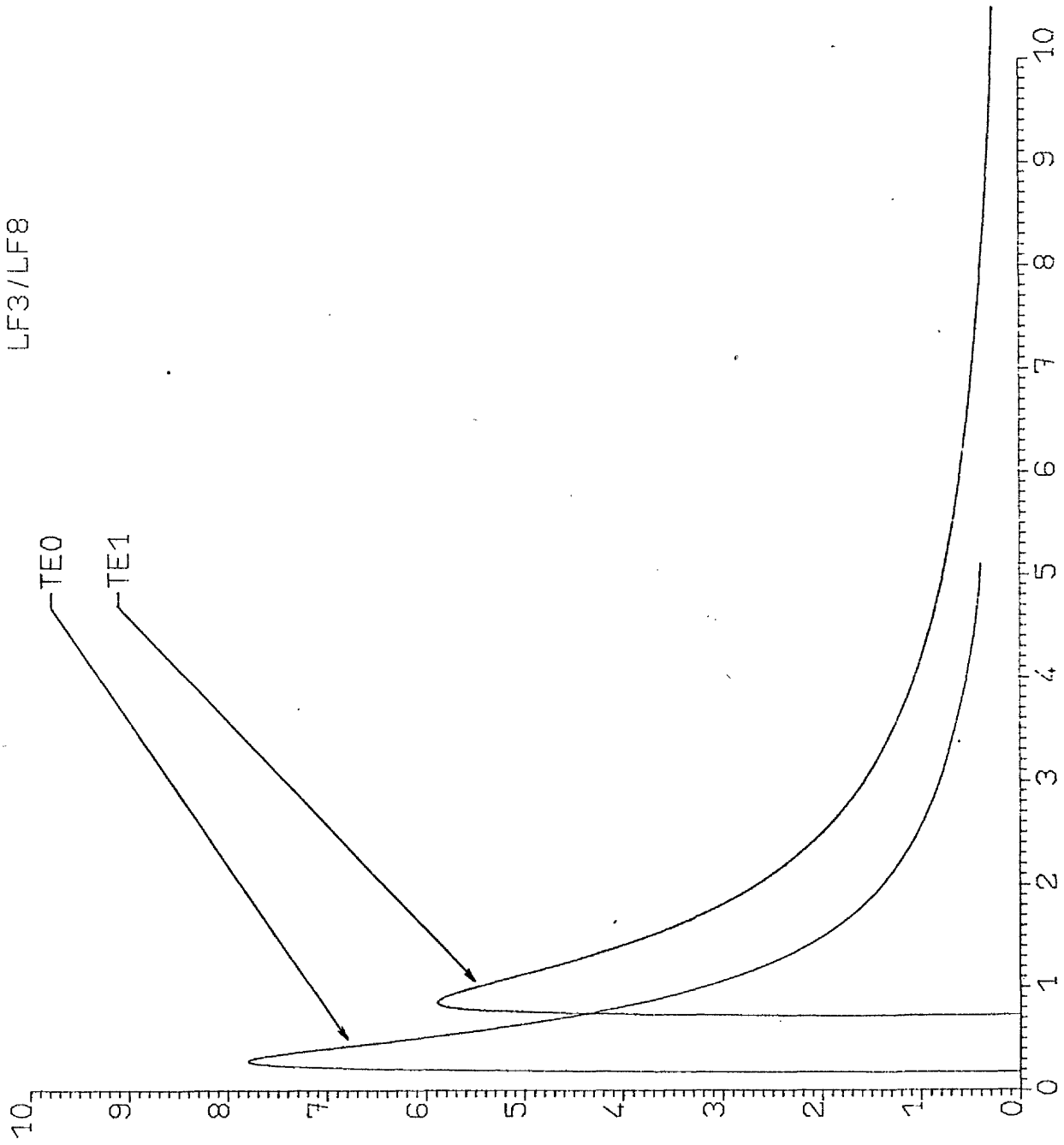


FIG:7.4: Coupling Coefficient VS Film Thickness

COUPLING COEFFICIENT IN CM-1

FILM INDICES: $n_{m0}=1.5125$ $n_{m1}=1.568$
SR FIBRE INDICES: $n_{s0}=1.5618$ $n_{s1}=1.5793$
GRATING DEPTH: $2H$

MODE TE0

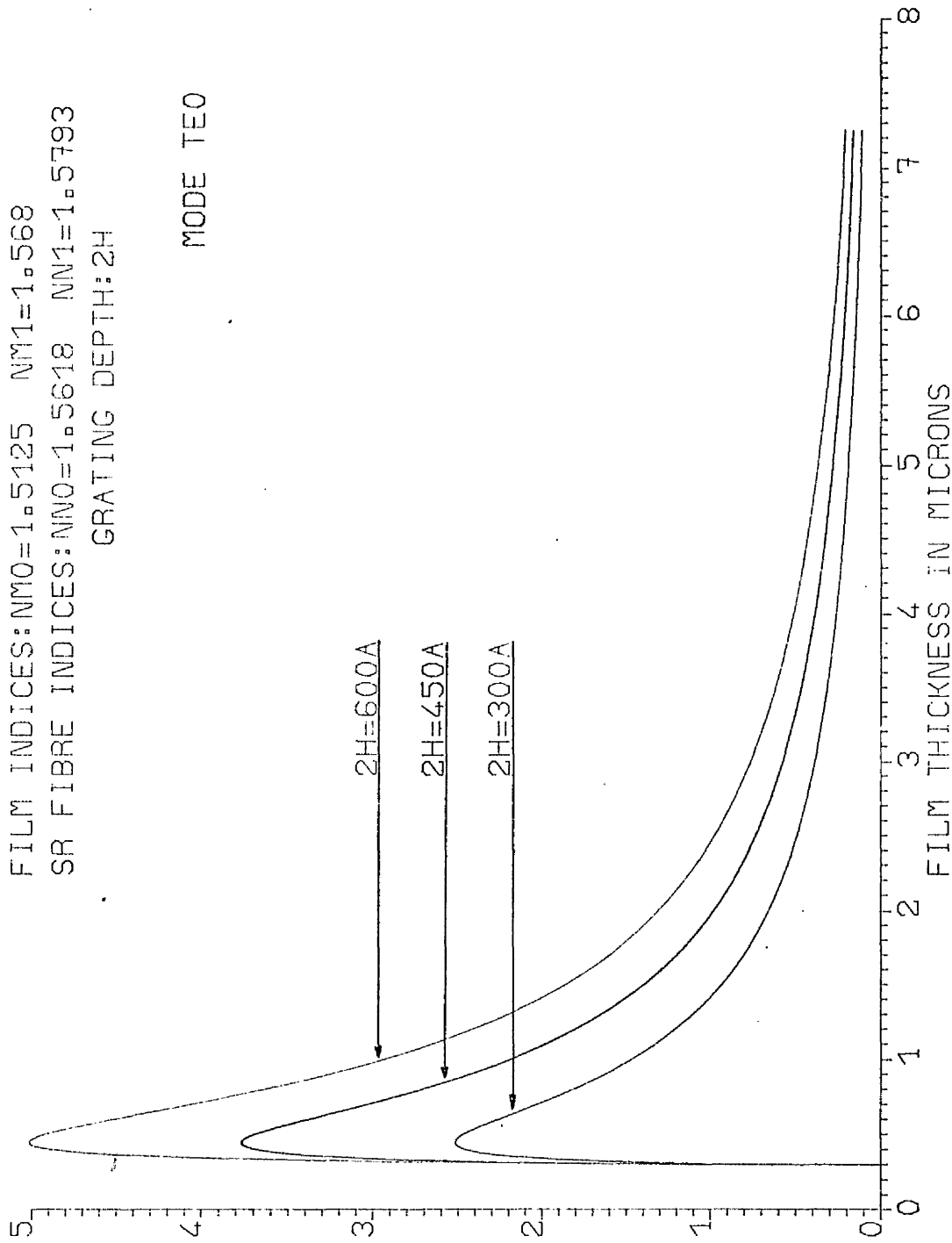


FIG: 7.5: INFLUENCE OF THE GRATING DEPTH

COUPLING COEFFICIENT IN CM-1

FILM INDICES: $n_{m0}=1.5125$ $n_{m1}=1.568$
SR FIBRE INDICES: $n_{s0}=1.5618$ $n_{s1}=1.5793$
GRATING DEPTH: $2H=600\text{\AA}$

MODE TE0

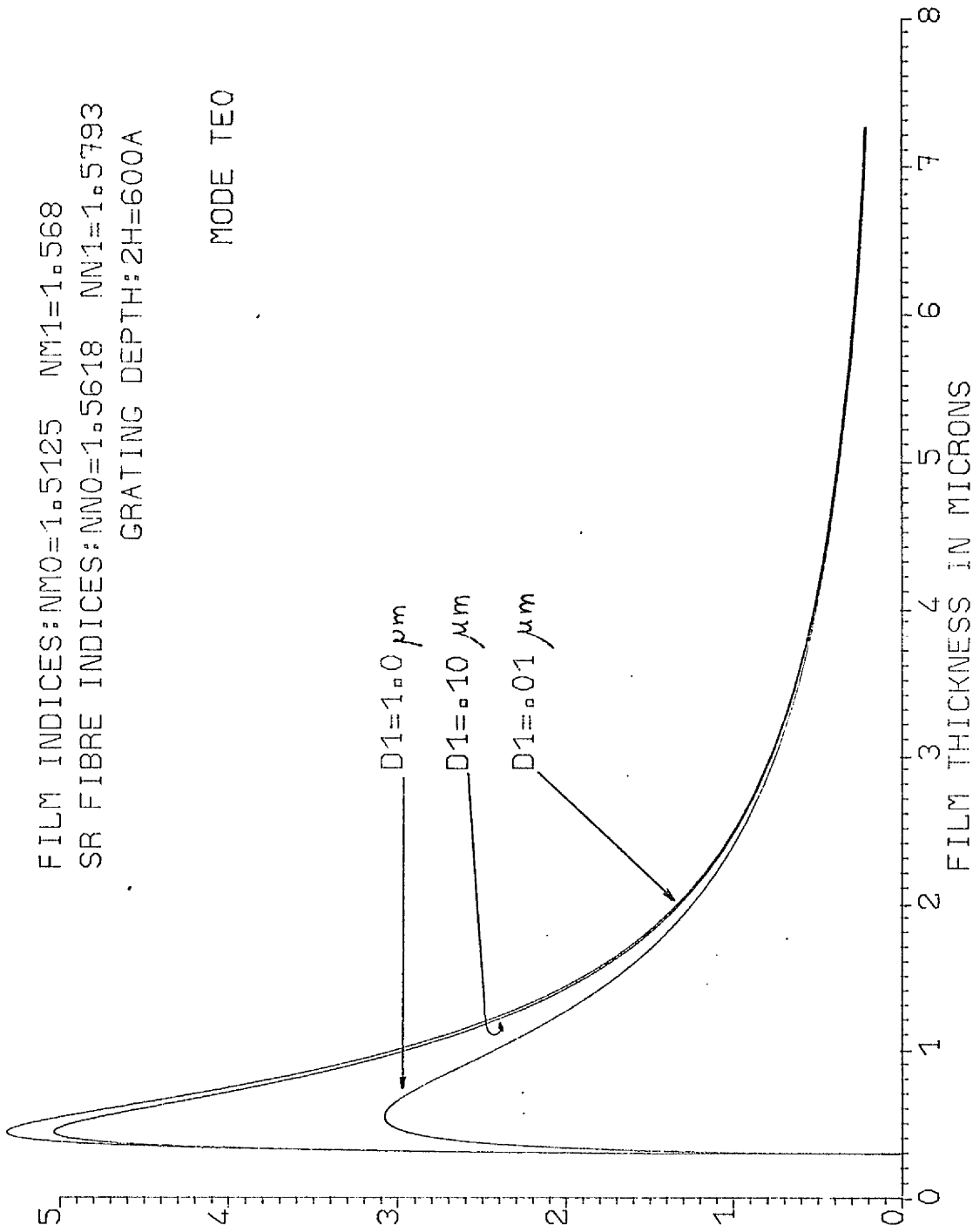


FIG: 7.6: INFLUENCE OF THE GAP

COUPLING COEFFICIENT IN CM-1

FILM INDICES: $n_{m0}=1.5125$ $n_{m1}=1.568$
GRATING DEPTH: $2H=600\text{\AA}$

MODE TEO

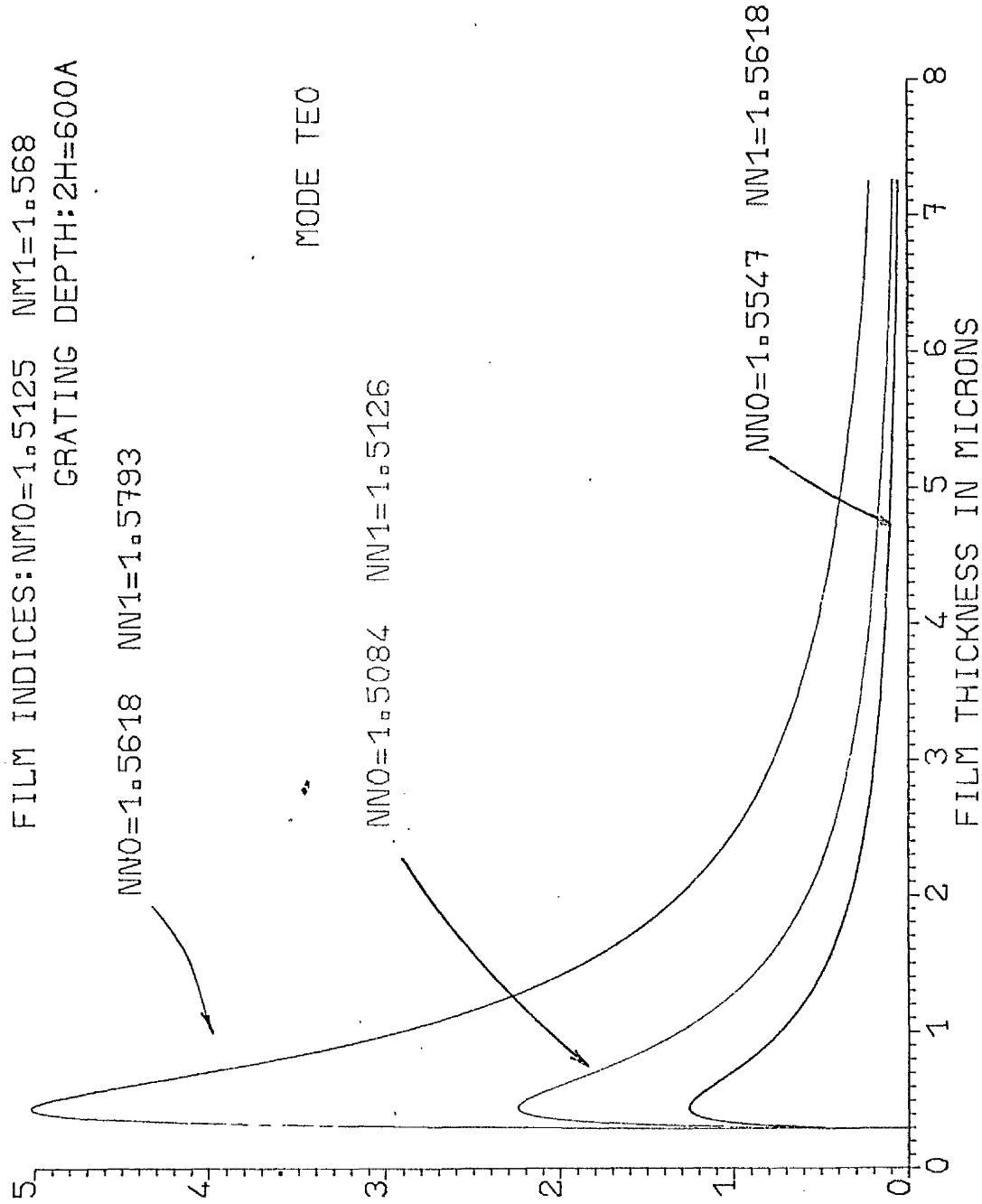


FIG: 7.7A: COUPLING COEFFICIENT FOR VARIOUS FIBRES

COUPLING COEFFICIENT IN CM-1

FILM INDICES: $n_{m0}=1.5125$ $n_{m1}=1.568$
GRATING DEPTH: $2H=600\text{\AA}$

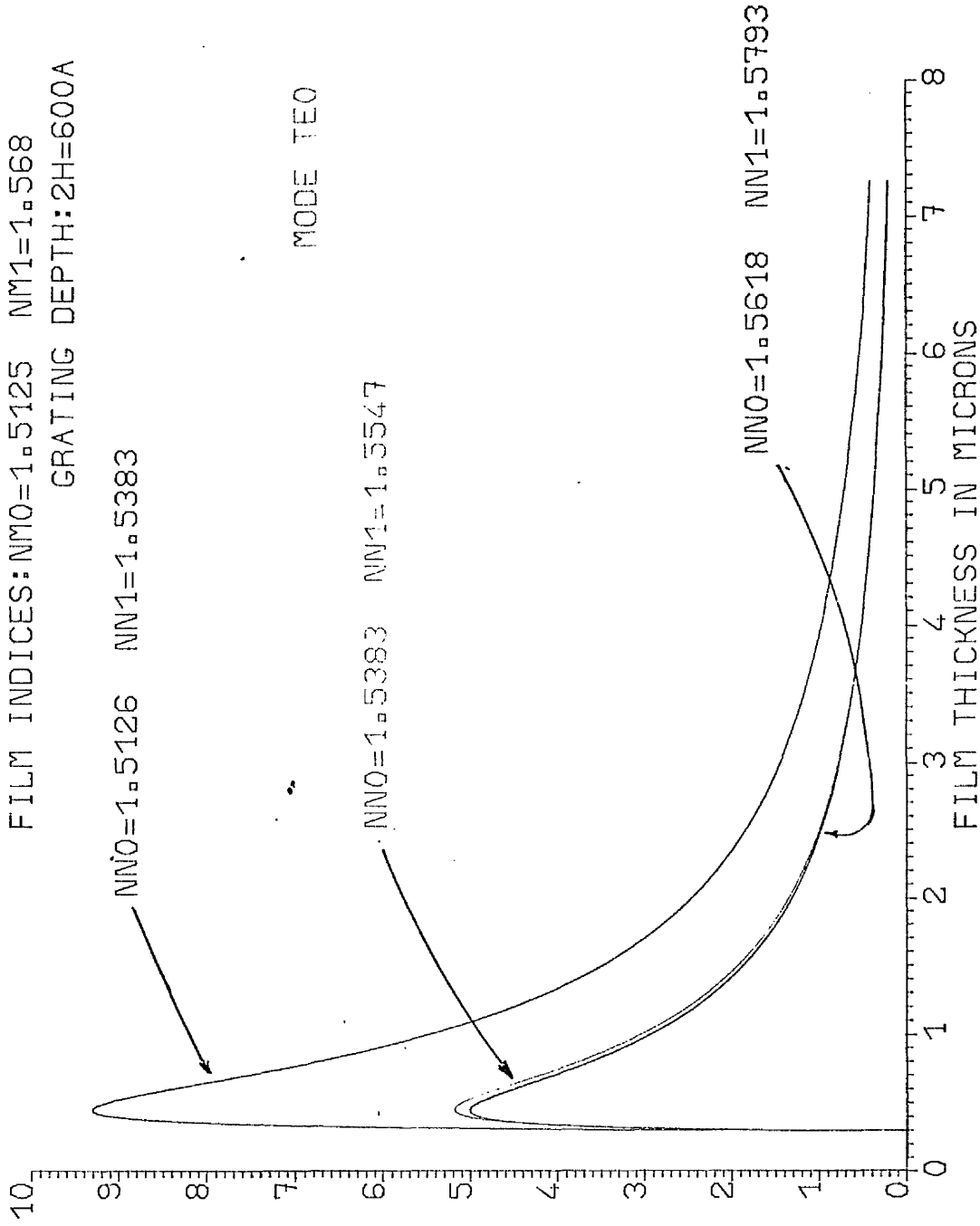


FIG: 7.7B: COUPLING COEFFICIENT FOR VARIOUS FIBRES

the fibre, the better the coupling efficiency. However, this leads to fibres with a very small core so a compromise must be reached.

For the film indices (Fig. 7-8) the same fact appears, but there the limitations are less strict since it is possible to deposit very thin films. The curves illustrate an Arsenic Trisulphide film deposited on soda lime glass and on Lithium Niobate. The very high coupling coefficient shows that this method can be used for high index films and the application of this method of coupling for linking integrated components appears to be very promising.

The gap between the fibre and the grating has been, up to now, considered to be filled with air. Fig. 7-9 shows that if an index matching fluid is used a much higher efficiency can be obtained. This is due to the alteration of the field pattern outside the film when the index in the superstrate is increased.

Finally Fig. 7-10 shows the actual coupling efficiency for three types of fibres and for a 4 mm grating etched on sputtered 7059 film on soda-lime glass substrate.

COUPLING COEFFICIENT IN CM-1

$\times 10^{-1}$

SR FIBRE INDICES: $n_{n0}=1.5618$ $n_{n1}=1.5793$
GRATING DEPTH: $2H=600\text{\AA}$
SUBSTRATE INDEX $n_{m0}=1.5125$

$n_{m1}=2.60$

MODE TE0

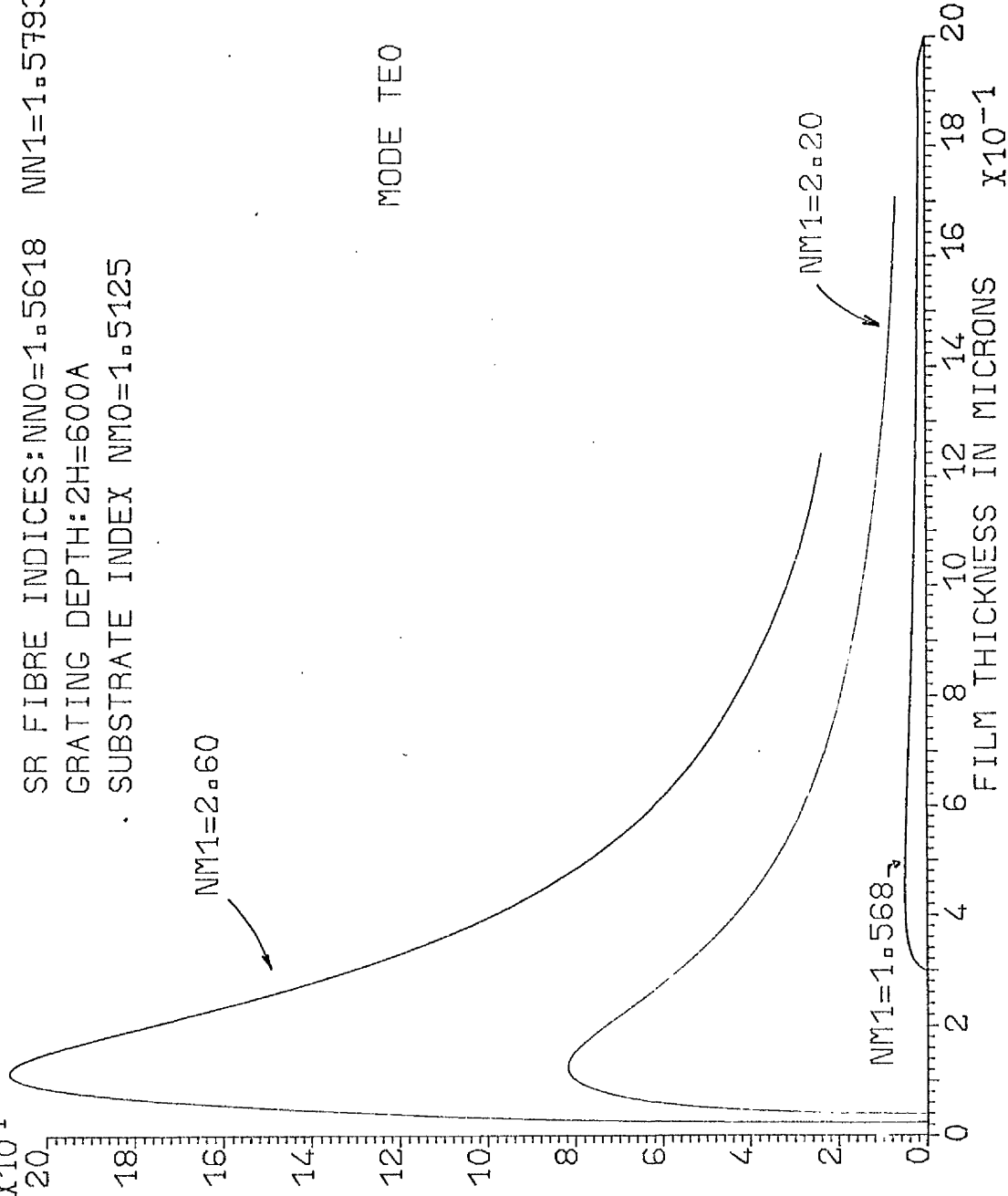


FIG: 7.8: INFLUENCE OF THE FILM

COUPLING COEFFICIENT IN CM-1

FILM INDICES: NMO=1.5125 NM1=1.568
SR FIBRE INDICES: NNO=1.5618 NN1=1.5793
GRATING DEPTH: 2H=600A

MODE TE0

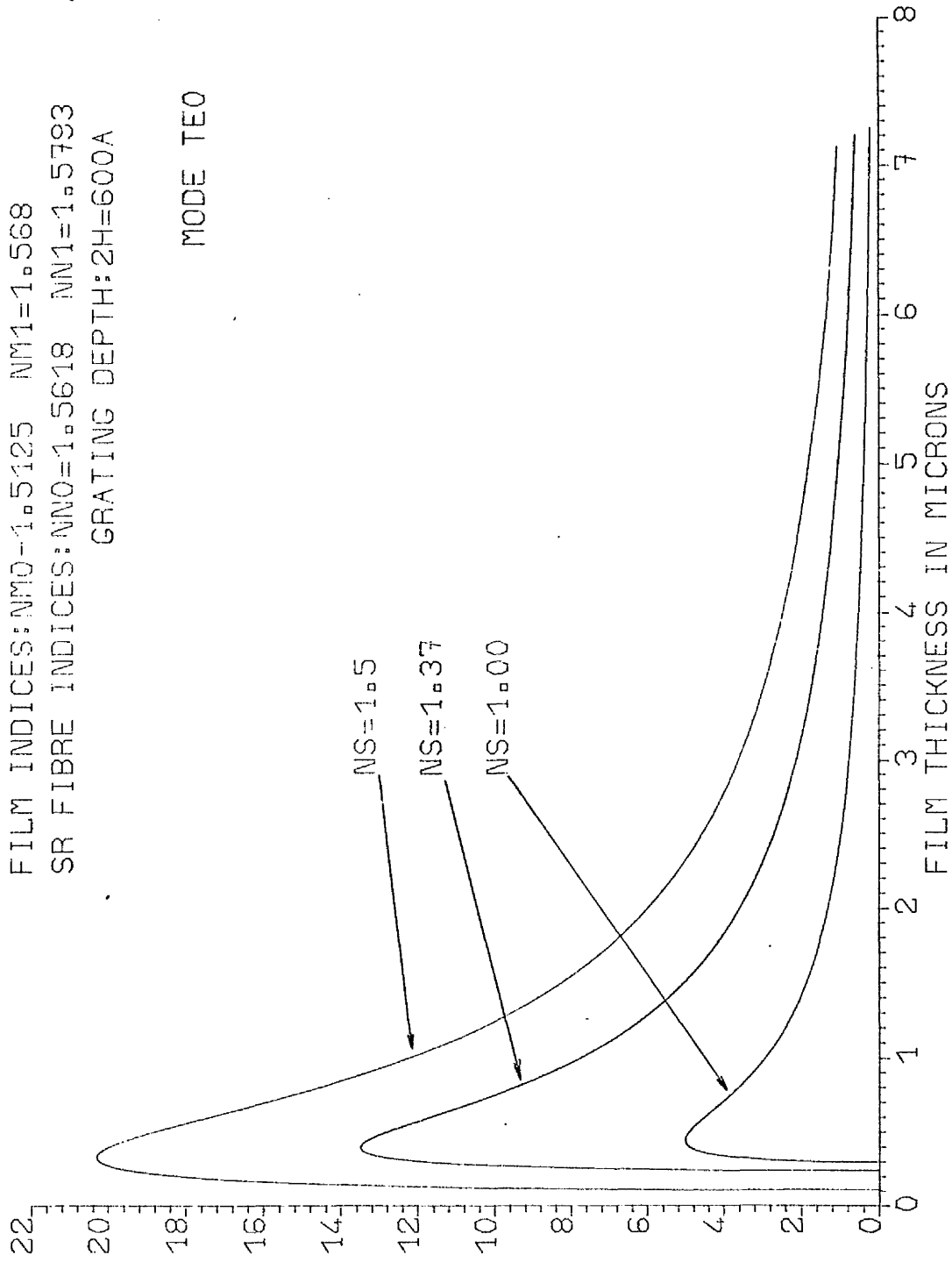


FIG:7.9: INFLUENCE OF THE IML

COUPLING EFFICIENCY FOR A 4MM GRATING

FILM INDICES: $n_{m0}=1.5125$ $n_{m1}=1.568$
GRATING DEPTH: $2H=600A$
SR FIBRES INDICES: $n_{n0}=1.5618$ $n_{n1}=1.5793$

$n_{n0}=1.5547$ $n_{n1}=1.5618$ $2H=600A$
 $n_{n0}=1.5084$ $n_{n1}=1.5126$ $2H=600A$

FIRST TWO MODES

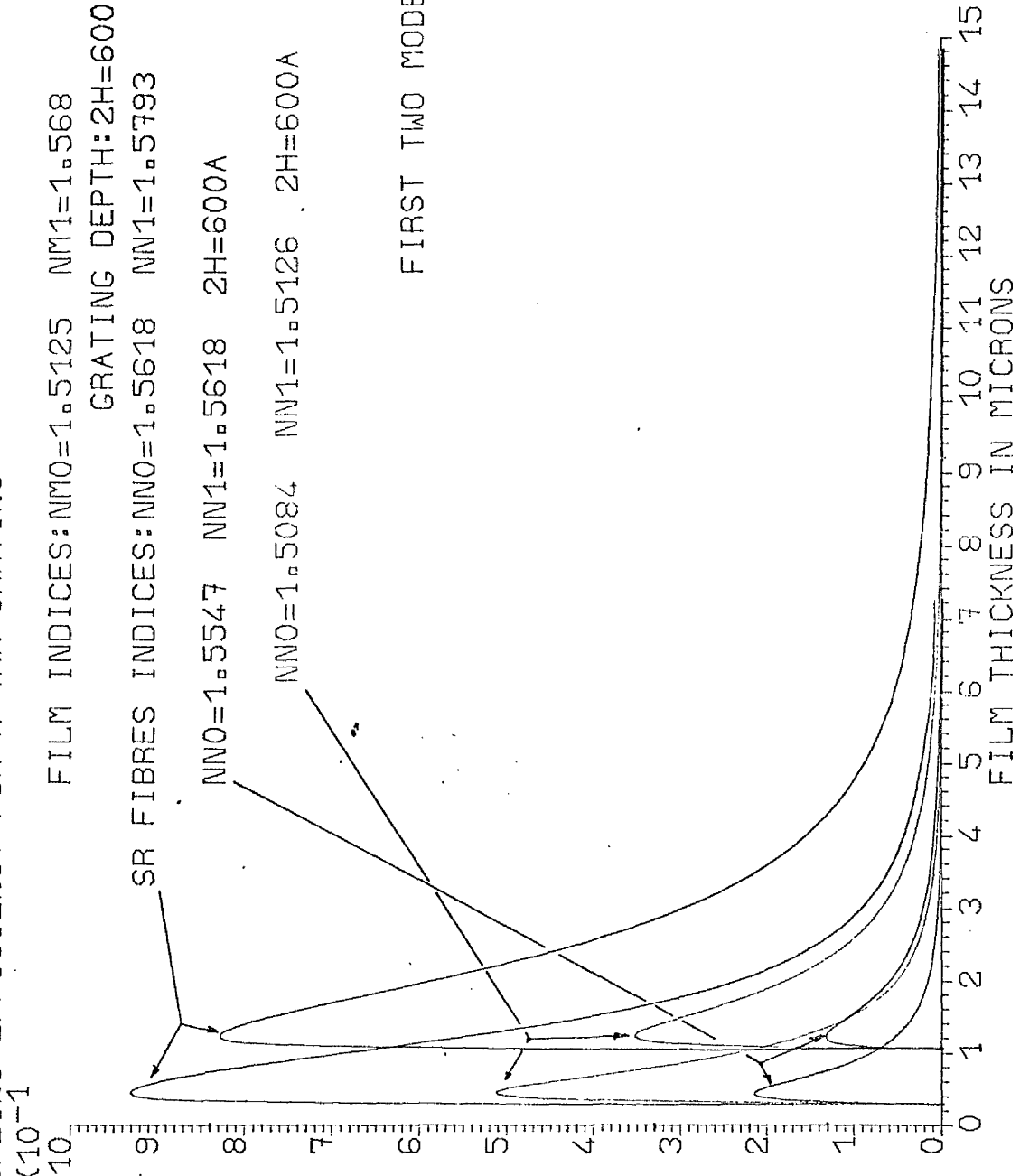


FIG: 7.10: COUPLING EFFICIENCY VS FILM THICKNESS

CHAPTER IV

EXPERIMENTAL RESULTS AND CONCLUSION

Due to a lack of gratings, very few experiments were done. However the results gained were very promising.

II 4.1. Experimental apparatus

The apparatus used is shown in Fig. 8-1. As the gratings used were not always exactly as specified, a dye laser was used to compensate for any discrepancy in periodicity. This also allowed the observation of the response of the system with changing frequency. The wavelength range used was $6100 \text{ \AA} - 6400 \text{ \AA}$.

The set of three mirrors is used to change the polarisation of the laser light (TE) in order to launch the TE_0 mode in the slab which is sitting horizontally.

The fibre is pressed onto the grating by means of a pressure pad whose dimensions are such that it covers the whole grating. It is tightened by a screw (Fig. 8-1b).

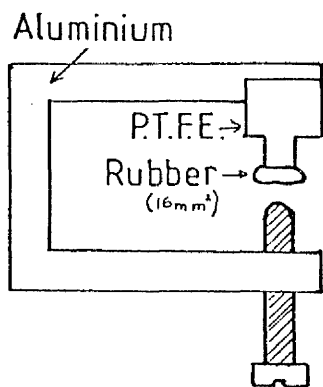
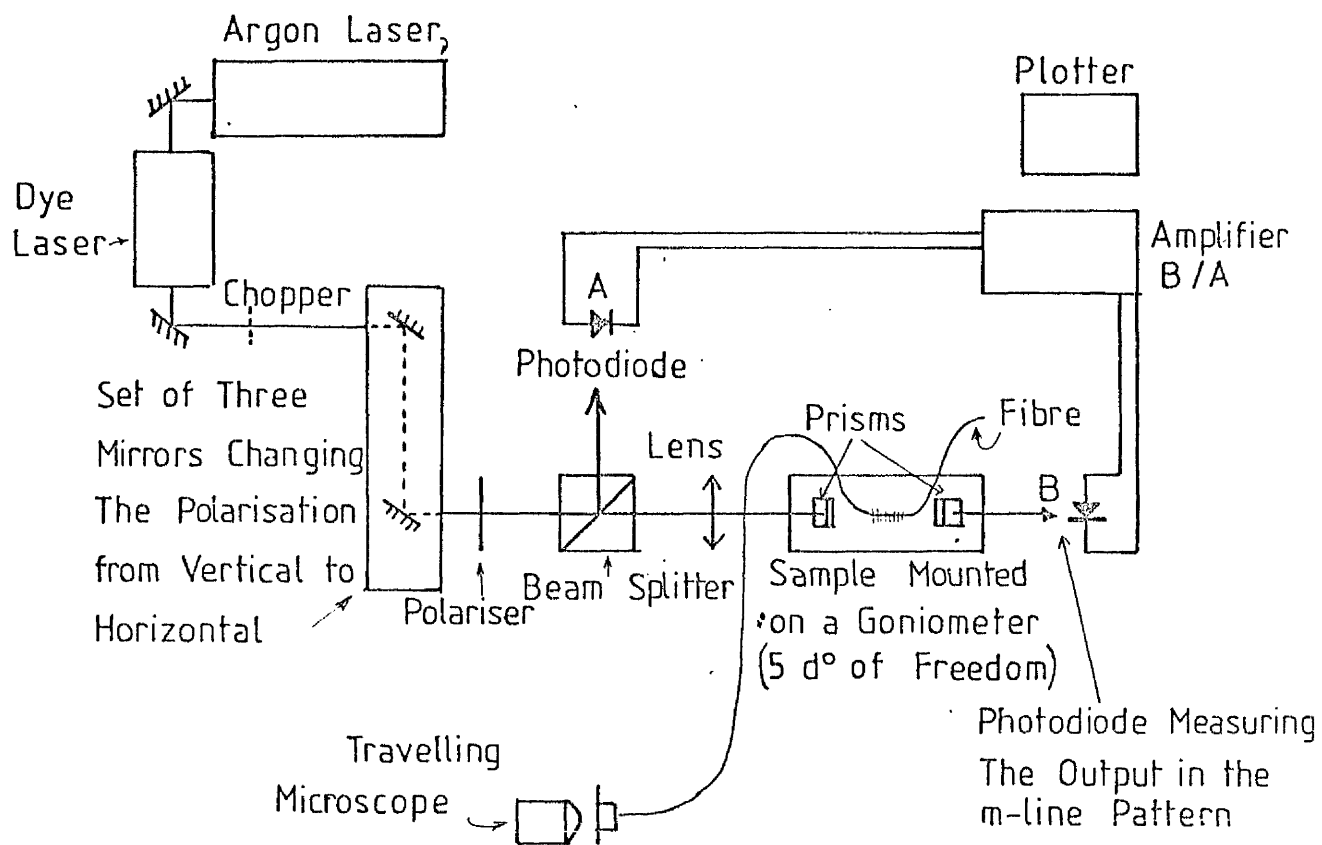
An output prism allows one to measure the quantity of light which is not trapped by the fibre. The intensity of the m line is measured by a photodiode and is compared to the power in the input beam. The ratio $\frac{P_{out}}{P_{in}}$ is plotted versus the wavelength.

The end of the fibre was placed in a cell and could be observed through a travelling microscope or measured by a photodetector.

II 4.2. The fibres

The fibres used were sandwich ribbon fibres. They were made from various glasses from the Schott catalogue [87], which were chosen according to the following criteria:

- i) The indices were to range from 1.5 to 1.6.
- ii) The expansion coefficients were to be similar.
- iii) The softening points were to be close enough to give the same



Clamping Device Used to Press the Fibre onto the Grating.

Fig.8.1 Experimental Apparatus

pulling temperatures.

The glasses chosen are listed in table 8.1.

The Bragg wavelength of the gratings being around 6250 \AA the fibre effective index has to be chosen so that it satisfies 5-1 for a wavelength λ where:

$$\lambda_B \leq \lambda \leq \lambda_B + \Delta\lambda \quad (8-1)$$

($\Delta\lambda$ being the half width of the Bragg peak) so that there is no risk of having coupling occurring at the Bragg wavelength or above the high frequency cut-off of the grating (Fig. 8-2).

The Bragg frequency was measured for each sample and the fibre chosen accordingly.

In order to manufacture the fibres the core preforms were produced first. Two methods were investigated. The first one consisted in pulling a slide down, reducing the cross section from $25 \text{ mm} \times 1 \text{ mm}$ to, typically, $2.5 \text{ mm} \times 0.1 \text{ mm}$, with a conventional pulling machine (Fig. 3-2) at the temperature of 800°C . As this tended to produce round cores a second method was investigated. It consisted in cutting a preform with a quartz saw and then polishing it down to the required dimensions (2.5 mm width \times five hundred times the required thickness to achieve monomode guiding). This last method had the disadvantage of being very time consuming and to be sometimes rather cumbersome when the required thickness was small. However it allowed a better dimensioning of the core.

Once the preform of the core was made, it was clamped on a slide of the chosen material for the substrate. The latter had frequently to be polished. The assembly was then put in the pulling machine to be pulled down to the required dimensions.

The resulting fibre was then visually checked with a microscope and its effective index was measured with a prism. The results found

```

*****
*          *          *          *          *          *
*   GLASS  *(theoretical)* (measured)*   Tg (°C)* α 10-7/°C*
*          *          *          *          *          *
*****
*   BK1    * 1.50084 * 1.50979 * 547 * 89 *
*          *          *          *          *          *
*****
*   KF3    * 1.51257 * 1.51338 * 470 * 94 *
*          *          *          *          *          *
*****
*   LLF2   * 1.53834 * 1.53894 * 442 * 91 *
*          *          *          *          *          *
*****
*   BAK5   * 1.55471 * 1.55537 * 580 * 90 *
*          *          *          *          *          *
*****
*   LF8    * 1.56177 * 1.56027 * 439 * 96 *
*          *          *          *          *          *
*****
*   LF3    * 1.57930 * 1.57220 * 463 * 92 *
*          *          *          *          *          *
*****
*   BaK1   * 1.57041 * 1.57047 * 602 * 87 *
*          *          *          *          *          *
*****
*   BaK3   * 1.56259 * 1.56164 * 583 * 84 *
*          *          *          *          *          *
*****
*   BaK4   * 1.56670 * 1.56715 * 552 * 81 *
*          *          *          *          *          *
*****
*   BaK2   * 1.53806 * 1.53424 * 562 * 91 *
*          *          *          *          *          *
*****

```

n : refractive index at 0.6328 micron.

T_g: transformation temperature.

α: coefficient of thermal expansion.

TABLE 8.1: CHARACTERISTICS OF THE GLASSES.

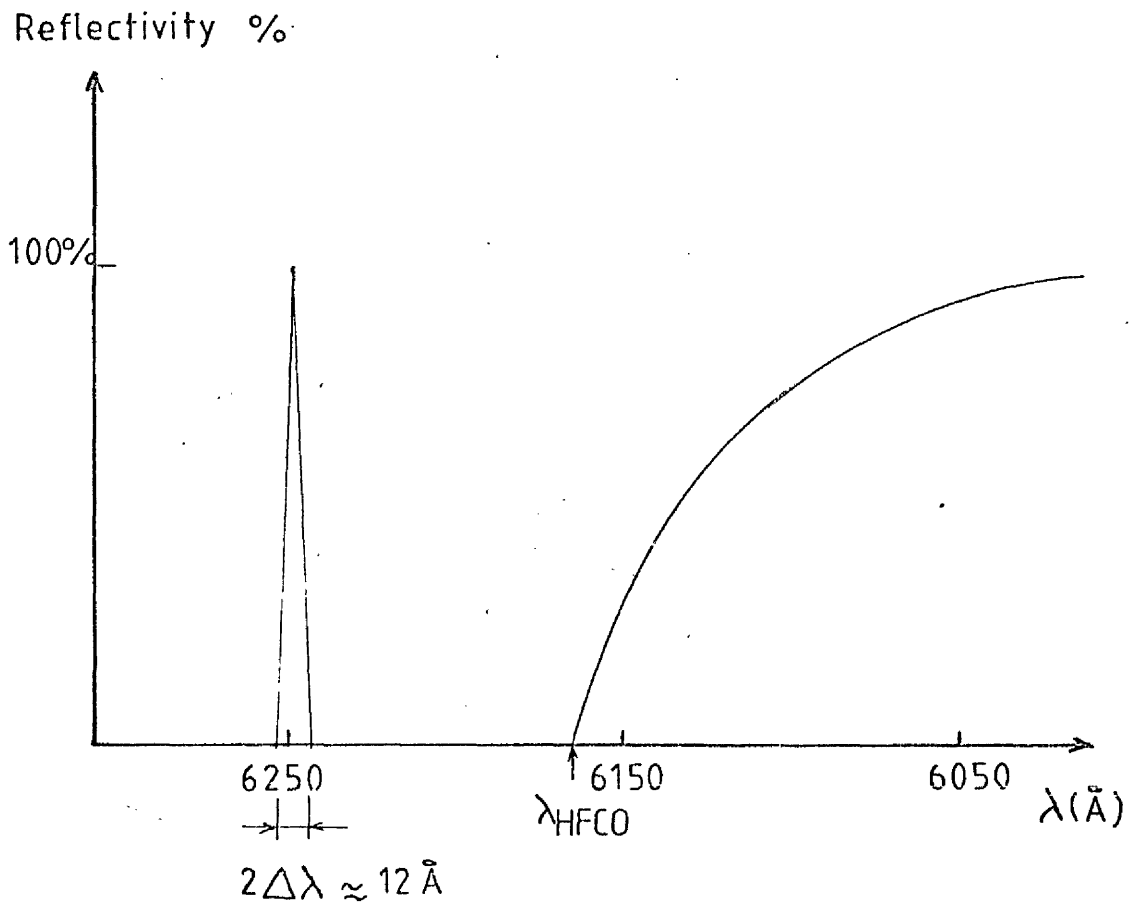


Fig. 8.2 Bragg Interaction and High Frequency Cut-off Properties

	n_{no}	TN ₁₁	β_{11}	K_{x11}	K_{y11}	C_{max11}
FIBRE						
	n_{n1}	TN ₂₁	β_{21}	K_{x21}	K_{y21}	C_{max21}
	1.53834	0.575	15.018714	.619289	2.713612	7.159
LLF2/KF3						
	1.51257	0.728	15.056825	.619289	2.493490	5.933
	1.55471	0.778	15.274504	.619633	2.146256	4.463
BaK5/LLF2						
	1.53834	1.076	15.312084	.619833	1.859299	3.3335
	1.57930	0.737	15.507164	.620115	2.245423	4.209
LF3/LF8						
	1.56177	0.998	15.54422	.620115	1.972631	3.222
	1.56177	1.417	15.437009	.619775	1.355911	0.898
LF8/BaK5						
	1.55471	3.147	15.474262	.619775	0.795683	0.806
	1.51257	2.236	14.977078	.618706	0.928494	1.439
KF3/BK1						
	1.50839					

$n_{m0} = 1.5125$ $n_{m1} = 1.568$ $2h = 400 \text{ \AA}$

TN: Thickness at Cut-off For The Considered Mode

C_{max} : Maximun Coupling Coefficient Value

$n_s = 1$ $\lambda = 0.6328 \text{ micron}$ $d = 5 \text{ micron}$

TABLE 8.2: COUPLING COEFFICIENT FOR VARIOUS S.R. FIBRES.

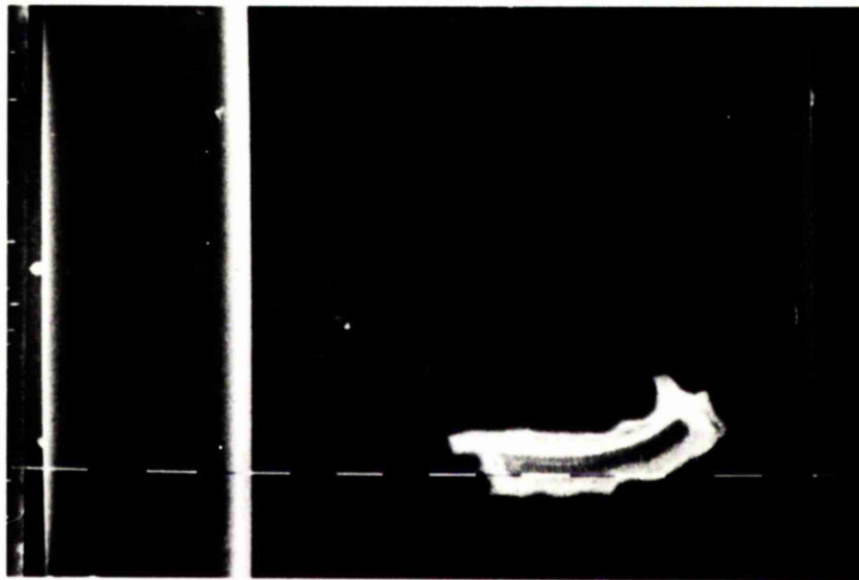


Figure 8.3: S.E.M. PHOTOGRAPH OF A LARGE S.R. FIBRE
SHOWING A DEFECT IN THE SUBSTRATE.
(10 micron markers)

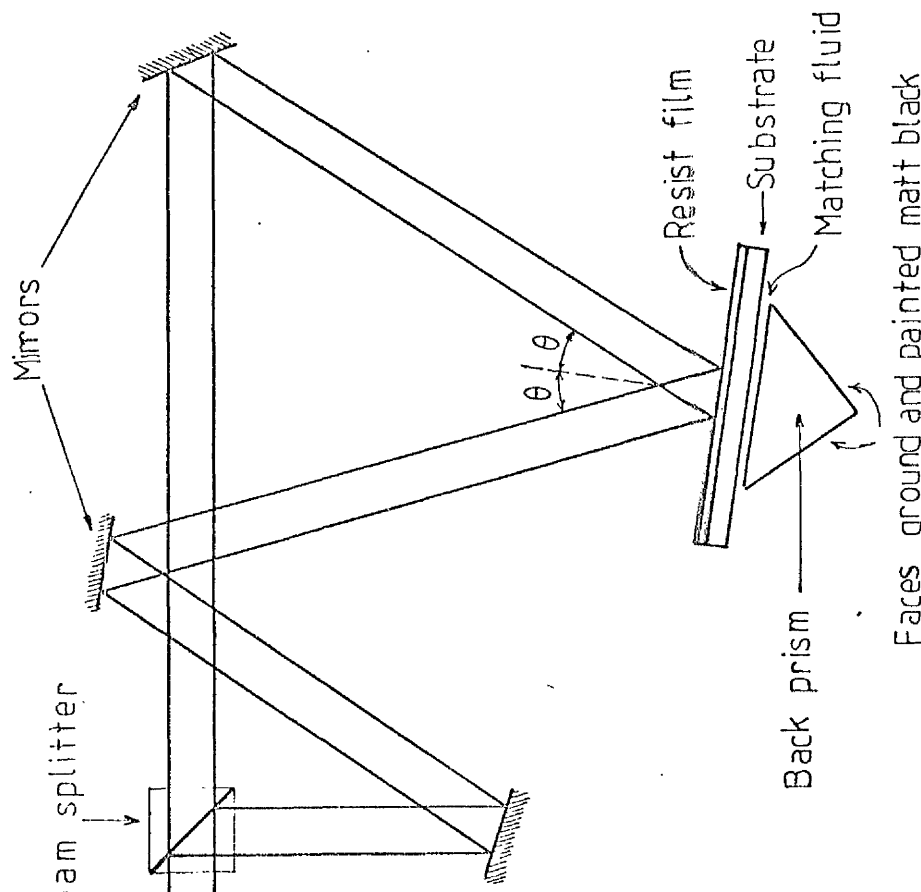
showed a variation in the index which was lower than expected ($4 \times 10^{-3} \leq N_{\text{initial}} - N_{\text{measured}} \leq 5 \times 10^{-3}$). It was thus necessary to anneal the fibres after pulling in order to regain the original indices as far as possible [84]. For this the fibre was clamped above the furnace and, using the feeding motor, was allowed to go through the furnace at a very slow rate (1 μm every five seconds), the furnace temperature being set at 550°C. This process proved to be very lengthy but achieved good results since the index change was reduced to one third of its original value.

III 4.3. Slab waveguides and gratings

The slab waveguides were made by sputtering 7059 glass on a soda-lime or amorphous silica slide, using a conventional technique [85]. The measurement of the synchronous angles gave the effective index and, with the help of a computer programme, the thickness of the guide [86].

The gratings were produced by Dr. A. Yi Yan. They were made by exposing the slide, covered by photoresist, to the diffraction pattern of two amplitude divided beams from a single laser [85] as shown on Fig. 8-4). After exposure the photoresist was developed, yielding a grating pattern of 4 mm x 4 mm whose periodicity ranged from 1995 to 2017 Å. The resulting slab was then etched in an ion beam etcher. The grating depth obtained varied between 400 Å and 600 Å. Finally the remaining resist was taken off with an asher before being cleaned with acetone.

This method for producing etched gratings is usually very efficient but, in this case, some problems occurred. The ion-beam etcher of the Department being out of use for a very long time (7 months) several alternatives were looked for. Consequently the gratings were etched in the Rutherford Laboratories in a machine



Grating period $\Lambda = \frac{\lambda}{2 \sin \theta}$

Fig.8.4 Three-Mirror Experimental Interferometer for the Production of Holographic Diffraction Gratings

usually used to etch chrome and aluminium masks. This led to contamination of the samples, inducing high losses and a very poor coupling efficiency. What happened is that during the etching process a layer of chrome and aluminium (mainly chrome) was deposited on the sample, this layer being strongly oxidised during the removal of the resist in the asher. It was then impossible to remove the chrome oxide layer in spite of all the methods tried. Some achieved a good etching of the chrome film but destroyed the sputtered film at the same time as shown on picture (8-5), (8-6).

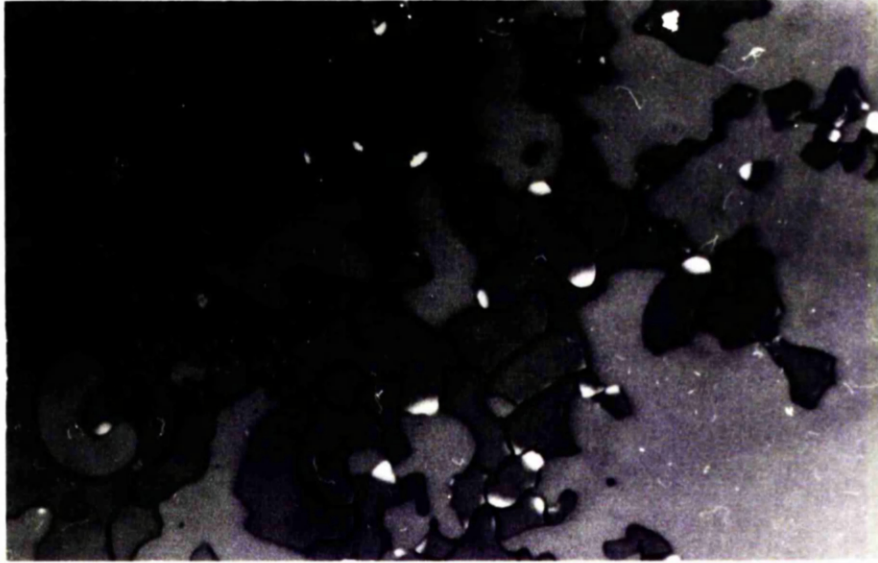
Another ion-beam etcher was tried but it gave very poor results because of its poor resolution (Fig. 8-7).

III 4.4. Experimental results

The very poor quality of the gratings considerably altered the experimental results. The efficiency measured did not tally at all with the theory. But, in spite of this, contradirectional coupling occurred. Fig. 8-8 shows the light in several fibre ends. The fibres are slightly over-moded but the coupling is evident.

One of the main problems in achieving good coupling was to have a beam impinging the grating at an angle of 90° and to align the fibre on it exactly. The first part was done by setting the wavelength at the Bragg value (typically 6250 \AA) so that the reflected beam in the substrate could be aligned exactly with the incoming beam. However, due to the poor quality of the samples, the reflected beam was not always visible. The fibre was then pressed as exactly as possible to the beam.

The recording of the light output from the second prism allowed one to see when coupling occurred. Fig. 8-9 shows such a recording.

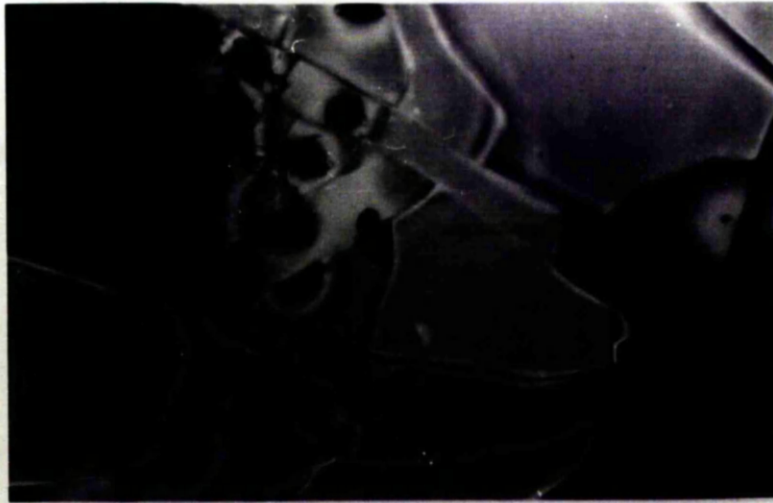


A. SPUTTERED 7059 FILM: ACTION OF CHROME ETCH. (X20)

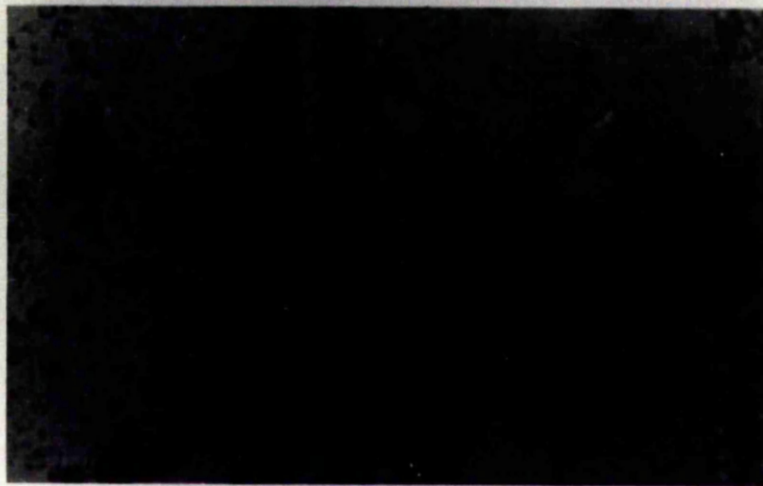


B. ION-BEAM ETCHED SPUTTERED 7059 FILM: ACTION OF CHROME ETCH AND AQUA REGIA. (X100)

Figure 8.5: PHOTOGRAPHS OF THE SAMPLE SURFACE AFTER REMOVAL OF THE CHROME OXIDE LAYER.



A. ETCHED WITH AQUA REGIA. (X100)



↑ 7059 film edge

B. INFLUENCE OF CHROME ETCH ON SPUTTERED 7059 FILMS.(X10)

Figure 8.6: PHOTOGRAPHS OF A SAMPLE SURFACE AFTER
ETCHING THE CHROME OXIDE FILM.

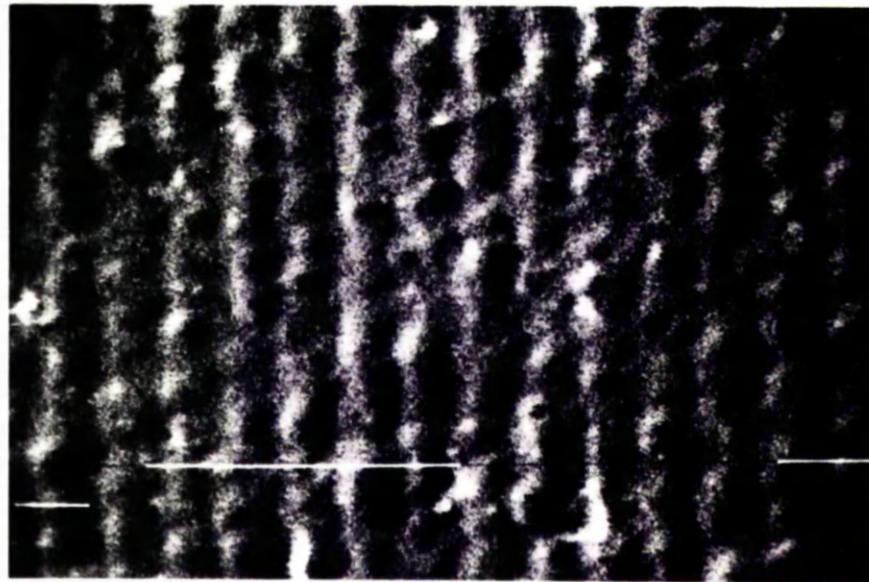
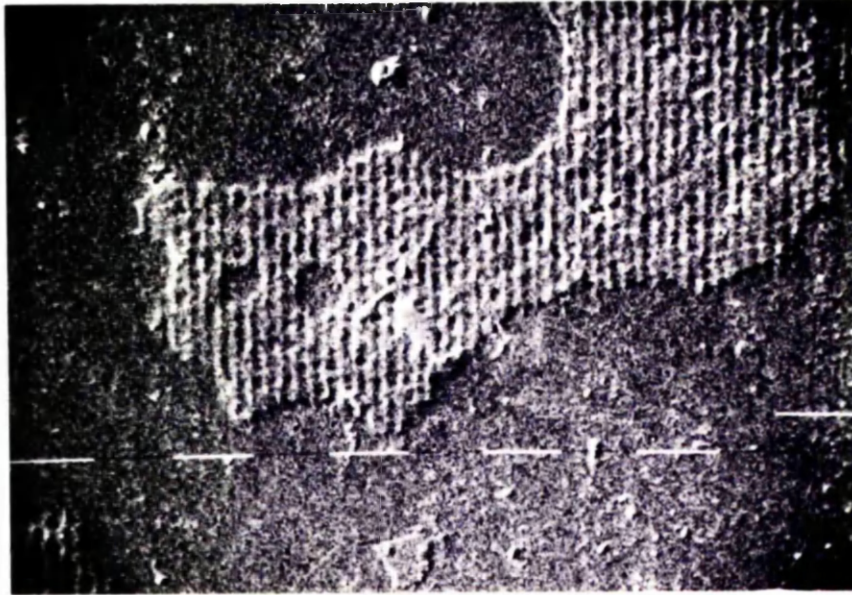


Figure 8.7: S.E.M. PHOTOGRAPHS OF AN ION-BEAM ETCHED GRATING. (1 micron markers)

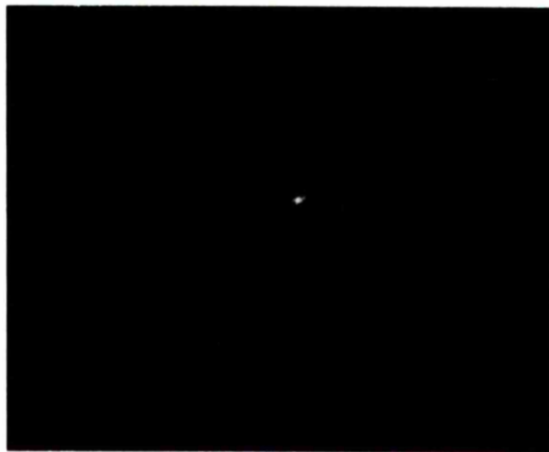
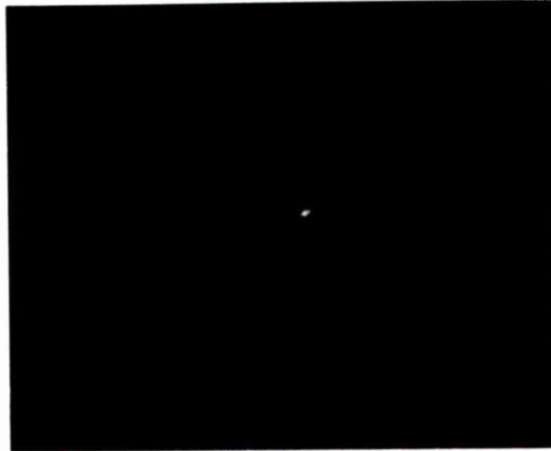


Figure 8.8: PHOTOGRAPHS OF COUPLED LIGHT IN A S.R.
FIBRE. (NEARFIELD) (— : 20 micron)

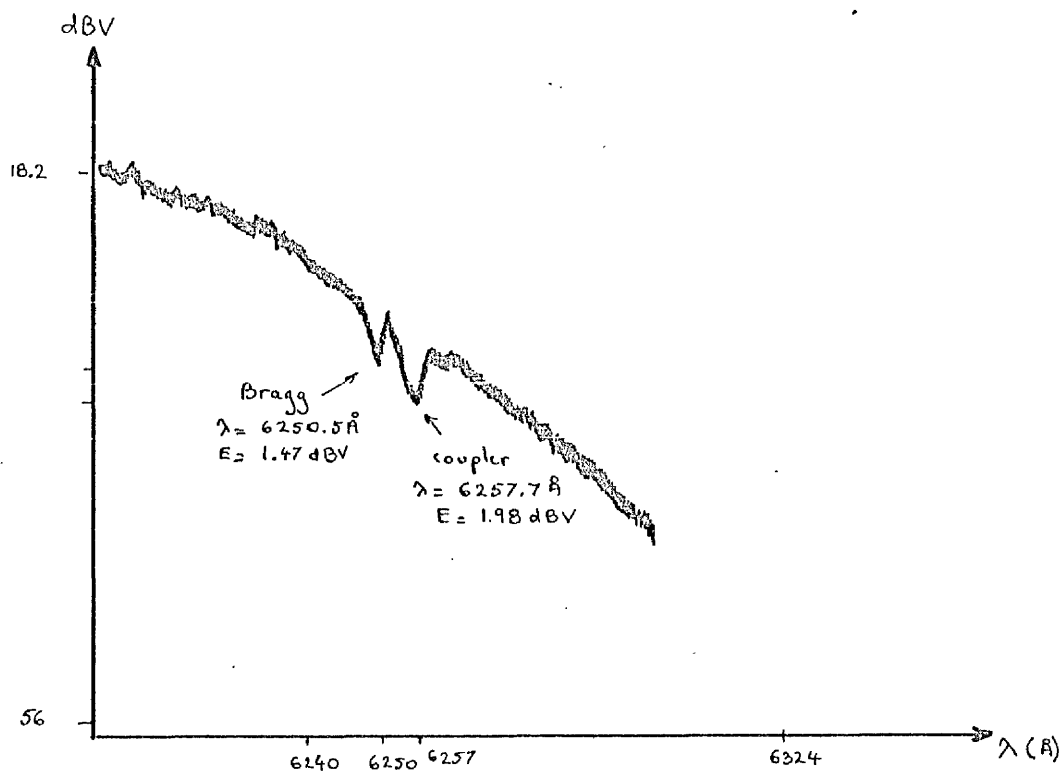


Fig.89 Recording of the Output

III 5. Conclusion

The experimental results given in this part are not very conclusive. However it may be seen that this method for coupling thin films to fibres is very promising since, in spite of the very poor quality of the films and gratings, coupling occurred and showed a good response with frequency.

The efficiency of the coupler was estimated to be 20% but it must be remembered that the films and gratings were covered with a layer of oxide. On top of this the beam waist was very large (0.5 mm) when compared to the fibre core and to achieve a better efficiency it would be necessary to have either a beam whose dimensions are equivalent to the fibre core width (5 μm) or a three dimensional waveguide.

The alignment of the fibre, sample and beam is very critical and, here again, better results are to be gained if a much more sophisticated set up is used.

Finally a better knowledge of the fibre must be gained. It seems necessary to study in detail the changes in material characteristics during the pulling and annealing so that the preform dimensions could be worked out beforehand to achieve a given effective index instead of having to use a trial and error method.

PART IV

CONCLUSION

IV 1. First Part

The bulk of this part has been concerned with gaining an understanding of the coupling phenomenon between two round fibres. Many of the conclusions reached have been detailed at the end of each chapter. These will now be summarised and some further observations made.

We started by studying the ion exchange process. It was shown that the presence of monovalent ions was necessary and that such oxides as Al_2O_3 played an important role as they determine the ions "preferred" by the glass. On the other hand other oxides such as CaO were inhibiting the diffusion process.

The kinetics of ion exchange are related to the interdiffusion process of the two ions in the glass. We looked especially at the case when the two interacting ions are in the melt (i.e. a dilute melt). This particular situation allows control over the index change produced at the glass surface and the phenomenon is studied for the case of Silver/Sodium ion exchange. The concentration-dependent diffusion equation is solved by the finite difference method since this method can be applied for both planar and cylindrical systems.

The theory of propagation was studied next. Maxwell's equations are solved for graded index fibres after a few approximations are made (for weakly guiding fibres). However, as this leads to expressions which are still cumbersome to handle, the ray optics approach and the WKBJ method were employed, yielding the eigenvalue equation.

In order to study the multimode fibre coupler even more drastic approximations were made in order to avoid the use of the modified Hankel functions for the case of step index multimode fibres. A simplified coupling coefficient was thus derived and a computing programme was written to plot the results in different cases. The

results showed that good coupling could only be achieved with high order modes and that the two coupled fibre cores had to be as close as possible. The evaluation of the coupling efficiency led to the determination of the most suitable coupling length.

The fabrication and measurement of graded index fibres were then described. The manufacturing process uses the ion diffusion method with a dilute melt of silver nitrate and sodium nitrate. This method gives the following advantages:

- i) control over the index change
- ii) reduction in the silver staining effects
- iii) easy application of the results gained to Selfoc fibres
- iv) good repeatability.

However the fabrication of graded index fibres did not prove to be altogether successful since:

- a) the staining of the fibres could not be completely avoided
- b) it allowed only very small lengths to be made (≤ 2 cm)
- c) the fibres were excessively fragile.

Another method was thus investigated but, although successful, the cladding dimensions were then too large to allow an efficient index modification.

Experimental methods for observing refractive index profiles were tested. The most successful consisted in measuring the amount of light refracted at the fibre end. In spite of the fact that the apparatus could be much improved, it gave good results and allowed one to measure accurately index profiles.

Finally index modification and coupling were examined. The results gained are in accordance with the theory except for the coupling efficiency. The figures obtained are less than predicted and this can be explained by deficiencies in the method used. However

no attempt was made to improve it since the aim of the coupling is only to tap a small amount of power.

In conclusion, the coupling method achieved what was aimed for except for the fact that the low order modes could not be efficiently tapped. But this is inherent in the system and cannot be improved. Following the method described here it thus seems possible to make a multimode fibre directional coupler as long as the useful signal is carried by the high order modes. Therefore mode mixing is desirable in any system used.

Some further work could be done with single mode fibres or with fibres carrying a small number of modes.

IV 2. Second Part

The second part of the thesis started with a brief review of propagation in a slab waveguide. The field expressions in a rectangular waveguide was derived, using Marcatili's approach, in five distinct zones defined by the waveguide geometry.

The formulation of the coupling coefficient was undertaken next. For this the coupled mode theory was briefly reviewed and the perturbation induced by a grating described. A perturbation analysis was then used to calculate the coupling coefficients. A computer programme was written to plot the coupling coefficient as a function of the film thickness. These curves are used to evaluate the influence of the various parameters. It is shown that the nature of the film and of the fibre have a strong influence on the efficiency of the coupler as well as the dimensioning of the grating.

Finally the experimental results were described. Due to the poor quality of the gratings no decisive measurements were done; however, the method proved to be successful qualitatively, since the efficiency of the coupling was estimated at 20% and the response with wavelength

showed a distinct peak.

It thus seems that the contradirectional coupler can be very efficient if the following conditions are achieved:

- a) good quality of the gratings
- b) good monomode fibres, and knowledge of their characteristics
- c) a more accurate coupling device is designed, allowing a very accurate alignment of the components.
- d) the laser beam waist is reduced to the dimensions of the fibre.

IV 3. Suggestions for future work

First of all, as soon as it is possible to make good gratings again, the experimental work should be finished so that conclusive results are established.

Considering the high efficiency yielded by an arsenic trisulphide film on glass and that gratings having suitable periodicity ($\sim 1500 \text{ \AA}$) are feasible [88], the use of such couplers to link integrated optical systems seems to be very promising. Fig. 9-1 shows what the experimental set up could be to test such a link. Light from a laser beam is launched into an arsenic trisulphide film deposited on a fused silica substrate [89] through an input prism. The guided beam is then contradirectionally coupled to a S.R. fibre by means of a first grating, to be coupled from the fibre into a phosphosilicate or a germano silicate glass film by means of another grating [90]. An output prism allows one to observe the efficiency of the arrangement through the m-line pattern.

Such a study would also lead to the study of fibre-to-film coupling which might need a good knowledge of the behaviour of the polarisation in a S.R. fibre.

Another possible use of such a coupler would be in a demultiplexer. It has been seen that the frequency response of a contradirectional

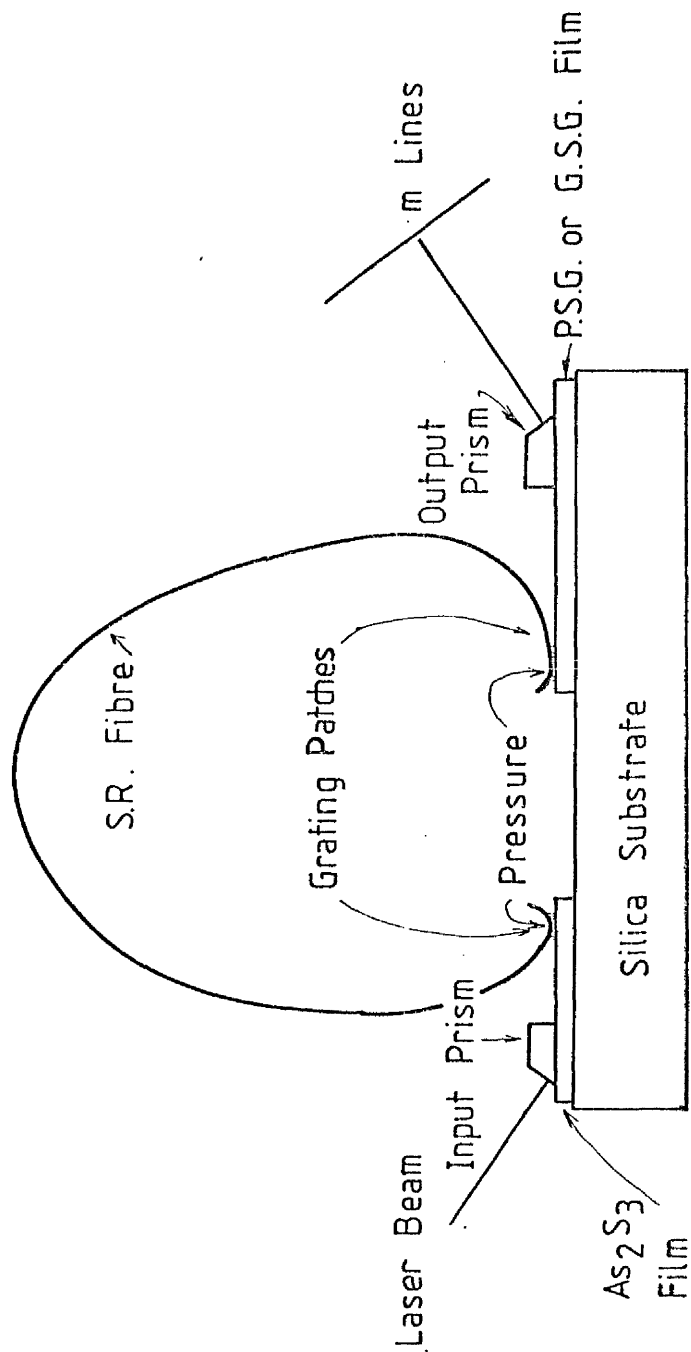


Fig.9.1 Linking Experimental Set-up

showed a peak. The bandwidth is rather large ($\sim 5 \text{ \AA}$) but could be reduced with better samples and set-up. The proposed demultiplexer is depicted in Fig. 9-2.

Several gratings of various periodicity would be etched onto a film and matching fibres pressed on them in order to tap given wavelengths contained in the input beam.

Eventually, by carefully designing the grating length, only a portion of the power could be tapped out of the film for a given frequency, yielding a highly sophisticated demultiplexer.

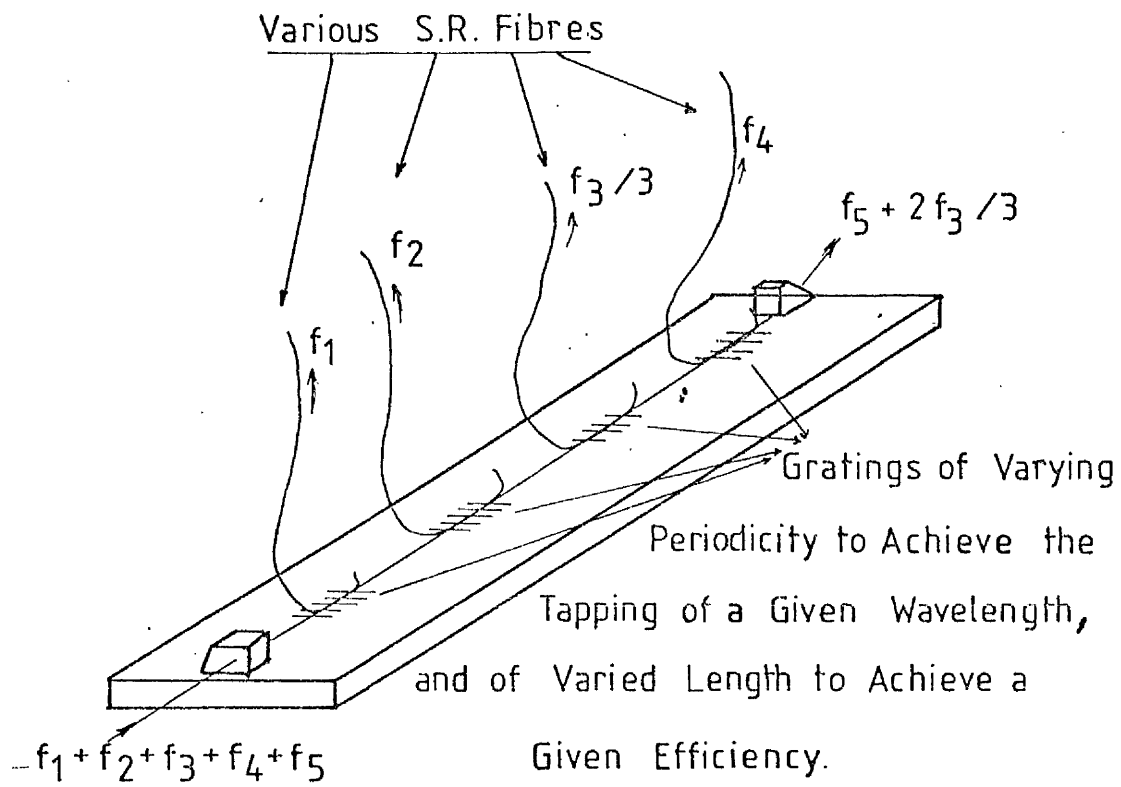


Fig.9.2 Demultiplexer

REFERENCES

- 1 K.C. KAO, G.A. HOCKHAM
Dielectric Fibre Surface Waveguides for Optical Frequencies
Proc. I.E.E.E., 113, 7, p.1151, 1966
- 2 S. TAKANA, H. YOKOTA, M. HOSHIKAWA, T. MIYA, N. IGAKI
Ultra-low-loss Single-Mode Fibre with double synthetic cladding layers
Proceedings of the 6th European Conference on Optical Communication ;
p. 37, York 16-19 sept. 1980
- 3 Y. IKEDA, M. YOSHIYAGAWA
Développement de verres à faibles pertes pour fibres Selfoc.
Communication 1.2, Materials and Technologies, Part I, p.27
- 4 K.J. BEALES
Proceedings of the 3rd European Conference on Optical Communications, p.2
18-20, 160-165, NTG Munich Germany, Sep. 14-16 1977
- 5 J.B. MACCHESNEY, P.B. O'CONNOR, H.M. PRESBY
A New Technique for the Preparation of Low-loss and Graded Index Optical
Fibres
Proc. I.E.E.E., 62, 9, p.1280, sept. 1974
- 6 T. AKAMATSU, K. OKAMURA, Y. UEDA
Fabrication of Long Fibres by an Improved Chemical Vapour Deposition Method
A.P.L., 31, 3, P.174, August 1977
- 7 G.W. TASKER, W.G. FRENCH
Low-Loss Optical Waveguides with Pure Fused SiO₂ Cores
Proc. I.E.E.E., 62, 9, p.1281, Sep. 1974
- 8 D.N. PAYNE, W.A. GAMBLING
A Borosilicate Cladded Phosphosilicate Core Optical Fibre
Opt. Comm., 13, 4, p.422, April 1975

- 9 D.N. PAYNE, W.A. GAMBLING
New silica Based Low-loss Optical Fibre
Elect. Lett., 10, 15, p.289, July 1974
- 10 S. SENTSUI, K. YOSHIDA, Y. FURUI, T. HOSAKA
Low-loss Monomode Fibres with $P_2O_5 - SiO_2$ Cladding in the Wavelength Regi
1.2 - 1.6 μ m
Proceedings of the 5th European Conference on Optical Communication. Amste
Dam, 17-19 sept. 1979.
- 11 D.B. OSTROWSKI
L'Optique Intégrée
La Recherche, 6, 59, p.740, 1975
- 12 W.J. MURRAY
Proceedings of the sixth European Conference on Optical Communications
University of York, United Kingdom, 16-19 september 1980
- 13 J.E. MIDWINTER
Evanescent Field Coupling Into a Thin Film Waveguide
I.E.E.E. J. Quant., Elect., QE6, p.583, october 1970
- 14 D. MARCUSE
The Coupling of Degenerate Modes in Two Parallel Waveguides
B.S.T.J. 50, 6, p.1791, August 1971
- 15 L.P. BOIVIN
Thin Film To Laser Coupler
Appl. Opt., 13, 2, p.391, February 1974
- 16 P.J.R. LAYBOURN, C.A. MILLAR, G. STEWART, C.D.W. WILKINSON,
Optical Coupling Between Thin Films and Circular Fibres
Elect. Lett., 11, 1, p.2, january 1975
- 17 A. CARDAMA, E.T. KORNHAUSER
Modal Analysis of Coupling Problems in Optical Fibres
I.E.E.E. Trans. MTT, 23, 1, p.162, January 1975

- 18 C.A. MILLAR, P.J.R. LAYBOURN
Coupling of Integrated Optical Circuits Using Sandwich Ribbon Fibres
Opt. Comm., 18, 1, p.80, July 1976
- 19 C.A. MILLAR, R.H. HUTCHINS
Measurement of the Coupling Coefficient for two Coupled Optical Waveguides
by Detuning
Opt. Comm., Bd 31, p140, 1978
- 20 G. STEWART
Refractive Index Modification by Ion Exchange
Ph.D. Thesis, Glasgow University, 1979
- 21 G. STEWART, C.A. MILLAR, P.J.R. LAYBOURN, C.D.W. WILKINSON, R.M. DELARUE
Planar Optical Waveguides Formed By Silver Ion Migration in Glass
I.E.E.E. J. Quant. Elect., QE13, 4, p192, April 1977
- 22 G. STEWART, P.J.R. LAYBOURN
Fabrication of Ion Exchanged Optical Waveguides from Dilute Silver Nitrate
Melts
I.E.E.E. J. Quant. Elect., QE14, 12, Dec. 1978
- 23 L.I. MAISSEL, R. GLANG
Handbook of Thin Film Technology
Mc Grawhill, N.Y., 1970
- 24 V. ROTHMUND, G. KORNFELD
Der Basenaustausch im Permutit
Z. Anorg. Allgem. chem., 103, p.129, 1918
- 25 R.H. DOREMUS
Exchange and Diffusion of Ions in Glass
J. Phys. Chem., 68, 8, p.2212, 1964
- 26 H. GARFINKEL
Membranes, a series of Advances Vol.1
Dekker, New-York, 1972

- 27 G. EISENMAN
Glass Electrodes for Hydrogen and other Cations
Dekker, New-York 1966
- 28 F. HELFFERICH
Ion Exchange
MacGraw Hill, New York 1962
- 29 J. CRANK
The Mathematics of Diffusion
Clarendon Press, Oxford, 2nd Edition, 1975
- 30 GLADSTONE, DALE
Researches on the Refraction, Dispersion and Sensitiveness of liquids
Ph. Trans. Roy. Soc. London, 153, p.317, 1863
- 31 SCHROEDER, MOHR, MACEDO, MONTROSE
Rayleigh and Brillouin Scattering in K_2O-SiO_2 Glasses
J. Am. Ceram. Soc., 56, p.510, 1973
- 32 M.L. HAGGINS, K.M. SUN
J. Am. Ceram. Soc., 26, p.4, 1943
- 33 D.G. HOLLOWAY
The Physical Properties of Glass
Wikeham Publications ltd, London, 1973
- 34 W.H. ZACHARIASEN
The Atomic Arrangement in Glass
J. Am. Chem. Soc., 54, 10, p.3841, 1932
- 35 J.A. MARINSKY
Ion Exchange : a series of Advances
DEKKER, New York, 1969
- 36 GALLENKAMP Catalogue, 19th Edition
- 37 L. HOLLAND
The Properties of Glass Surfaces
Chapman and Hall, London, 1964

- 38 S. KAWAKAMI, T. NISHIZAWA
An Optical Waveguide with the Optimum Distributions of The Refractive Index with reference to wave-front distortion IEEE, Trans. MTT, 16, p.814, 1968
- 39 D.B. OSTROWSKI
Fibres and Integrated Optics
Plenum Press London New York 1979
- 40 H.G. HUNGER
Planar Optical Waveguides and Fibres
Oxford Engineering Science Series, Clarendon Press, Oxford 1977
- 41 D. GLODGE
Weakly Guiding Fibres
Appl. Opt., 10, 10, p.2252, 1971
- 42 D. MARCUSE
Cut-off Condition of Optical Fibres
J. Opt. Soc. Am, 63, 11, p.1369, 1973
- 43 D. GLODGE
Propagation Effects in Optical Fibres
I.E.E.E. Trans. MTT, 23, 1, p.106, 1975
- 44 A.W. SNYDER
Coupled Mode Theory of Optical Fibres
J. Opt. Soc. Am., 62, 11, p.1267, 1972
- 45 J.A. ARNAUD
Transfer Coupling in Fibre Optics. Part IV : Crosstalk
B.S.T.J., 54, 8, p.1431, 1975
- 46 A.W. SNYDER, P. MAC INTYRE
Crosstalk between Light Pipes
J. Opt. Soc. Am, 66, 9, p.877, 1976

- 47 K. OGAWA
Simplified Theory of the Multimode Fibre Coupler
B.S.T.J., 56, 516, p.729, 1977
- 48 D. MARCUSE
Light Transmission Optics
Van Nostrand Reinhold, New York - 1972
- 49 C.A. MILLAR, R.H. HUTCHINS
Manufacturing Tolerances for Silver-sodium in exchanged planar optical waveguides. J. Phys. D: Appl. Phys., Vol.11, p.1567, 1978
- 50 C.A. MILLAR, G. STEWART, R.H. HUTCHINS
Improved repeatability of ion exchanged waveguides by melt dilution
5th European Conference on Optical Communication, Amsterdam 1979.
- 51 T.G. GIALLORENZI, E.J. WEST, R. KIRK, R. GINTHER, R.A. ANDREWS
Optical Waveguides formed by thermal migration of ions in glass
Appl. Opt. 12, 6, p.1240, June 1973
- 52 K. KOIZUMI, Y. IKEDA, I. KITANO, M. FURUKAWA, T. SUMINOTO
New Light Focusing Fibres Made by a Continuous Process.
Appl. Opt., 13, 2, p.255, 1974
- 53 R.D. MAURER
Glass Fibres for Optical Communications
Proc. I.E.E.E., 61, 4, p.452, april 1973
- 54 K. KOIZUMI, Y. IKEDA
Lowloss Light Focusing Fibres Made by a Continuous Process
Proceedings of the 1st European Conference on Optical Fibre Communicati
IEE, London, England, Sept. 16-18, 1975 P.
- 55 Quartz et Silice, Catalogue, 1979
- 56 J.P. DAKIN, W.A. GAMBLING, D.N. PAYNE, H.R.D. SUNAH
L^unching Light into Glass Fibre Optical Waveguide
Opt. Comm., 4, 5, p.354, January 1972

- 57 C.A. MILLAR
Evanescent Field Coupling of Thin Films and Fibre Optical Waveguides
Ph. D. Thesis, Glasgow University, 1976
- 58 W.E. MARTIN
Refractive Index Profile Measurements of Diffused Optical Waveguides
Appl. Opt., 13, 9, p.2112, Sept. 1974
- 59 C.E. TRACY
Micromethod For Refractive Index Determination of Thin Films Using
Liquid Standards
J. Electrochem. Soc., 126, 1, p.103, January 1979
- 60 W. EICKHOFF, E. WEIDEL
Measuring Method For the Refractive Index Profile of Optical Glass Fibre
Opt. Quant. Elec., 7, p.109, 1975
- 61 R. OKOSHI, K. HOTATE
Refractive Index Profile of an Optical Fibre : its Measurement by the
Scattering Pattern Method.
Applied Opt., 15, 11, p.2756, Novembre 1976
- 62 H.M. PRESBY, D. MARCUSE, L.M. BOGGS
Rapid and Accurate Index Profiling of Optical Fibres
Proceedings of The 4th European Conference on Optical Communications,
p.162, Genova, 12-15 sept. 1978
- 63 H.M. PRESBY, D. MARCUSE, H.W. ASTLE, L.M. BOGGS
Rapid Automatic Index Profiling of Whole Fibre Samples
Part I, B.S.T.J., 58, 4, p.867, April 1979
- 64 Ibid. Part II, B.S.T.J., 58, 4, p.883, April 1979
- 65 B. DAINO, S. PIAZZOLLA, A. SAGNOTTI
A New Method for Measuring the Index Profile of Optical Fibre
Proceedings of the 4th European Conference on Optical Communications
p.156, Genova, 12,15 sept. 1978

- 66 F.M.E. SLADEN, D.N. PAYNE, M.J. ADAMS
Determination of Optical Fibre Refractive Index Profiles by a Near Field Scanning Technique
Appl. Phys. Lett., 28, 5, p.255, March 1976
- 67 W.J. STEWART
A New Technique for Determining the Values of Refractive Index Profiles of Optical Fibres
Optical Fibre Transmission Technical Digest, TUD8, 1975
- 68 W.J. STEWART
Proceedings of the Conference on Integrated Optics and Optical Communication, C.2.2. Japan, 1977
- 69 K.I. WHITE
The Measurement of The Refractive Index Profiles of Optical Fibres by the Refracted Near Field Technique.
Proceedings of the 4th European Conference on Optical Communications, P.146, Genova, 12,15 sept. 1978
- 70 M.J. ADAMS, D.N. PAYNE, F.M.E. SLADEN
Leaky Rays on Optical Fibres of Arbitrary Index Profile
Elect. Lett., 11, 11, p.238, May 1975
- 71 D. GLODGE, E.A.J. MARCATILI
Multimode Theory of Graded Core Fibres
B.S.T.J., 52, 9, p. 1563, Novembre 1973
- 72 J.M. HAMMER, R.A. BARTOLINI, C.C. NEIL
Optical Grating Coupling between Low Index Fibres and High Index Film Waveguides
Appl. Phys. Lett., 28, 4, p.192, February 1976
- 73 C.H. BULMER, M.G.F. WILSON
Single Mode Grating Coupling between Thin Films and Fibre Optical Waveguides
I.E.E.E. Jour. Quant. Elect., QE14, 10, p.741, October 1978

- 74 H.P. HSU, W.S.G. CHANG
Coupling Methods in Prospective Single Mode
Fibre Integrated Optics System : A progress Report
Fibre and Integrated Optics, 1, 2, p.153, 1977
- 75 J. GUTTMAN, O. KRUMPHOLZ, E. PFEIFFER
Optical Fibre - Stripline Coupler
Appl. Opt., 14, 5, p.1225, 1975
- 76 D.G. DALGOUTTE, R.B. SMITH, G. ACHUTARAMAYYA, T.H. HARRIS
Externally Mounted Fibres for Integrated Optics Interconnections
Appl. Opt., 14, 8, p.1860, 1975
- 77 D. MARCUSE
Theory of Dielectric Optical Waveguides
Academic Press, New York and London, 1974
- 78 E.A.J. MARCATILI
Dielectric Rectangular Waveguides and Directional Coupler for Integrated
Optics
B.S.T.J., 48, p.2071, Septembre 1969
- 79 A. YARIV
Coupled Mode Theory for Guided Wave Optics
I.E.E.E. Jour. Quant. Electr., QE9, 9, p.919, 1973
- 80 C.H. BULMER
Optical Directional Coupling between Thin Film and Fibre Waveguides
Ph. D. Thesis, University College, London, 1976
- 81 K. OGAWA, W.S.C. CHANG, B.L. SOPORI, F.J. ROSENBAUM
A theoretical Analysis of Etched Grating Couplers for Integrated Optics
I.E.E.E. Jour. Quant. Electr., QE9, 1, p.2942, 1973
- 82 W.S.C. CHANG
Periodic Structures and Their Applications in Integrated Optics
I.E.E.E. Trans. MTT, 21, 12, p.775, 1973

- 83 W. STREIFER, D.R. SCIFRES, R.D. BURNHAM
Coupling Coefficients for Distributed Feed Back Single and Double
Heterostructure Diode Lasers
I.E.E.E. Jour. Quant. Electr., QE11, 11, p.867, November 1975
- 84 W.H. OHO
Compaction Effects in Glass Fibres
Jour. Am. Ceram. Soc., 44, 2, p.68, 1961
- 85 A. YI YAN
Frequency Selective Grating Filters for Integrated Optics
Ph. D. Thesis, Glasgow University, 1978
- 86 R. ULRICH, R. TORGE
Measurement of Thin Film Parameters with a Prism Coupler
Appl. Opt., 12, 12, p.1901, 1973
- 87 Schott Catalogue, 1978
- 88 Dr. A. YI YAN, Private Communication
- 89 Dr. G. STEWART, Private Communication
- 90 C.J. FRANCOIS-KERR
Ph. D. Thesis, GLASGOW University, 1980

